Middle Rio Grande

San Acacia Reach: Morphology and Silvery Minnow Habitat Analysis

September 2019
Plan B Technical Report

Prepared by:
Sydney Doidge

Prepared for:
Dr. Pierre Julien
Dr. Peter Nelson
Dr. Ellen Wohl

Colorado State University
Engineering Research Center
Department of Civil and Environmental Engineering
Fort Collins, Colorado 80523

Abstract

The San Acacia reach spans 11.6 miles of the Middle Rio Grande (MRG), from the San Acacia Diversion Dam to the Escondida Bridge in central New Mexico. This reach report aims to better understand the morpho-dynamic processes of this reach, which is divided into four subreaches (SA1, SA2, SA3 and SA4) to better recognize the spatial and temporal trends in channel geometry and morphology.

The river is dynamic, still changing in response to anthropogenic impacts over the last century (Posner 2017). The mean annual discharge and suspended sediment discharge have been declining since around 1995. Significant channel degradation has occurred in all subreaches. In subreach SA1, there has been over 10 feet of degradation since 1962. Analysis of the bed material also shows evidence of coarsening downstream of the San Acacia Diversion Dam, where bed material samples with d_{50} larger than 1 mm are only found above 22,000 ft downstream of the dam.

GIS analysis of digitized aerial photographs dating back to 1918 was also performed. The current channel width has decreased dramatically over time. The width of subreach SA3 is currently ten times less than it was in 1918. Other reaches have exhibited a similar but less drastic transformation. All are within 50% of the Julien-Wargadalam equation predicted width. Sinuosity drops for all reaches after 1949. In all reaches, except SA4 which maintains a value of around 1.02, sinuosity begins to increase again around 1985.

Application of Massong et al.'s 2010 geomorphic conceptual model for the Middle Rio Grande finds that most subreaches are currently in the M4 stage, which represents excessive transport capacity and constraint by vegetation.

Finally, additional work in understanding habitat for the endangered Rio Grande Silvery Minnow (RGSM) was performed using HEC-RAS analysis. Subreach SA3 was the main driver of habitat available on the MRG. Areas with velocities suitable for silvery minnow habitat were the limiting factor compared to depth in the availability of total habitat.

Acknowledgements

I would like to thank the Colorado State University civil engineering department for the opportunity to learn at CSU. My appointment as a Graduate Teaching Assistant Fall 2018 to Spring 2019 enabled me to attend CSU. I would also like to thank the United State Bureau of Reclamation (USBR) for funding the work done in this report and enabling me to serve as a Graduate Research Assistant. I would like to thank Dr. Pierre Julien for his support as a teacher and as my advisor. I would not have accomplished what I did without his guidance and his faith in me and my abilities. I would also like to thank Dr. Peter Nelson and Dr. Ellen Wohl for serving on my committee. I greatly appreciate the students who worked on the Rio Grande before me, specifically Chun-Yao Yang and Kristin LaForge. Their work set a great foundation for my own efforts. I would also like to thank Tori Beckwith for joining the team; I am sure she will accomplish a lot as she continues our research on the Middle Rio Grande. Finally, I would like to thank my friends and family who supported and encouraged me over the last year and half here at CSU.

Table of Contents

List of Tables

List of Figures

1. Introduction

The purpose of this reach report is to evaluate the morpho-dynamic conditions on the MRG. Specific objectives include:

- Delineate the reach into subreaches based on shared geomorphic characteristics;
- Summarize the flow and sediment discharge history for the period of record available from United State Geologic Survey (USGS) gages;
- Analyze geomorphic characteristics at a subreach level (sinuosity, width, bed elevation, bed material, and other hydraulic parameters);
- Link changes in the river geomorphologic with shifts in sediment and flow trends;
- Apply a geomorphic conceptual model to help predict future river changes; and
- Model and understand RGSM fish habitat.

1.1 Site Description and Background

The Middle Rio Grande (MRG) has historically been characterized by large spring flooding events from snowmelt and periods of drought. These floods often caused large scale shifts in the course of the river and rapid aggradation (Massong et al 2010). Floods helped maintain aquatic ecosystems by enabling connection between water in the main channel and the floodplains (Shurlock 1998), but at the same time, these events also threatened human establishments. Starting in the 1990s, levees were used to prevent flooding, while dams were used to store and regulate flow in the river. In the 1950s, the USBR undertook a significant channelization effort involving jetty jacks, river straightening and other techniques. While these efforts enabled agriculture and large-scale human developments along the MRG, they have also fundamentally changed the river, reducing peak flows and sediment supply, and altering channel geometry and vegetation (Posner 2017). Narrowing of the river continues, with channel degradation due to limited sediment supply and the formation of vegetated bars which encroach into the channel (Varyu 2013; Massong et al 2010). The river continues to adjust to anthropomorphic impacts (Posner 2017). These factors have created an ecologically stressed environment, as seen in the decline of species such as the Rio Grande Silvery Minnow (Mortensen et al 2019).

The San Acacia reach is part of the Middle Rio Grande located in central New Mexico. This reach begins at the San Acacia Diversion Dam in Socorro County in New Mexico. It continues approximately 11.6 miles downstream to the bridge that crosses the Rio Grande near Escondida, New Mexico.

1.2 Subreach Delineation

To analyze hydraulic trends, the reach was subdivided into four sections. These subreaches were primarily delineated by confluences or by cumulative plots of hydraulic variables such as top channel width and flow depth. Subreaches were designated when there was a noticeable change in the slope in cumulative plots. These plots were developed using a HEC-RAS model with 2002 and 2012 geometry provided by the USBR. A flow of 3,000 cfs was selected based on past precedent and correspondence with the USBR (LaForge et al. 2019; Yang et al. 2019).

Subreaches were delineated at aggradation/degradation lines (agg/deg lines) which are “spaced approximately 500-feet apart and are used to estimate sedimentation and morphological changes in the

river channel and floodplain for the entire MRG" (Posner 2017). Each agg/deg line is surveyed when the USBR performs monitoring, and is adapted as a cross-section into the HEC-RAS models of the Rio Grande.

Subreach SA1 (San Acacia 1) begins at the San Acacia Diversion Dam and continues downstream on the confluence with the Alamillo Arroyo, encompassing agg/deg lines 1207-1245. SA2 begins at the confluence with the Alamillo Arroyo and continues until a cumulative change in depth was seen (ie this subreach is deeper than the downstream subreach). SA2 includes agg/deg lines 1245-1264. SA3 begins where the cumulative depth plots indicate that the river is shallower, and continues until the cumulative width plot indicates narrowing, agg/deg lines 1264-1300. SA4 is a narrower section of the river and continues until Escondida Bridge at the conclusion of the entire San Acacia reach and at agg/deg line 1313. See Appendix 7.1 Subreach Delineation for all cumulative mass plots used in these determinations. Table 1 describes these delineations along with the mean and median widths from the HEC-RAS results in feet.

Table 1 San Acacia Subreach Definition

San Acacia Reach			Width in 2012		
Subreach	Agg/deg lines	Justification	Mean	Median	Standard Deviation
SA1	1207-1245	San Acacia Diversion Structure	197	179	64
SA2	1245-1264	Confluence with Alamillo Arroyo	227	216	83
SA3	1264-1300	Change in cumulative depth (shallower)	378	369	136
SA4	1300-1313	Change in cumulative width (narrower)	182	144	72

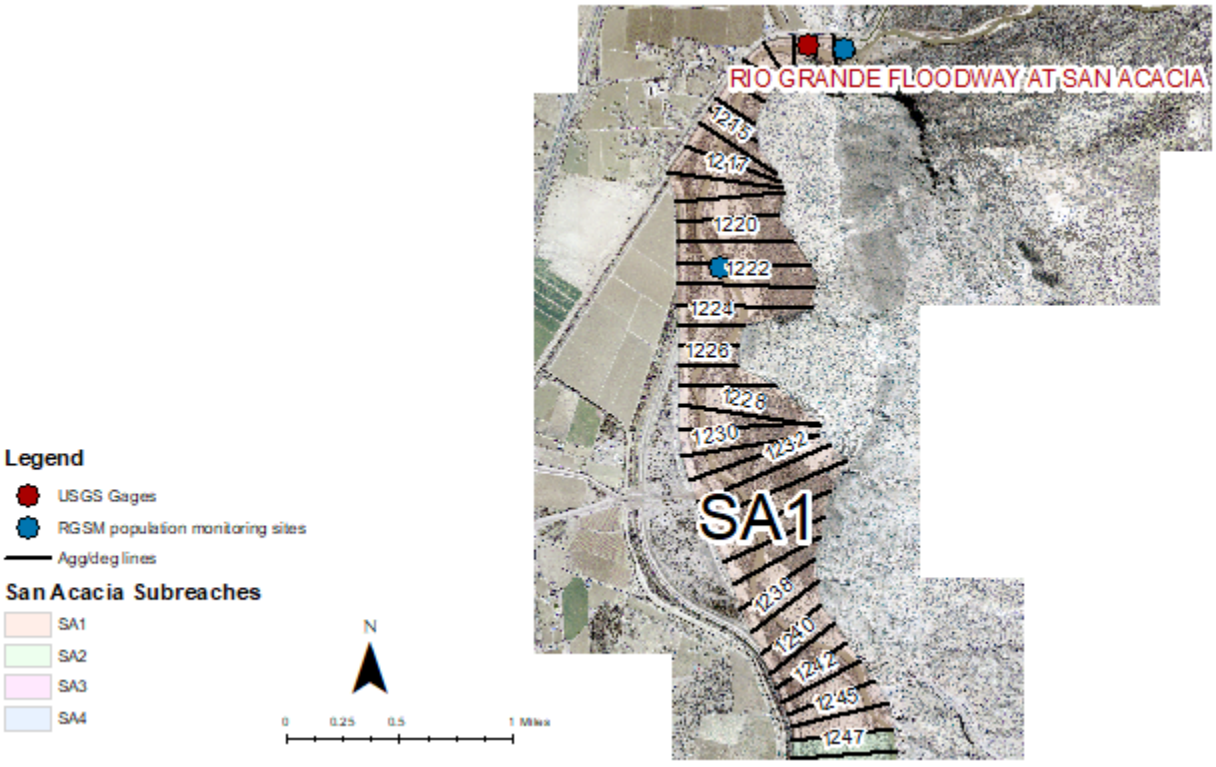

Figure 1 Subreach SA1; flow direction is north to south

Figure 2 Subreach SA2; flow direction is north to south

Figure 3 Subreach SA3; flow direction is north to south

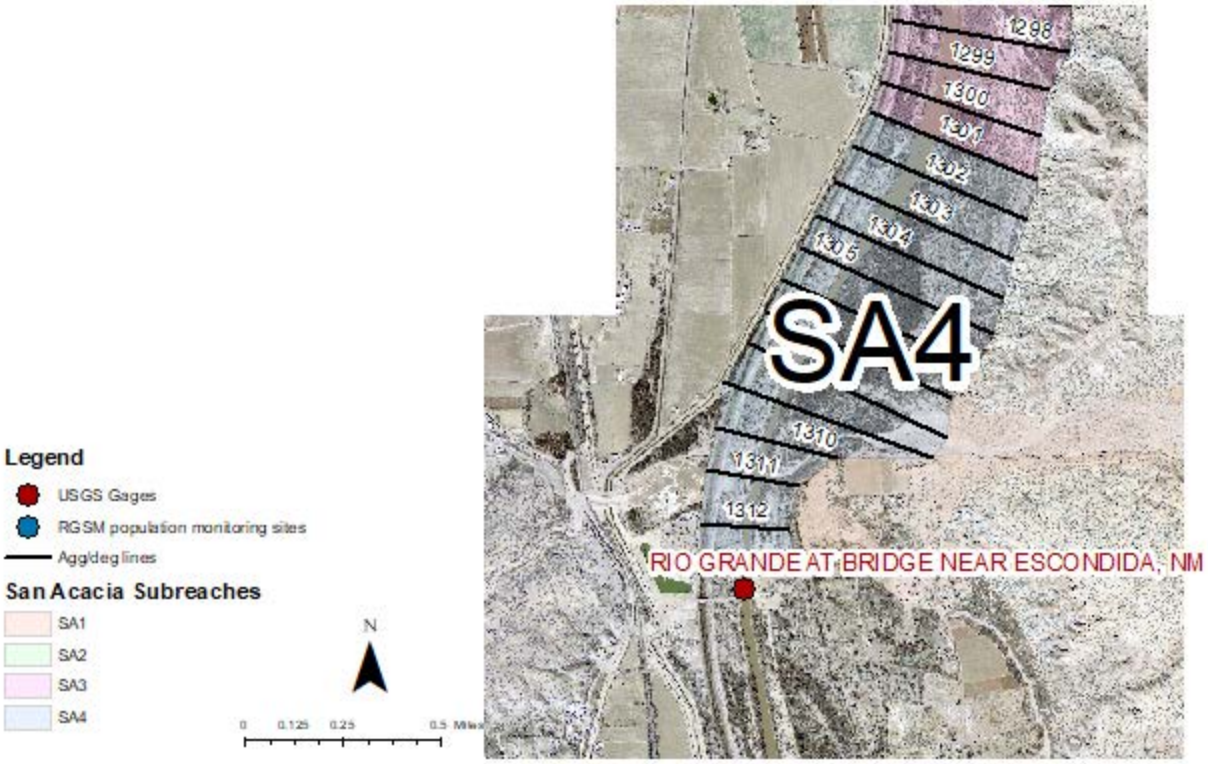

Figure 4 Subreach SA4; flow direction is north to south

2. Precipitation, Flow and Sediment Discharge Analysis

2.1 Precipitation

Precipitation data are collected along the MRG by the Bosque Ecosystem Monitoring Program from University of New Mexico (BEMP Data 2017). The locations of data collection are shown in Figure 5.

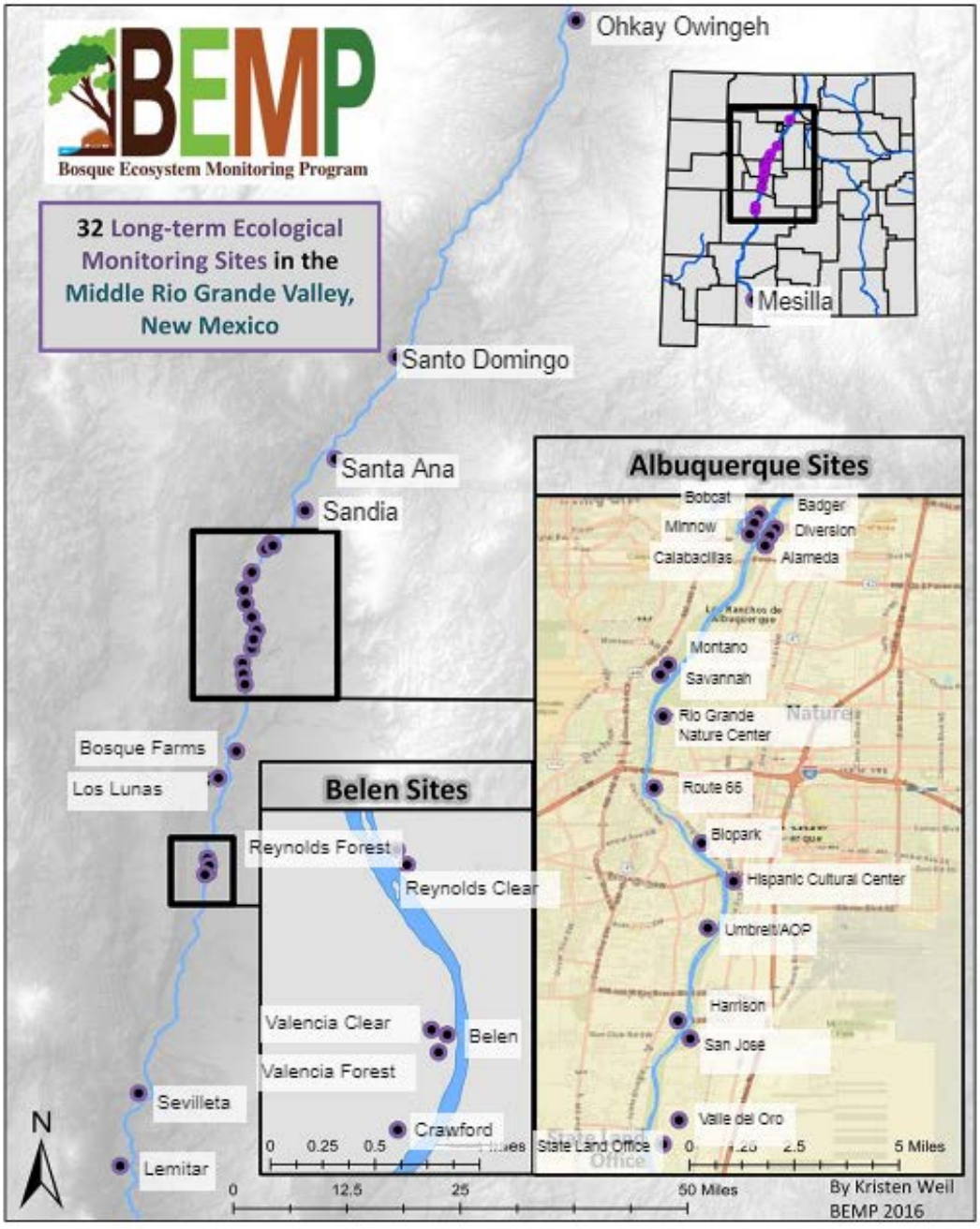

Figure 5 BEMP data collection sites (figure source: http://bemp.org)

The Sevilleta site is near the San Acacia Diversion Dam, and the Lemitar site is between the San Acacia Diversion Dam and Escondida, just outside of Lemitar, New Mexico. Both sites were used in the

precipitation analysis. The average annual and monthly precipitation data accounts for both open and vegetated areas. The precipitation data are shown in Figure 6. By far, the highest precipitation peak was in August of 2006 at the Lemitar gage, with 140.55 mm of rainfall total. A general trend was observed with highest precipitation values during monsoon season (late July through early September), although some outliers were seen. A cumulative plot of rainfall (Figure 7) shows that individual rain events can greatly affect the overall trend of the data. It further highlights the monsoonal rains, which create a "stepping" pattern with higher rainfall in August and September, and lower levels (a nearly flat trend) through the rest of the year.

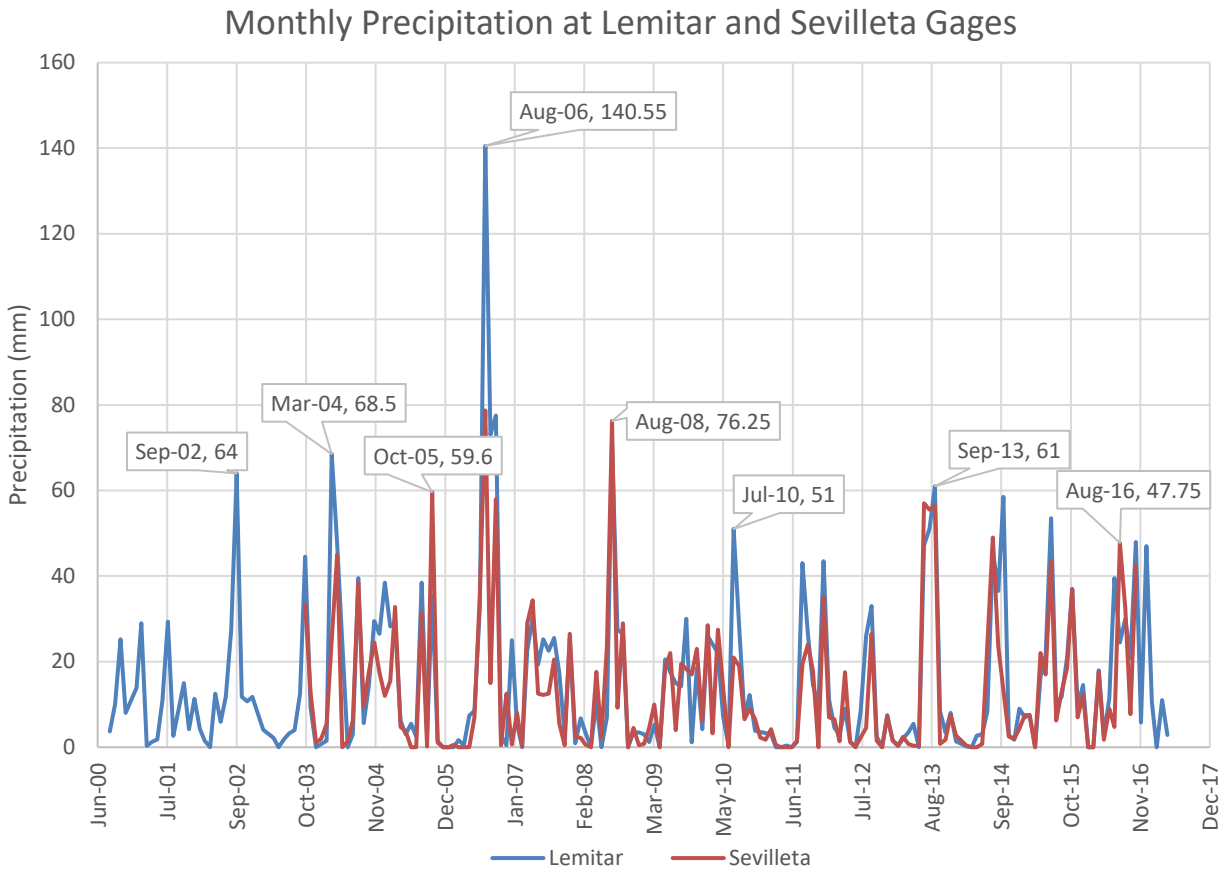

Figure 6 Monthly precipitation trends for the San Acacia reach

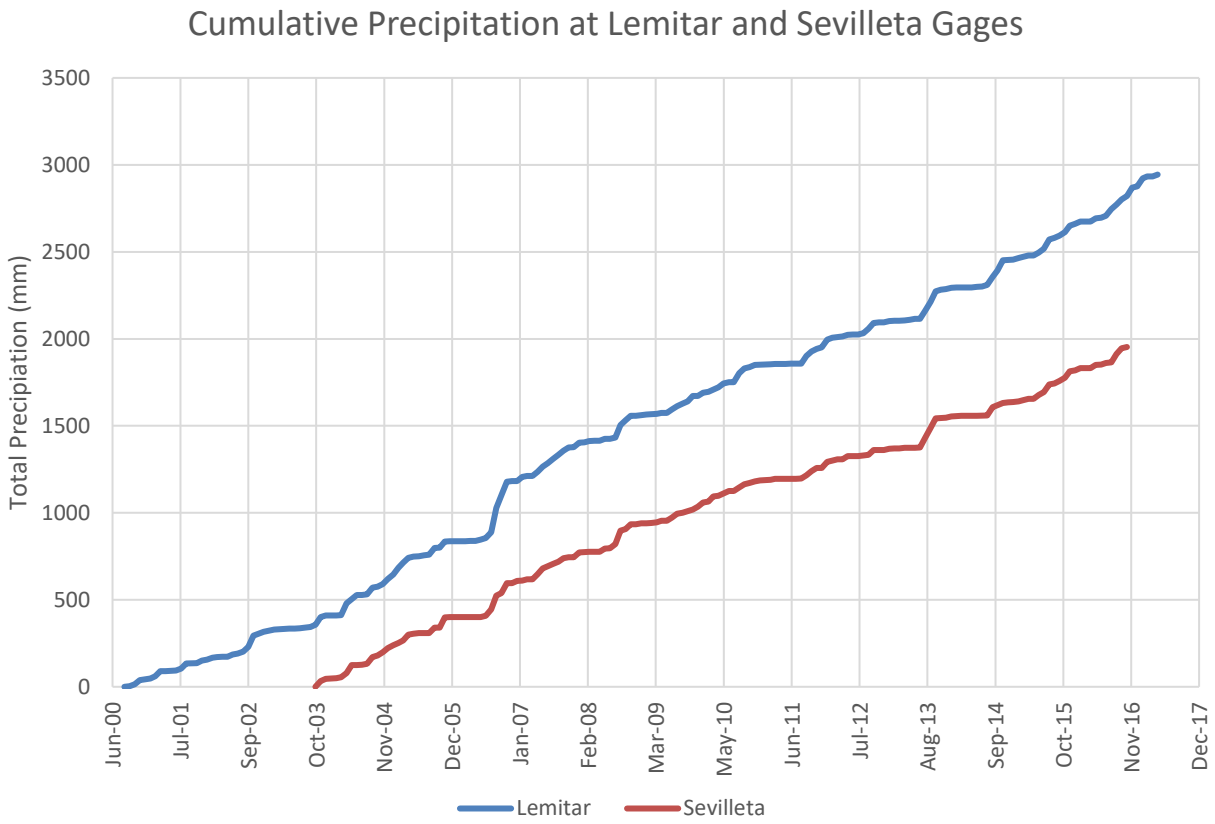

Figure 7 Cumulative precipitation for the San Acacia Reach

2.2 Flow Discharge

Available gages near the study area were found in the United State Geological Survey (USGS) National Water Information System. Table 2 lists the gages analyzed in this report. These gages can be seen relative to the reach in Figure 1 and Figure 4.

Table 2 List of gages used in this study

Station	Station Number	Mean Daily Discharge	Suspended Sediment
Rio Grande Floodway at San Acacia	08354900	October 1, 1958 to present	January 5, 1959 to September 30, 2018
Rio Grande At Bridge Near Escondida, NM	08355050	September 30, 2005 to present	No data

The daily discharge of the San Acacia (08354900) and Escondida (08355050) gages are plotted in Figure 8 and Figure 9. These show seasonal flow patterns, with peak flow occurring with snowmelt runoff April through June, low flow through much of the rest of the summer, and then medium flow from November onwards.

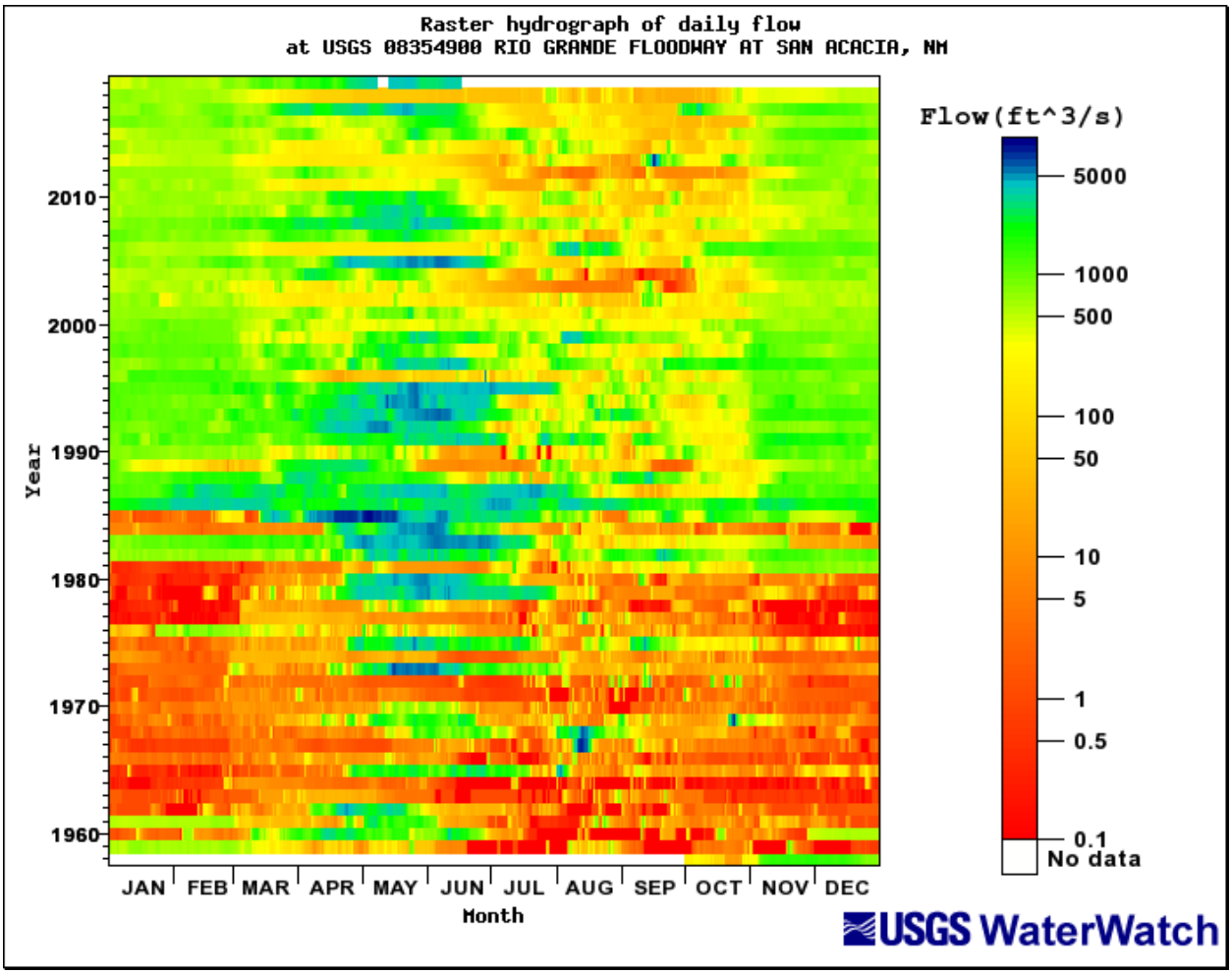

Figure 8 Raster hydrograph of daily discharge at USGS Station 08354900

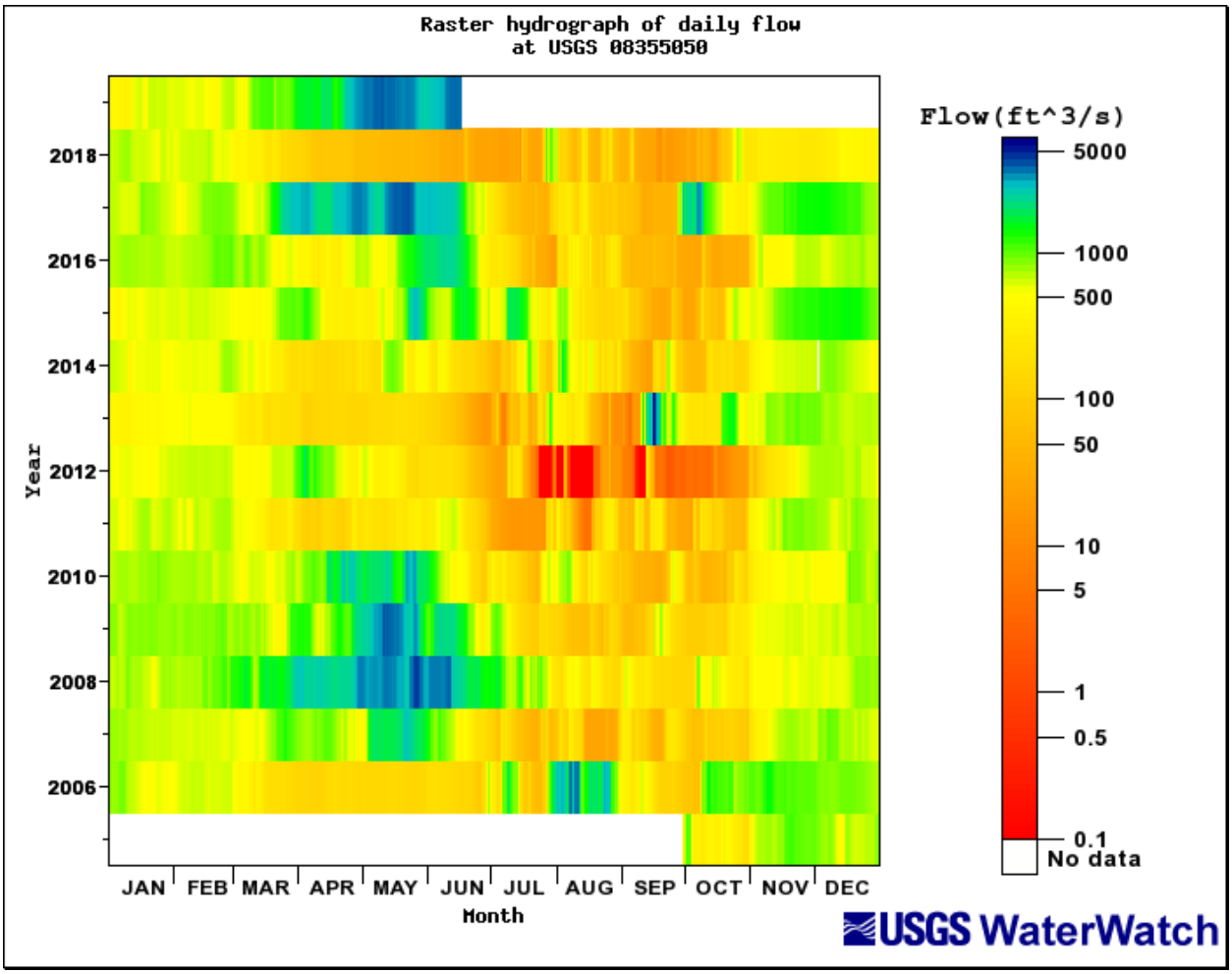

Figure 9 Raster hydrograph of daily discharge at USGS Station 08355050

2.1.1 Cumulative Discharge Curves

Cumulative discharge curves can show changes in annual flow volume over time. The slope of the line of the mass curve gives the mean annual discharge, where breaks in slope show changes in flow volume. Figure 10 shows the flow mass curves of gages at San Acacia and Escondida. The mass curves were divided into the following time periods in water years: 1958 to 1978, 1978 to 1980, 1980 to 1981, 1981 to 1983, 1983 to 1984, 1984 to 1987, 1987 to 1990, 1990 to 1995, 1995 to 1999, 1999 to 2004, 2004 to 2009, 2009 to 2016, 2016 to 2017 and 2017 to 2018. For each of these time periods the average annual discharge in acre-feet was calculated.

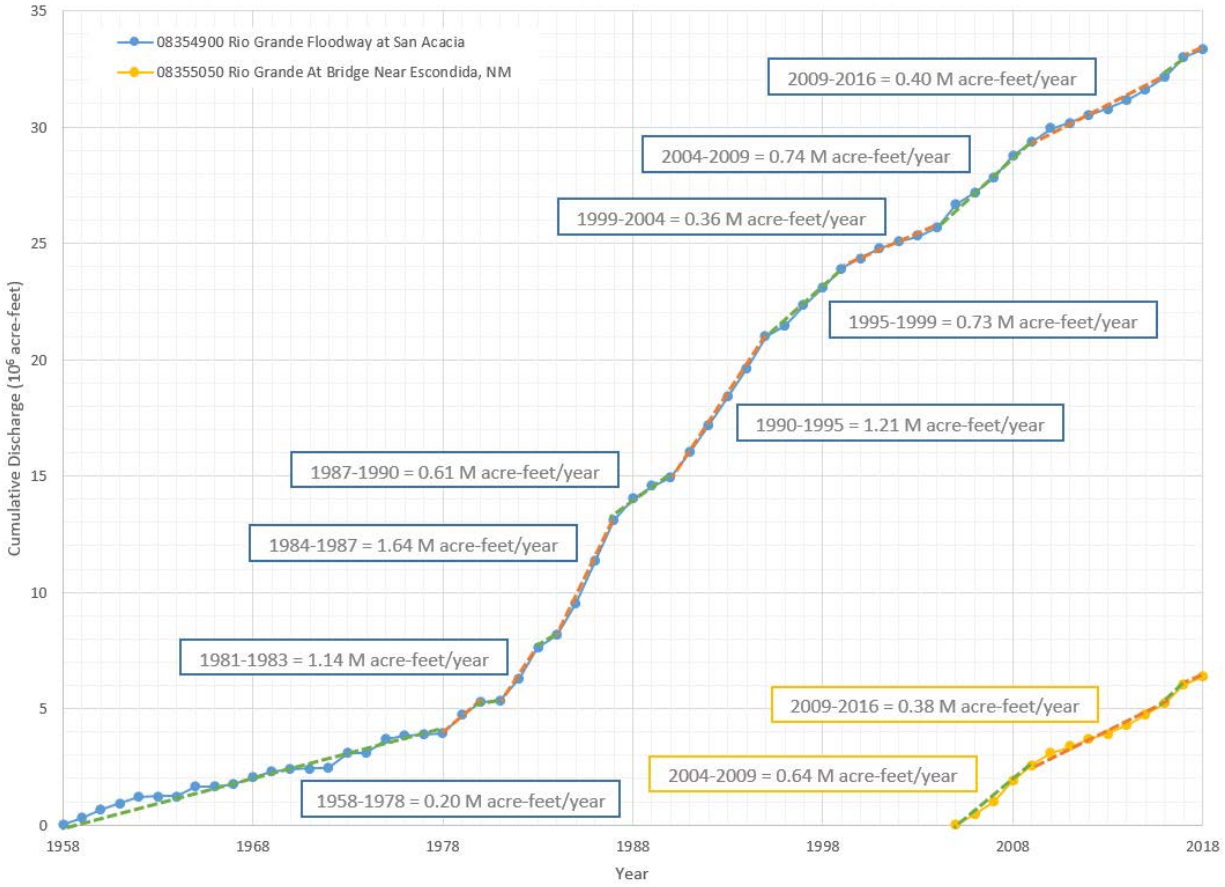

Figure 10 Discharge single mass curve at San Acacia and Escondida gages

Table 3 Average discharge at different time periods

Average Annual Discharge (10^6 acre-feet/year)		
Years	08354900 Rio Grande Floodway at San Acacia	08355050 Rio Grande At Bridge Near Escondida, NM
1958-1978	0.20	--
1978-1980	0.68	--
1980-1981	0.04	--
1981-1983	1.14	--
1983-1984	0.57	--
1984-1987	1.64	--
1987-1990	0.61	--
1990-1995	1.21	--
1995-1999	0.73	--
1999-2004	0.36	--
2004-2009	0.74	0.64
2009-2016	0.40	0.38
2016-2017	0.82	0.79
2017-2018	0.35	0.34

2.1.2 Flow Duration

A flow duration curve was developed for the San Acacia gage for the time period 1979 to 2018 and for the Escondida gage for the entire record, 2011 to 2018. Figure 11 and Figure 12 show the flow duration curves. Table 4 shows some exceedance values calculated from these flow duration curves. Note that the values for the Escondida gage are lower except for 90% exceedance. There is a shorter period of record for the Escondida gage; as a result, it has not experienced as many high flow events as since recording began as the San Acacia gage. Water is also taken from the river for agricultural purposes at the San Acacia Diversion Dam. Finally, the higher flow value calculated at Escondida for the 90% exceedance may be attributed to a station that pumps water into the river near agg/deg line 1300, just upstream of the gaging location, thus ensuring that this section of the river maintains a higher level of flow regardless of upstream flow conditions.

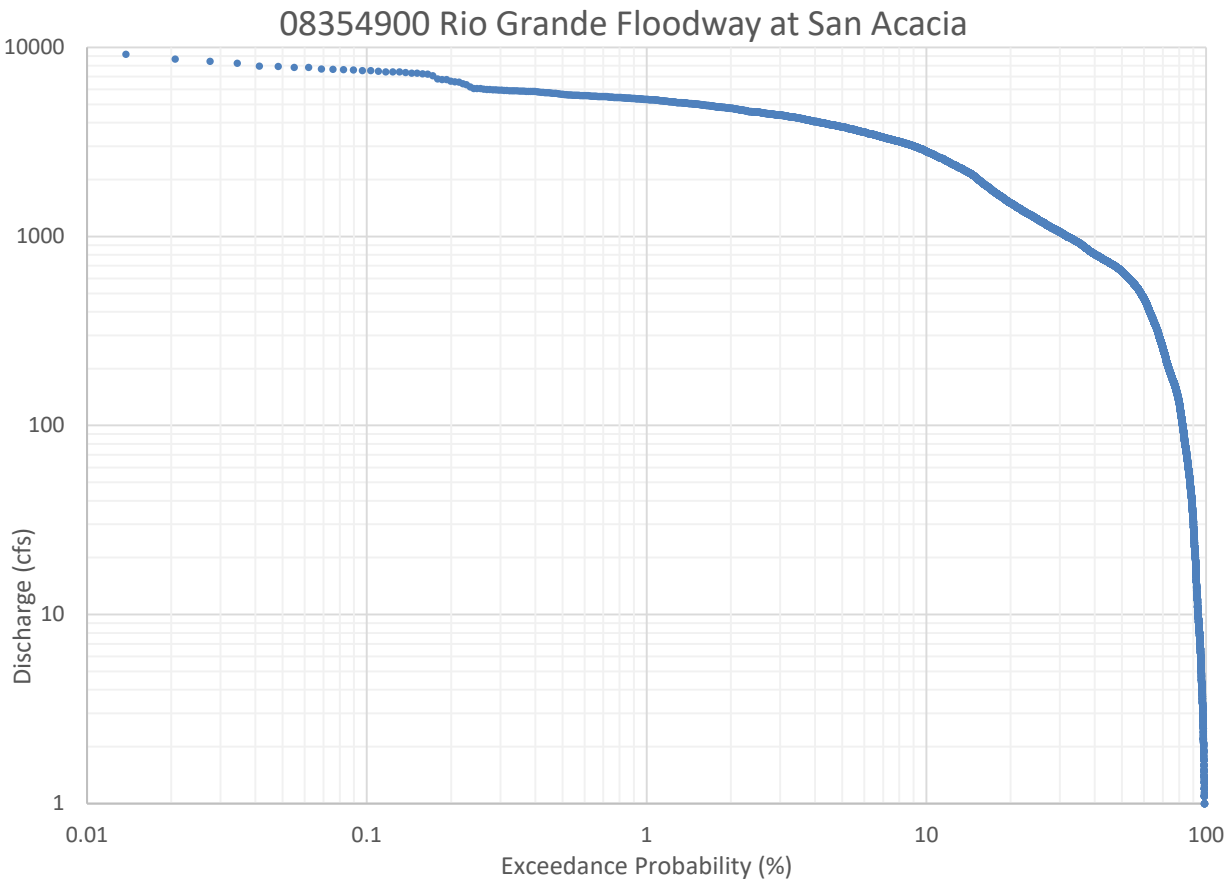

Figure 11 Flow duration curve for USGS gage 08354900

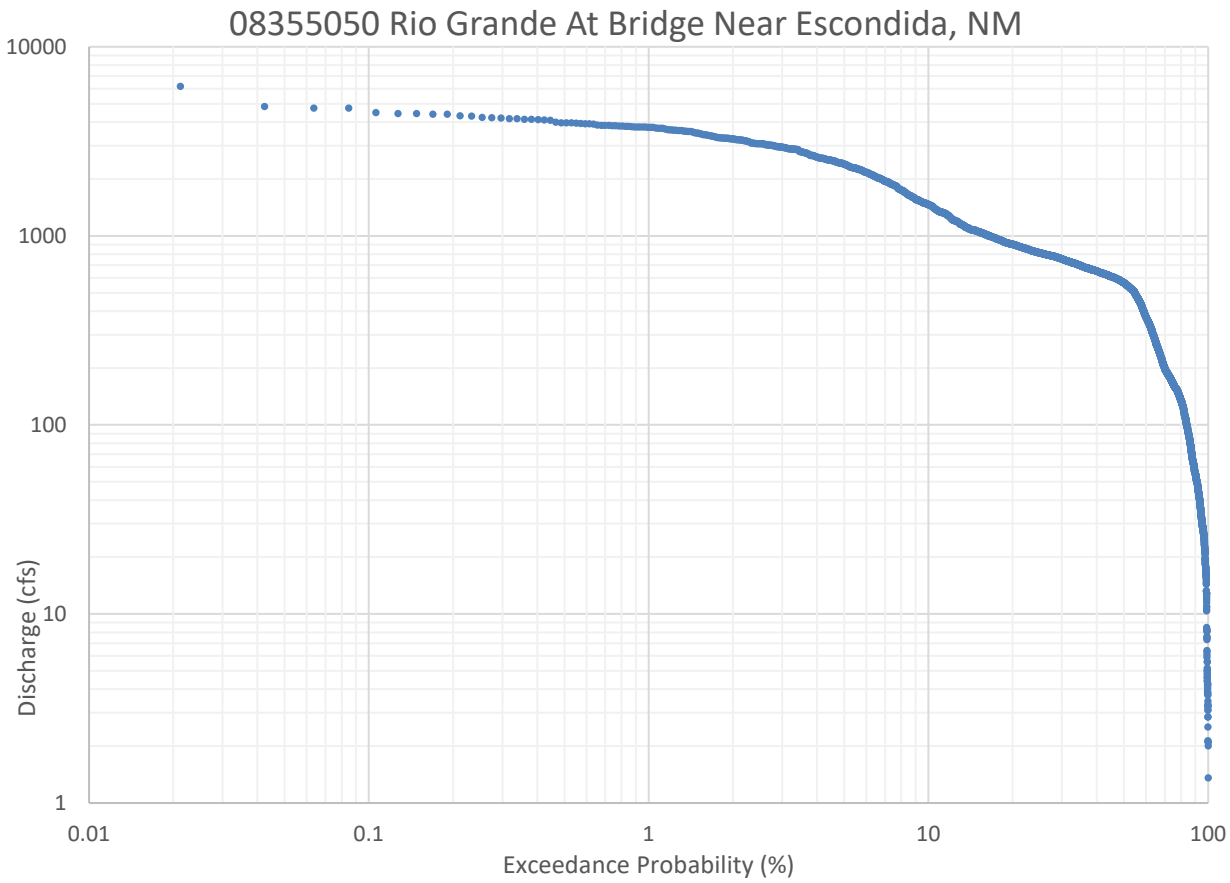

Figure 12 Flow duration curve for USGS gage 08355050

Table 4 Probabilities of exceedance for both gages from the flow duration curves

	08354900 Rio Grande Floodway at San Acacia	08355050 Rio Grande At Bridge Near Escondida, NM
Probability of Exceedance	Flow (cfs)	
1%	5310	3760
10%	2810	1470
25%	1230	815
50%	654	565
75%	183	164
90%	29	55

In addition to flow duration curves, the number of days in the water year exceeding target flow values (500 cfs, 1000 cfs, 2000 cfs, 3000 cfs, 4000 cfs, 5000 cfs and 6000 cfs) at each gage was analyzed. This is purely a count of days and does not consider consecutive days. Analysis was performed for the last twenty years for the San Acacia gage, and for the entire record for the Escondida gage. Table 5 and Table 6 show the number of days over these target values. There are two periods of lower peak flows, from 2002 to 2003 and from 2011 to 2013. 2013 is a particularly interesting year in that the fewest number of days over 500 cfs were seen while the greatest number of days over 6000 cfs were seen.

These outlying high values are not from snowmelt but are associated with a storm event in September of 2013.

Table 5 Number of days over a target discharge at the San Acacia gage

Year	500 cfs	1000 cfs	2000 cfs	3000 cfs	4000 cfs	5000 cfs	6000 cfs
1998	278	219	26	2	0	0	0
1999	287	151	48	20	6	0	0
2000	174	60	0	0	0	0	0
2001	232	25	2	0	0	0	0
2002	121	6	0	0	0	0	0
2003	135	2	1	0	0	0	0
2004	182	49	17	2	0	0	0
2005	242	111	75	70	48	24	0
2006	171	36	23	9	4	0	0
2007	257	157	22	2	0	0	0
2008	280	149	91	47	5	0	0
2009	229	68	43	19	1	0	0
2010	221	65	46	3	0	0	0
2011	131	1	0	0	0	0	0
2012	169	13	1	0	0	0	0
2013	95	11	6	4	3	2	2
2014	181	32	0	0	0	0	0
2015	223	45	10	2	0	0	0
2016	217	94	20	0	0	0	0
2017	235	102	87	53	12	1	0
2018	145	59	7	2	0	0	0

Table 6 Number of days over a target discharge at the Escondida gage

Year	500 cfs	1000 cfs	2000 cfs	3000 cfs	4000 cfs	5000 cfs	6000 cfs
2006	172	51	21	8	0	0	0
2007	249	95	13	1	0	0	0
2008	270	145	85	43	5	0	0
2009	254	81	43	19	4	0	0
2010	240	58	30	5	0	0	0
2011	131	1	0	0	0	0	0
2012	174	12	1	0	0	0	0
2013	92	13	6	4	2	1	1
2014	176	21	0	0	0	0	0
2015	224	49	7	2	0	0	0
2016	224	90	18	0	0	0	0
2017	230	96	87	48	10	0	0
2018	144	61	8	2	0	0	0

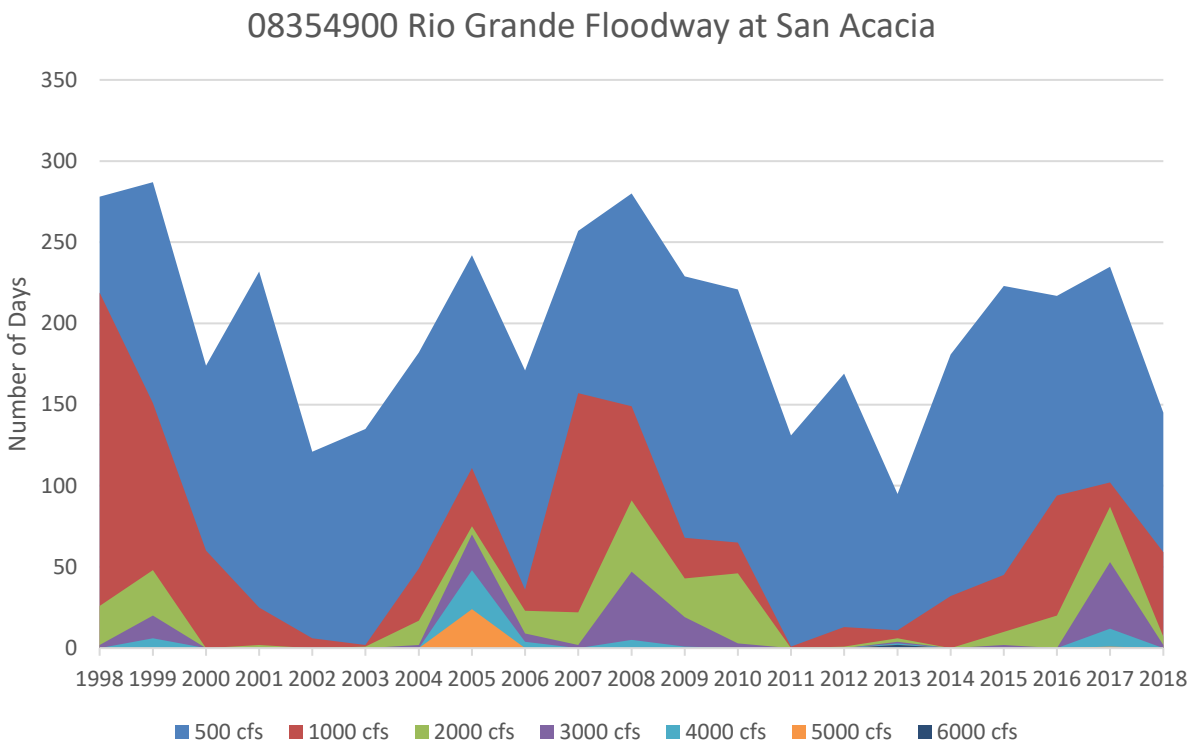

Figure 13 Number of days over a target discharge at the San Acacia gage

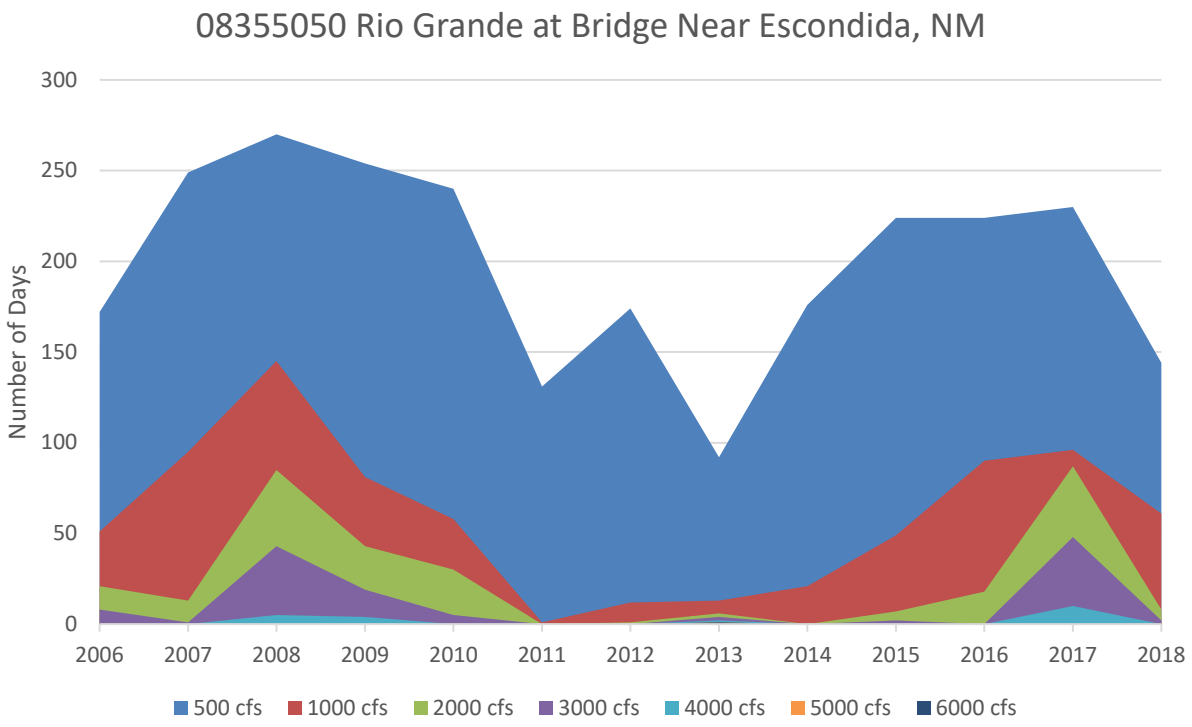

Figure 14 Number of days over a target discharge at the Escondida gage

2.1.3 Flood Frequency Analysis

Flood frequency analysis was performed using the Gumbel and Log-Pearson III distributions for both gages and the same time periods as outlined for the flow duration curve analysis; 1979 to 2018 for the San Acacia gage and 2011 to 2018 for the Escondida gage. Again, the discharges at all return intervals at Escondida were lower compared to the discharges at the San Acacia gage. This may be because the period of analysis for Escondida is only 13 years, as opposed to the 40 years used in the San Acacia analysis. Table 7 shows the results of the flood frequency analysis and Figure 15 shows them in graphical form.

Table 7 Discharges at different flood frequencies

	Gumbel Distribution		Log Pearson III Distribution	
Return period in years	Discharge San Acacia (cfs)	Discharge Escondida (cfs)	Discharge San Acacia (cfs)	Discharge Escondida (cfs)
2	4061	3204	4168	3313
5	5698	4428	5964	4678
10	6781	5238	6986	5448
20	7821	6015	7851	6096
25	8151	6262	8105	6286
50	9166	7021	8828	6825
100	10175	7775	9469	7302

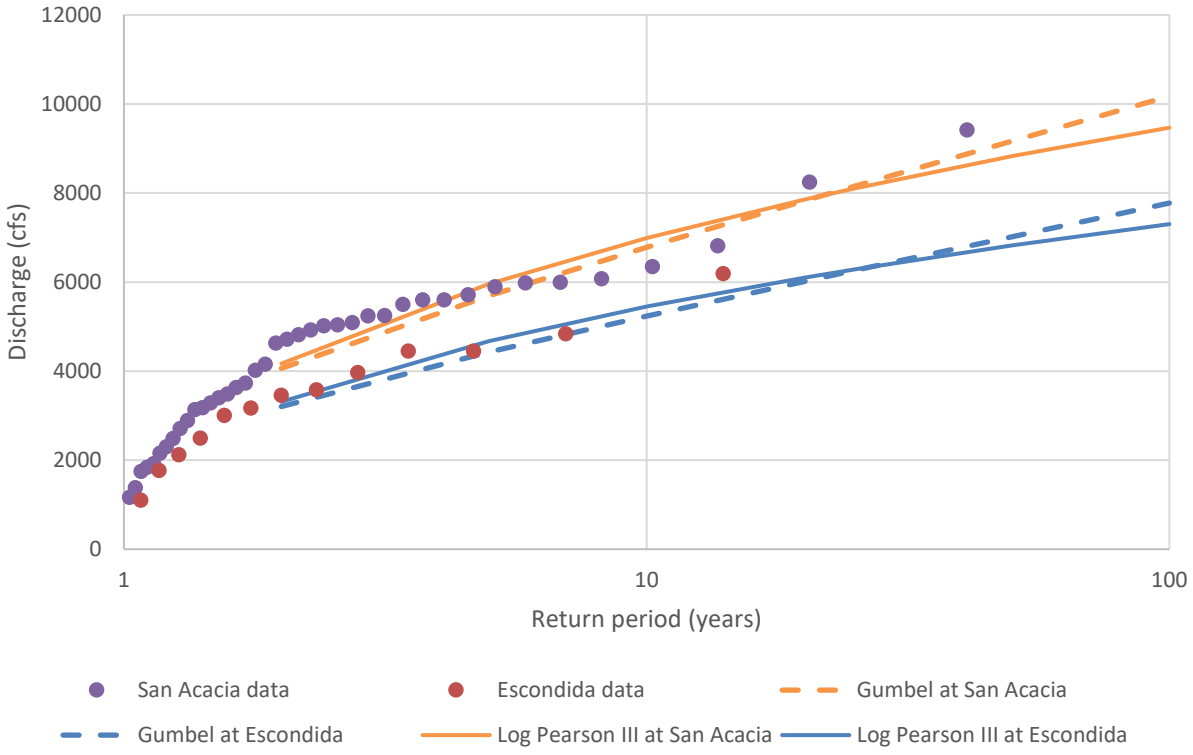

Figure 15 Flood frequency analysis

2.3 Suspended Sediment Load

2.3.1 Single Mass Curve

Single mass curves of cumulative suspended sediment (in millions of tons) are shown in Figure 16. Breaks in slope show the changes in flux. Data comes from the USGS gage at San Acacia (08354900) alone, as there is no sediment monitoring at the USGS gage at Escondida. Analysis is performed in water years. Years 1997 through 2000 were removed from the record as the data for those years is incomplete, some even missing several months of suspended sediment data. Since 2006, there has been an average of 2.1 million tons of sediment passing through the gage each year.

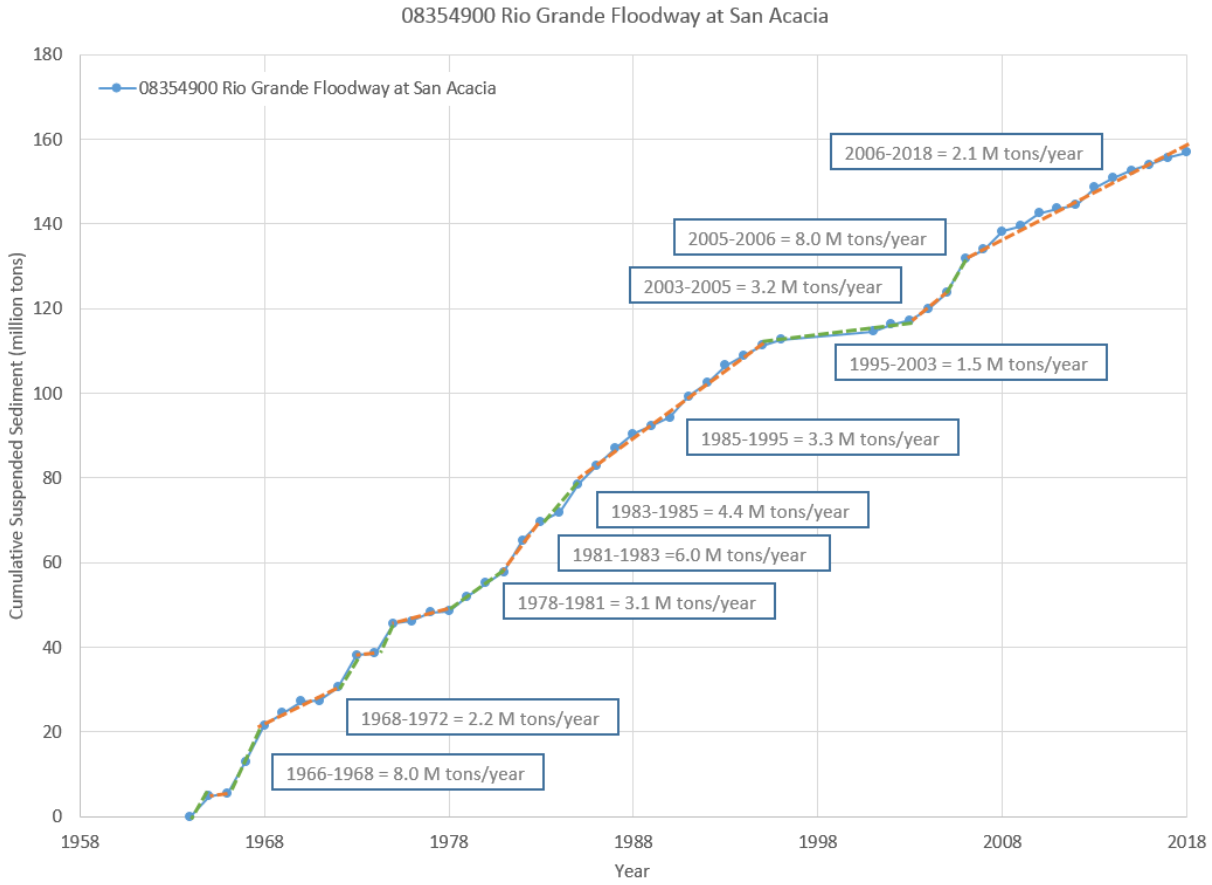

Figure 16 Suspended sediment discharge single mass curve for the San Acacia gage

2.3.2 Double Mass Curve

Double mass curves show how suspended sediment volume pairs with annual discharge volume. The slope of the double mass curve represents the mean sediment concentration. The double mass curve in Figure 17 is for USGS gage at San Acacia (08354900). Overall, the mean annual suspended sediment concentration has decreased since the 1960s. Table 8 shows the average suspended sediment concentration of groupings of years compared.

Table 8 Change in average suspended sediment concentration over time at the San Acacia gage

Years	Average Suspended Sediment Concentration (mg/L)
1965-1981	4056
1981-2005	2917
2005-2006	5037
2006-2012	3382
2012-2013	4642
2013-2018	2290

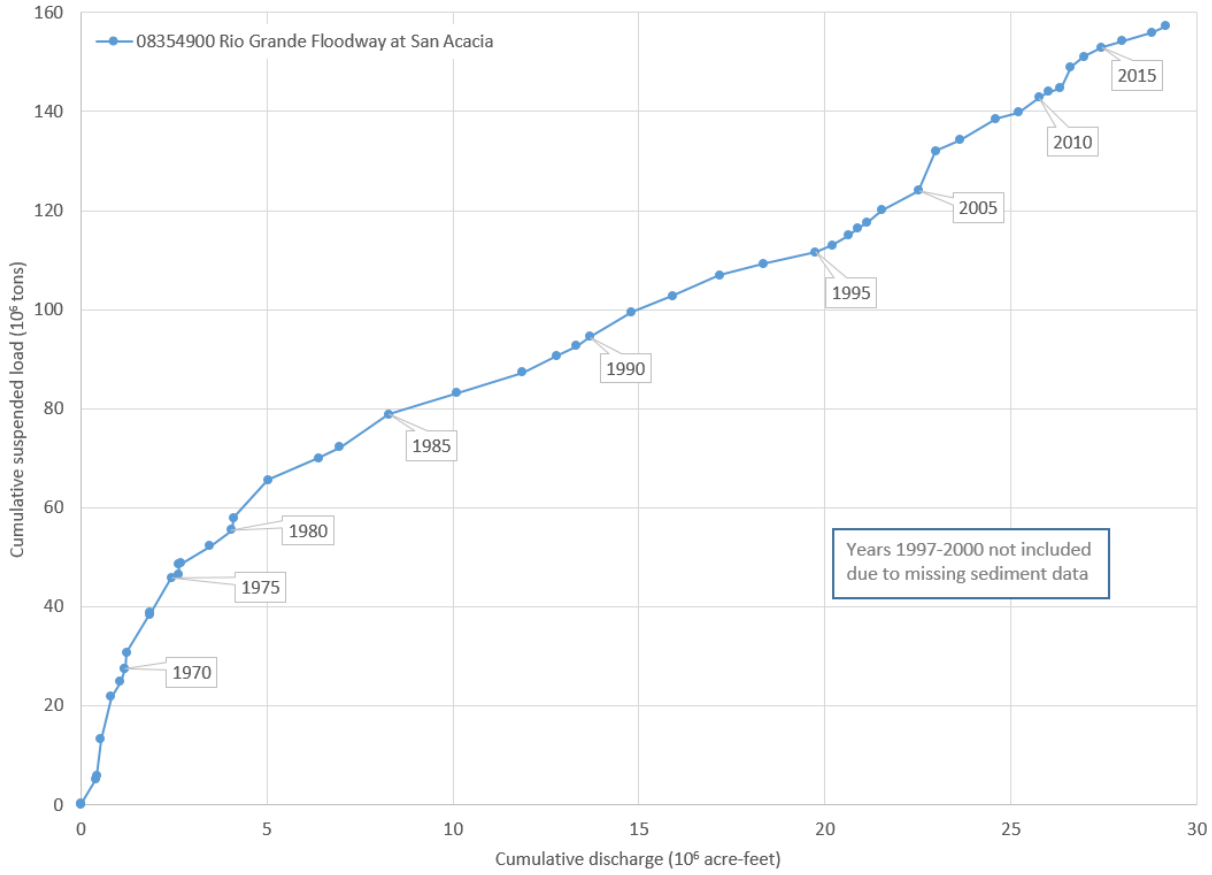

Figure 17 Suspended sediment discharge double mass curve for the San Acacia gage

Prior to 1981, the average suspended sediment concentration was 4,056 mg/L. In the 1980s and 1990s following the operation of the Cochiti Dam, this was reduced to an average of only 2,917 mg/L. Since 2013, the average suspended sediment concentration has been 2,290 mg/L.

It is important to note that with the Cochiti Dam, the main source of sediment now for the Rio Grande is the Rio Puerco. The confluence with the Rio Puerco occurs just upstream of the San Acacia reach. The Rio Puerco is undammed and still carries high sediment loads. Historic estimates indicate that values of sediment concentration in the Rio Puerco approached 150,000 to 165,000 mg/L in the 1940s and 1950s (MEI 2002); this has since been substantially reduced to only around 15,120 mg/L (Klein et al. 2018a).

2.3.3 Monthly Average Histogram and Sediment Movement Trends

A monthly average histogram, capable of revealing important seasonal trends, was created for the San Acacia gage. To compare the trends from 1980 to the present, the data was sorted by decade.

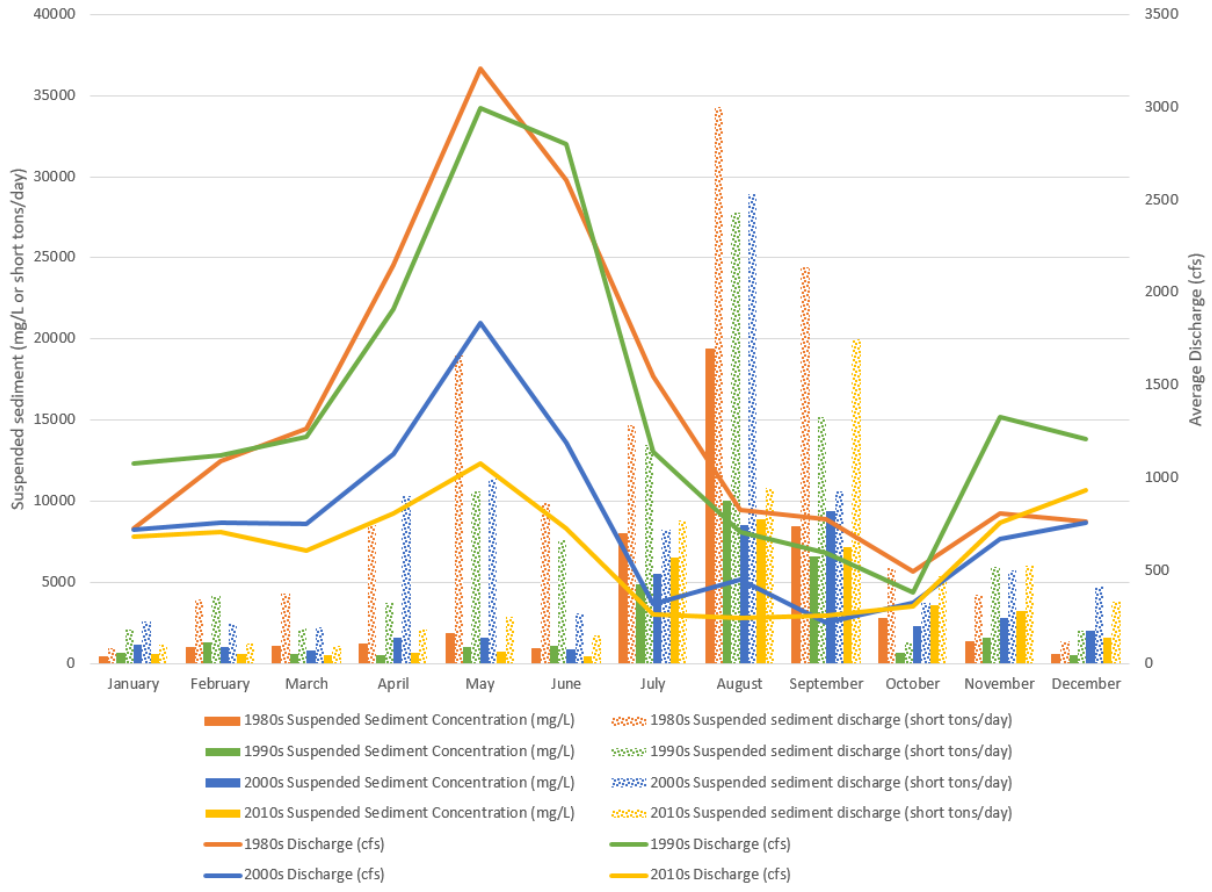

Figure 18 Monthly average histogram of sediment and discharge at the San Acacia gage

Although discharge peaks in late spring, April through June, the highest suspended sediment load occurs July through September. These high levels of transport are associated with monsoon events, which tend to be sudden and severe and cause widespread erosion. In flows associated with spring snowmelt during April, May and June, concentrations remain similar to what they are October through March, even though the total sediment discharge is higher than in the rest of the year. In contrast, the monsoon events have higher concentrations of sediment, in addition to higher volumes. Generally, average flows have been lower in the 2000s and 2010s.

To further demonstrate the effects of monsoon-related sediment movement, figures of precipitation versus discharge and precipitation versus suspended sediment discharge were generated. In Figure 19, when the line moves upward without moving across in the horizontal direction (as it does between April 2005 and August 2005, it means that there is a significant amount of discharge in the river despite a lack of rainfall (ie snowmelt related discharge can be seen). In contrast, from July 2006 to November 2006, where was a substantial increase in the amount of cumulative rainfall, while there was little change in

the discharge. Figure 20 compares the suspended sediment discharge with precipitation. Specific monsoon events can be clearly seen in this figure, such as from August 2006 to September 2006, and September 2013 to October 2013. These are the events that are substantially altering what sediment is in the river.

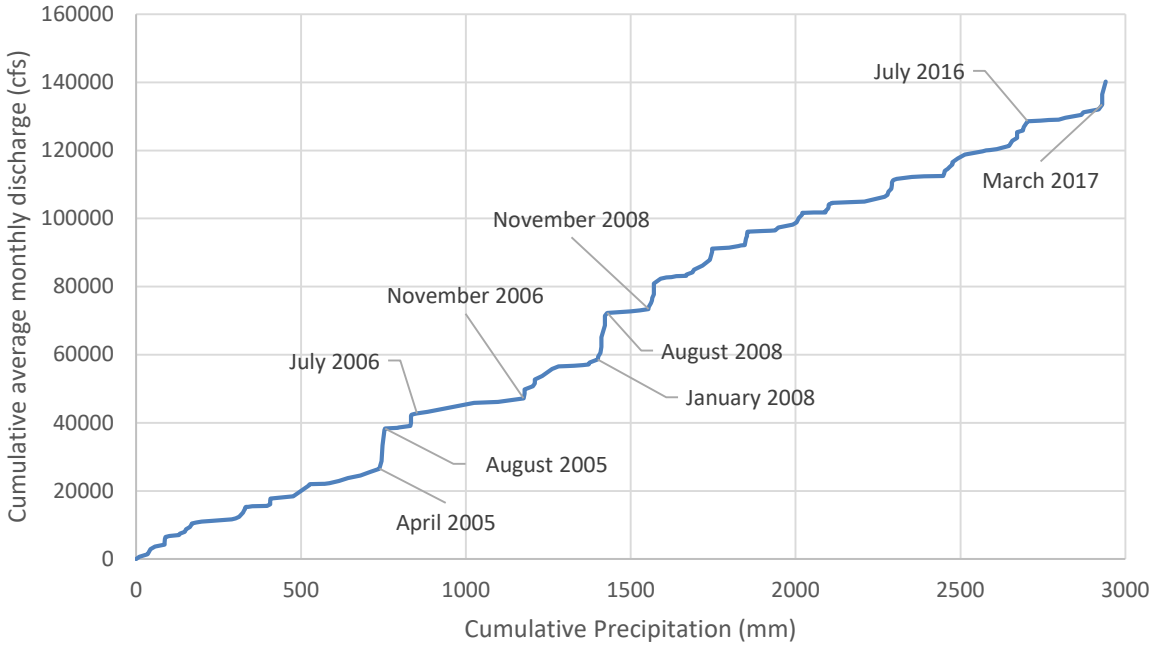

Figure 19 Cumulative discharge versus precipitation

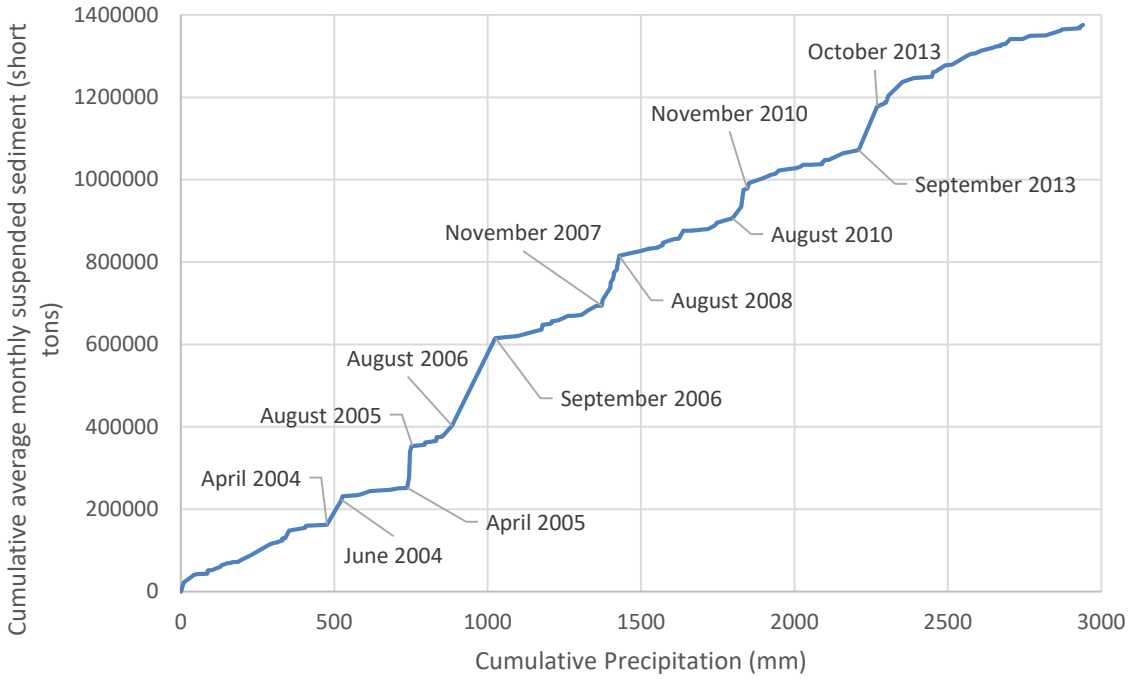

Figure 20 Cumulative suspended sediment vs precipitation

3. Geomorphic and River Characteristics

3.1 Wetted Top Width

Wetted top width can provide significant insight into at-a-station hydraulic geometry. A typical pattern would be a slow rate of width increase until connection with the floodplain is reached, when the width would increase dramatically. Then, the slow increase in width would continue. Analysis of the wetted top width can be used to help understand bankfull conditions and how they vary spatially and temporarily in the San Acacia reach. A HEC-RAS model was created to analyze the top width. This is the same model used for the results in Section 4. HEC-RAS Modeling for Silvery Minnow Habitat. An increment of 500 cfs up to 10,000 cfs was used. This data was then processed to analyze a variety of top width metrics.

Figure 21 shows a five cross-section averaged top width from HEC-RAS runs at 3,000 cfs and 6,000 cfs. Additional figures from this analysis can be found in Appendix 7.2 Additional Figures. Figure 21 shows that 2012 is the narrowest year, with the largest difference seen in subreach SA3. There is a different shape in 2012 and 1992 compared to 2002 in subreach SA3, where 2012 and 1992 are wider.

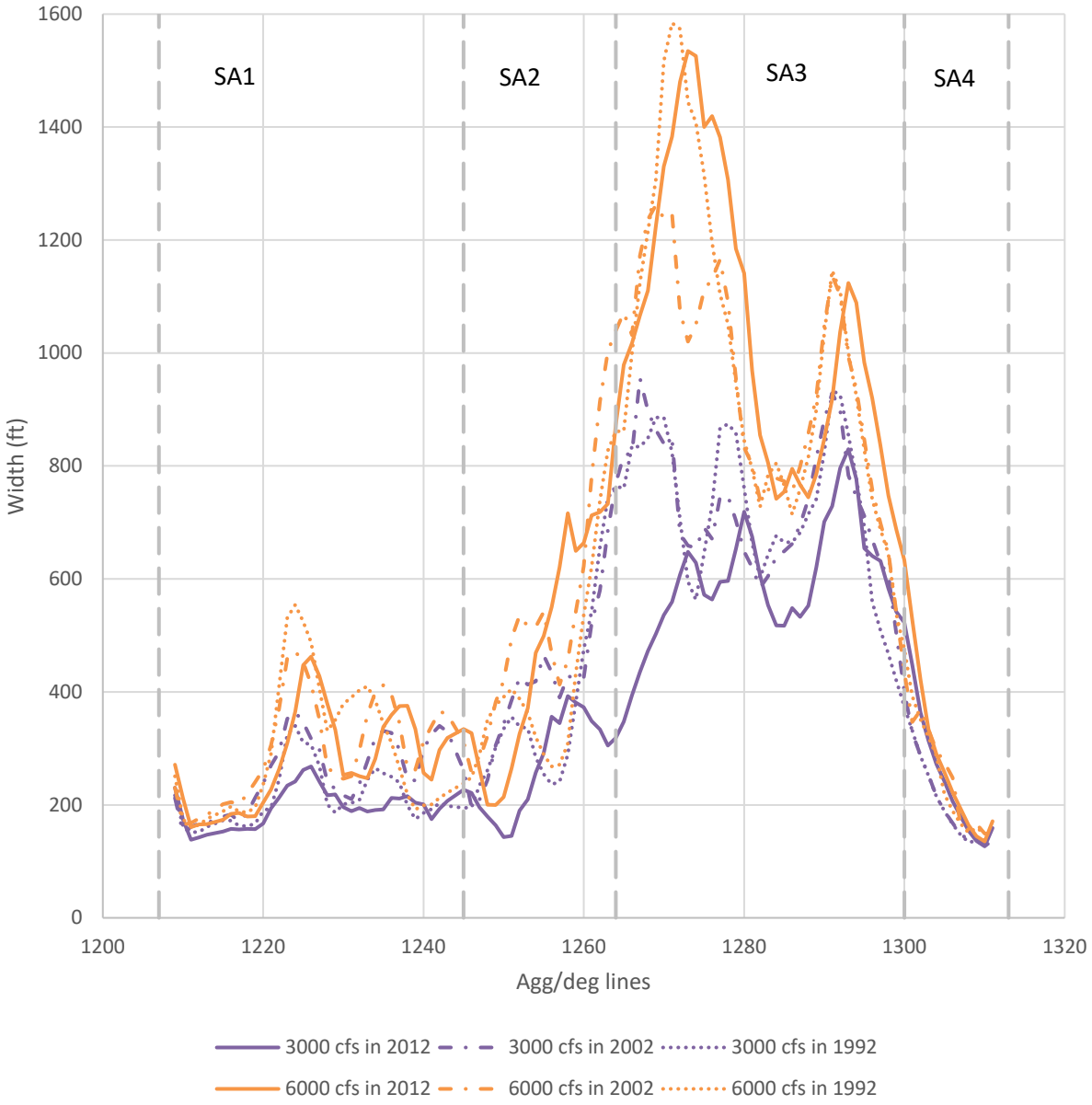

Figure 21 Five cross-section moving average width at 3,000 cfs and 6,000 cfs

Figure 22 shows the width-discharge relationship averaged across each subreach in 1992, 2002 and 2012. SA1 had a linearly increasing trend. The widest year was 2002, and the narrowest was 2012. SA2 showed more of the expected pattern of increase associated with floodplain connection. At discharges below 5,000 cfs, narrowing over time occurred, while above that value, widening over time occurred. Discharges of 6,000 cfs are rarely exceeded on this section of the river. It is likely that the narrowing reflects general trends seen with encroachment of vegetation. SA2 and SA3 had similar trends with narrowing and widening around a pivot point of about 5,000 cfs. SA3 increased the most from 2,000 to 4,500 cfs. Compared to the other subreaches, SA3 incised the least from 1962 to 2012 and has the widest non-vegetated width (Sections 3.5 Bed Elevation and 3.3 Width, respectively). SA4 does not

begin to significantly widen until discharges of around 8,000 cfs are reached, reflecting the heavily incised nature of this subreach.

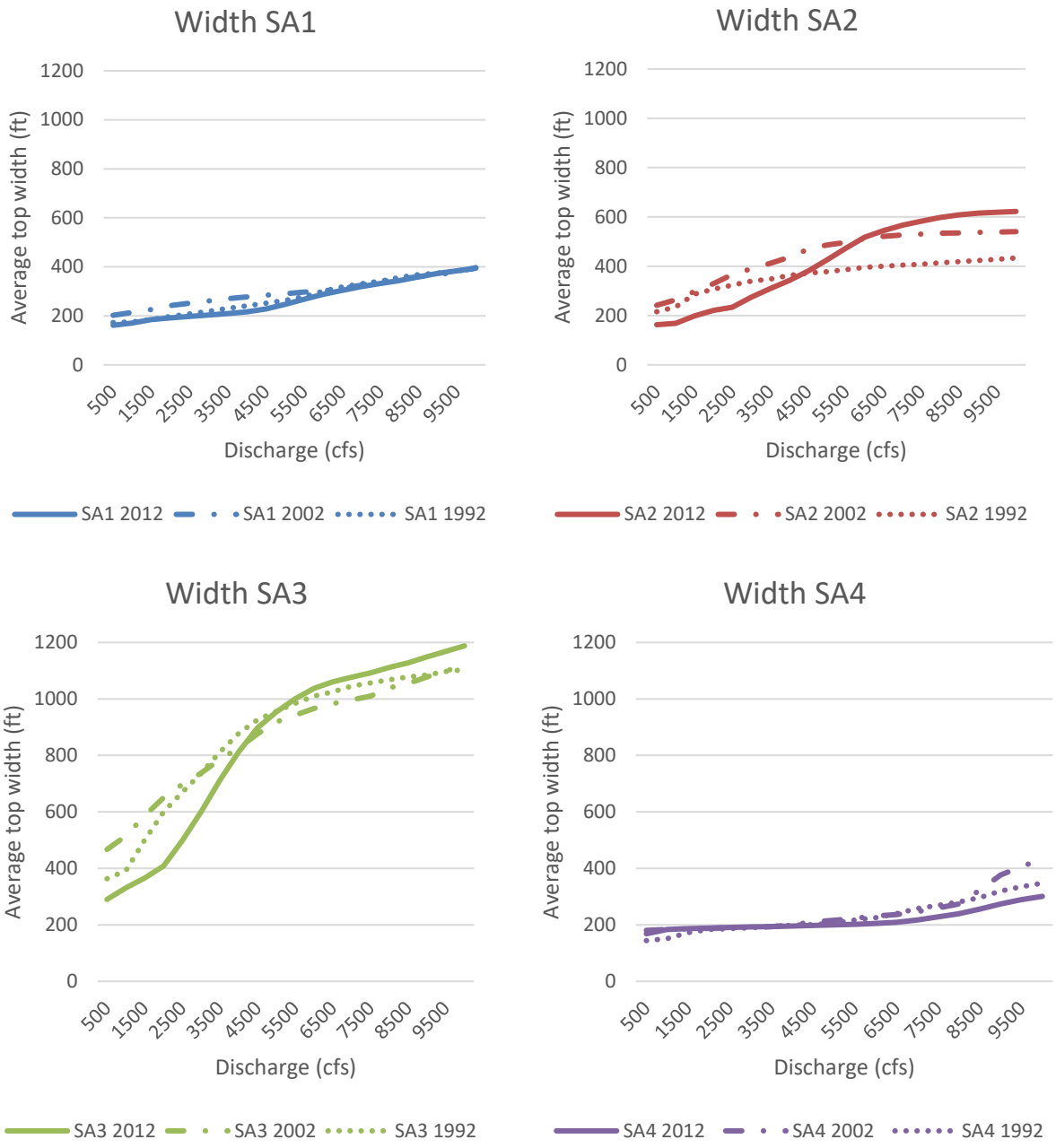

Figure 22 Subreach averaged width trends

Finally, narrow, average and wide cross-sections (25th, 50th and 75th percentiles, respectively) were selected from the entire reach. These representative cross-sections can illustrate in more detail the trends occuring at each reach. The average cross-section was represented by agg/deg line 1223, the narrow by 1248 and the wide cross-section by agg/deg line 1285. The wide cross-section followed a pattern of rapid increase in width before 3,000 cfs, at which point it remained mostly constant. In 2012,

the most dramatic increase (indicating bankfull discharge has been reached) happened from 2,500 to 3,000 cfs. The average cross-section remained consistent until 4,000 cfs was reached, when it began to increase. Bankfull discharge in 2012 appears to be around 6,000 cfs. Finally, the narrow cross-section maintained a linear trend throughout the entire range of discharges, making determining a bankfull discharge difficult. The largest increase in width in 2012 was seen at 6,000 cfs as well.

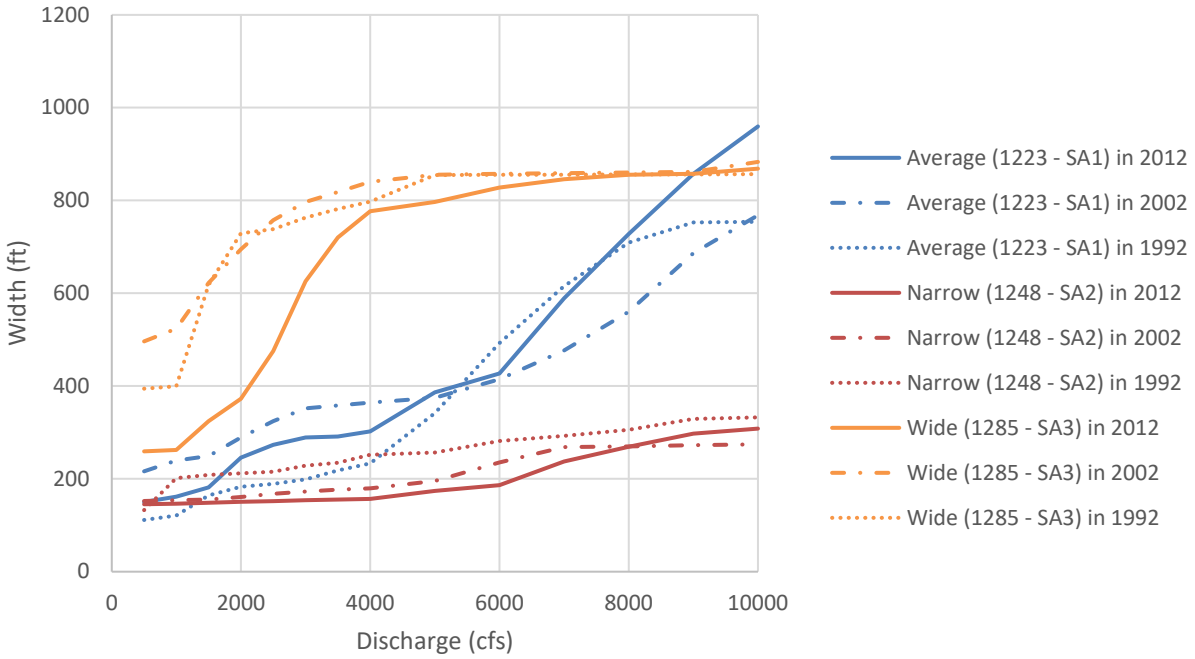

Figure 23 Width vs discharge at average, narrow and wide cross-sections

3.2 Sinuosity

Sinuosity was calculated at each subreach using digitized channel centerlines provided by the USBR's GIS and Remote Sensing Group. Aerial photographs and accompanying digital shapefiles were provided for years 1918, 1935, 1949, 1962, 1972, 1985, 1992, 2001, 2002, 2006, 2008, 2012 and 2016. The centerlines were split up by subreach and divided by the length of the subreach to calculate the sinuosity. Figure 24 shows the sinuosity of each subreach from year to year.

Overall, sinuosity values are low. They are highest in SA1, staying above 1.20 and lowest in SA4, staying around 1.01 to 1.02. In SA1, SA2 and SA4, the year with the highest sinuosity is 1935. In SA1 and SA2, sinuosity decreases from that point until 1985, and then begins to slowly increase again. SA3 also shows a slight increase from 1992 onwards but does not have the same decrease until then. SA4 shows the biggest change following the deliberate channelization of the MRG that occurred in the 1950s, which included channel straightening. Up until 1949, sinuosity values were over 1.20 in this subreach, however, these were reduced to 1.02 in 1962, where it approximately remained. This is the straightest subreach within the San Acacia reach and is experiencing very little change in channel centerline.

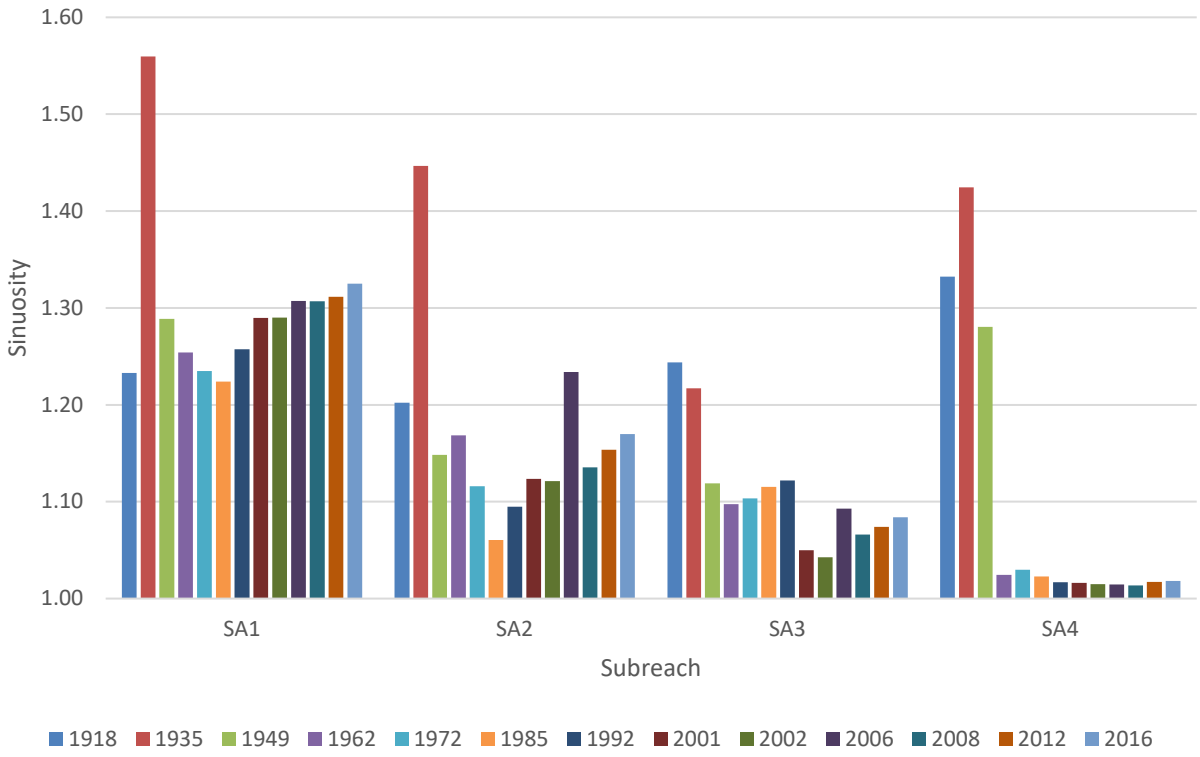

Figure 24 Sinuosity by subreach

3.3 Width

The active channel was defined as the non-vegetated channel. The width of the active channel was found by clipping the agg/deg line with the active channel polygon provided by the USBR's GIS and Remote Sensing Group. Then the width of each subreach was calculated by averaging the width of all agg/deg lines within the subreach. Data was available for the same years as was used to find the sinuosity in Section 3.2 Sinuosity.

These results are shown in Figure 25. There is a dramatic decrease in active channel width after 1949, due to channelization efforts by the USBR in the 1950s and 1960s. In subreaches SA1 and SA4, after this decrease, the width of the channel stays nearly constant. Subreaches SA2 and SA3 have a more gradual decline, but also appears to flatten out starting in the 2000s. In all subreaches but SA4, the narrowest year was 2016, where subreaches SA1, SA2, SA3 and SA4 had widths of 156, 171, 260 and 175 feet, respectively.

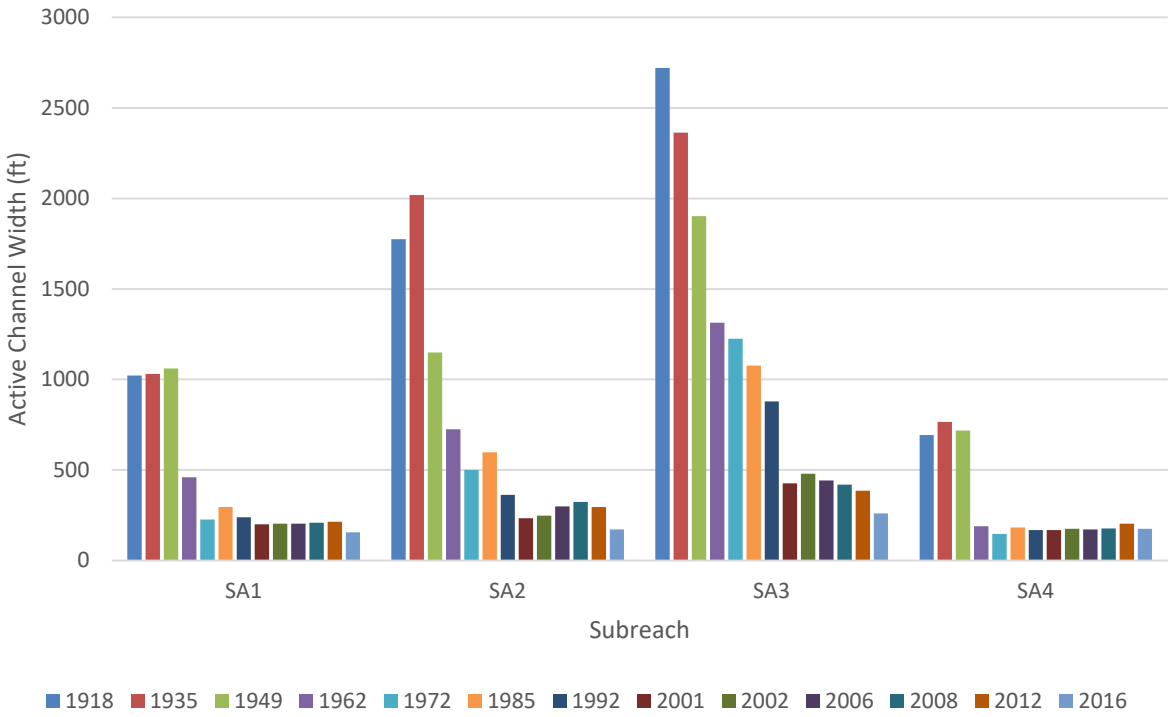

Figure 25 Averaged active channel width by subreach

3.4 Low Flow Channels

At low flows, the number of channels at each agg/deg line is measured from digitized planforms from the aerial photographs provided by the USBR. This is done using the same method as in Section 3.3 Width, where only the active channel polygon was used. In some locations, multiple channels were present at one agg/deg line. Figure 26 shows the results of this analysis. Subreach SA4 never has more than one channel, while the others shift inconsistently through time. For all subreaches, years 1985 and 1992 show only one channel. Overall, these results highlight how easily a sand-bedded channel shifts over time.

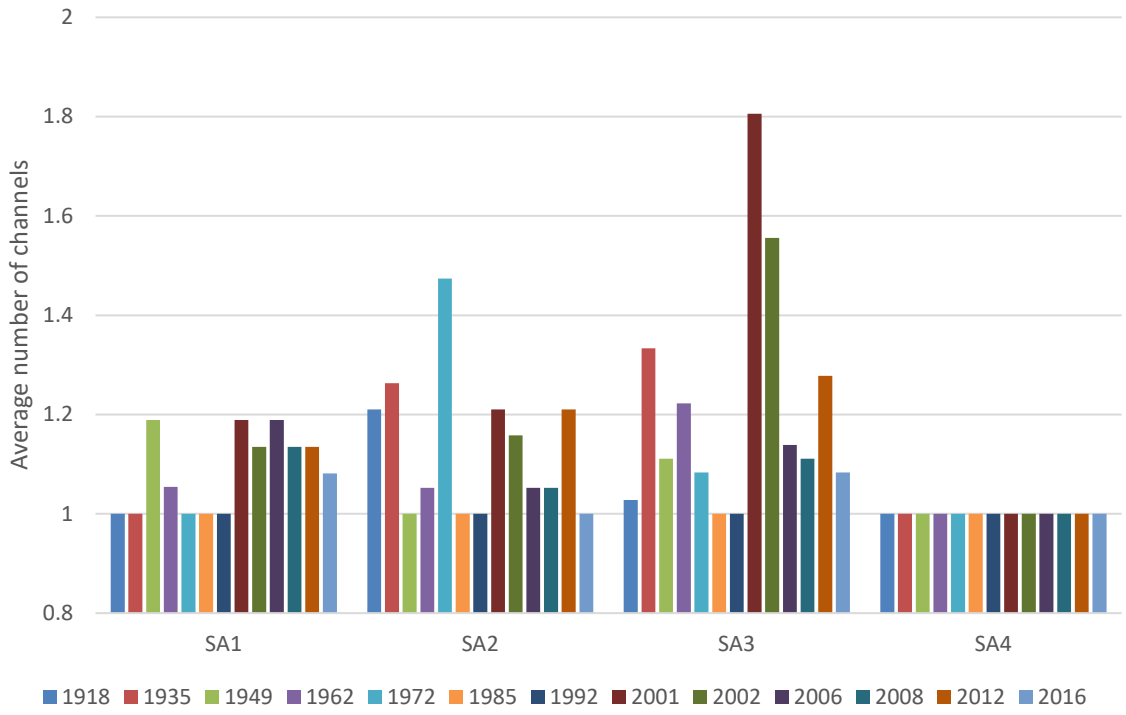

Figure 26 Average number of channels at each subreach through time

3.5 Bed Elevation

The mean bed elevation is used to compare the change in long profile in this report. Cross-section geometry at each agg/deg line was available from models developed by the Bureau of Reclamation Albuquerque Area Office. Models are available for 1962, 1972, 1992, 2002 and 2012. The 2012 model was developed from LiDAR data, but models prior to 2012 used photogrammetry techniques. All models use the NAV88 vertical datum. Figure 27 shows the long profiles of each of these years. Figure 28 shows the aggradation and degradation of each subreach.

Subreach SA1 had the most degradation over the period from 1962 to 2012, almost 10.5 ft. SA2, SA3 and SA4 had degradation of 8.4 ft, 5.0 ft and 5.2 ft, respectively. The most severe degradation is at the upstream end of this subreach. It is possible that scour is occurring downstream of the San Acacia Diversion Dam if sediment is being contained behind the diversion structure. The only time aggradation occurred was in subreach SA4 from 1992 to 2002; all other measurements were degradation. The most degradation occurred between 1972 and 1992, although this is a longer period than the others. Normalized to a ten-year period, the most degradation occurs between 2002 and 2012.

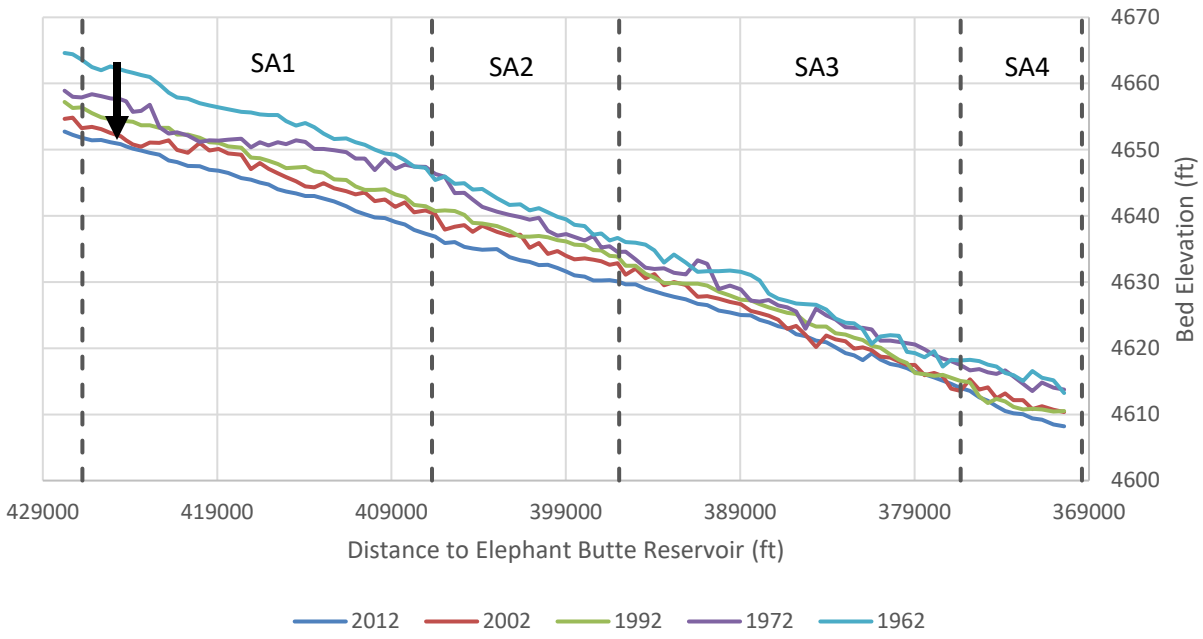

Figure 27 Long profile of bed elevations

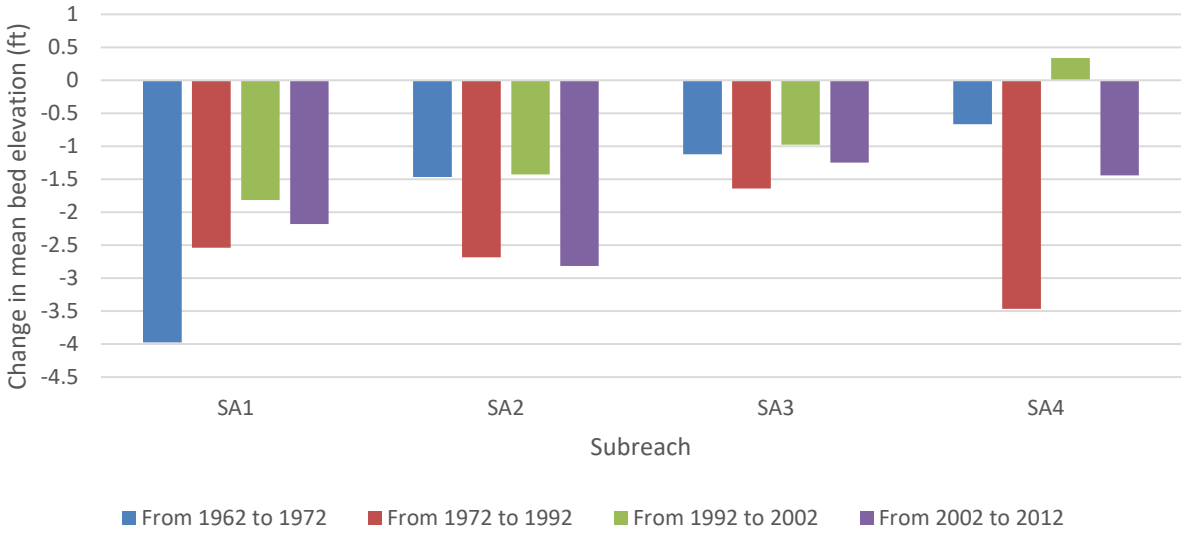

Figure 28 Degradation and aggradation by subreach

3.6 Bed Material

Bed material samples are collected at rangelines that differ from the agg/deg lines. These rangelines do not date back as far as the agg/deg lines and are spaced further apart. There are samples available for analysis in 1995, 1996, 1997, 1998, 1999, 2005 and 2014. Although samples were also collected in 2000, they were an order of magnitude higher than the mean of any other year and were sampled for the purpose of determining the size of the sediment in the gravel layer under the sand layer. Therefore, this

data was not included in Figure 29. Figure 29 shows the d_{50} of each sample in mm vs the distance downstream of the San Acacia Diversion Dam (ie the start of the San Acacia reach).

Some evidence of coarsening due to the San Acacia Diversion Dam in the bed material is seen in the first 22,000 ft downstream of the dam. As the dam holds back some sediment, scour occurs downstream of the dam, which in turn causes coarsening. This, plus the fact that the highest amount of degradation occurs in subreach SA1 (see Section 3.5 Bed Elevation), fits with the conceptual understanding of coarsening downstream of a dam. As scour occurs, the water transports the finer sediments in the bed until an armored layer with relatively larger gravel remains. After 22,000 ft downstream of the diversion, no samples were collected with a d_{50} larger than 1 mm.

Massong et al. (2010) also found that bed material coarsened from sand to gravel patches in some locations. Coherent patches of gravel in the channel were documented in 2000, when an extensive bed material survey was conducted. The channel bed is now considered gravel dominated, but the larger sediments are often covered by thick sand dunes migrating through the reach (Massong et al. 2010).

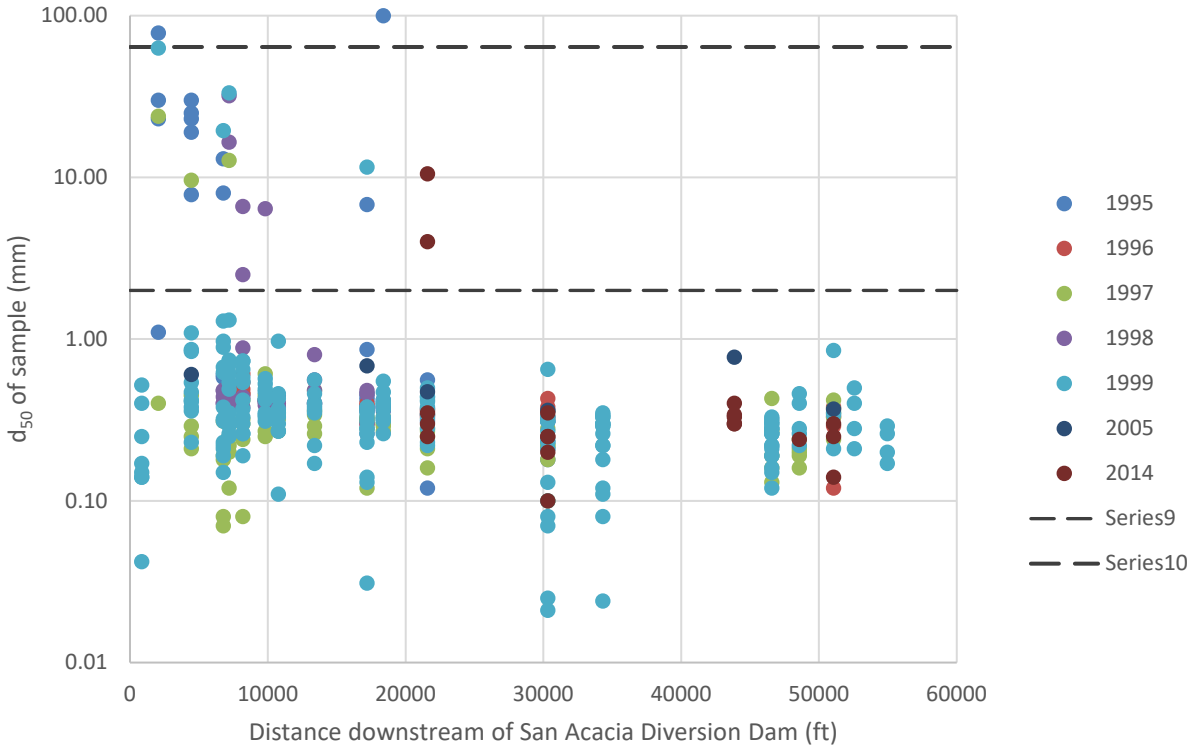

Figure 29 d50 measurements along the reach

Table 9 d50 in mm of the samples averaged by subreach and by sample year

Subreach	SA1	SA2	SA3	SA4
1995	14.25	0.29	--	--
1996	0.45	0.36	--	0.28
1997	1.26	0.22	0.22	0.34
1998	2.21	--	--	--
1999	1.48	0.29	0.25	0.34
2000	18.27	34.25	26.00	--
2005	0.64	0.42	0.77	0.37
2014	--	1.66	0.33	0.20
2016	--	--	0.24	0.30

3.7 Flow Depth, Velocity, Width, Wetted Perimeter and Slope

Flow depth, velocity, width, wetted perimeter, bed slope and energy slope are obtained using HEC-RAS 5.0.3 with a discharge of 3,000 cfs. A discharge of 3,000 cfs was selected based on past precedent (in LaForge et al 2019 and Yang et al 2019). Analysis was performed for years 1972, 1992, 2002, and 2012. Average values at each subreach are plotted in Figure 30.

There are dramatic decreases in width and wetted perimeter from 1972 to 2012. Width and wetted perimeter are closely linked, which indicates a wide and shallow channel. Depth decreases from 1972 to 2002, but then begins to increase again in 2012. In 1972, although much of the channel was shallow and wide, there were small sections (less than 50-100 feet across) that were deeper. In 2012, although similar depths were seen, these depths tend to be more uniform across an area of a couple hundred feet. Velocity, bed slope and energy slope show few trends.

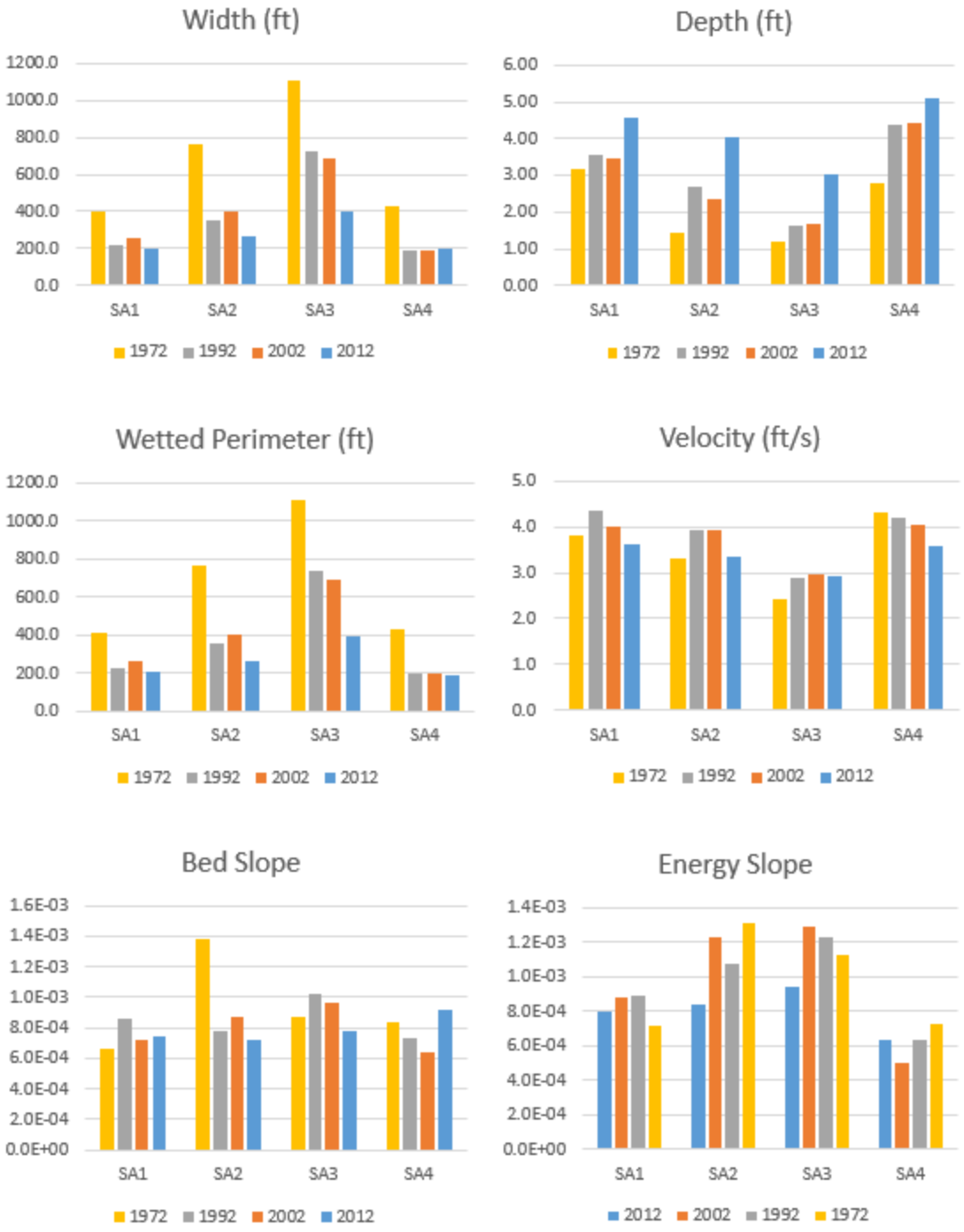

Figure 30 HEC-RAS analysis results

3.8 Equilibrium Width using the Julien and Wargadalam Equations

Equations to predict the downstream hydraulic geometry of rivers were derived by Julien and Wargadalam (1995). These equations were based on empirical analysis of over 700 single-threaded rivers and channels, and predicted the width and depth likely to result from a certain discharge, grain size and slope:

$$h = 0.2Q^{\frac{2}{6m+5}} d_s^{\frac{6m}{6m+5}} S^{\frac{-1}{6m+5}}$$

$$W = 1.33Q^{\frac{4m+2}{6m+5}} d_s^{\frac{-4m}{6m+5}} S^{\frac{-1-2m}{6m+5}}$$

Where $m = 1/\ln(12.2h/d_s)$, h is the flow depth, W is the channel width, Q is the flow discharge, d_s is the median grain size and S is the slope. A discharge of 3,000 cfs, the same as the previous HEC-RAS analysis, is used. The values for grain size and slope were obtained from Section 3.6 Bed Material and Section 3.5 Bed Elevation, respectively. The mean d_{50} of the 1990s was used for 1992, 2000s for 2002 and 2010s for 2012. The flow depth was iterated to calibrate m, then the width was calculated.

Historically, these equations would not have applied to the MRG as a braided, sand-bed channel. However, as the MRG became a single-threaded channel it became more appropriate to apply these equations as a method of estimating the eventual equilibrium width of the channel. Predicted widths were generally narrower than the observed widths. Over time, the percent difference between the predicted and observed widths decreased and in 2012, all widths were within 50% of the predicted widths. The JW equations seem to indicate that further narrowing is mostly likely to occur in subreaches SA2 and SA3.

Table 10 Julien and Wargadalam's equations results

Year	Subreach	Q (cfs)	ds (mm)	Slope	Predicted Width (ft)	Observed Width (ft)	Percent difference
	SA1	3000	3.93	0.000749	210.2	239.6	-12%
	SA2	3000	0.29	0.000686	222.3	363.4	-39%
	SA3	3000	0.23	0.000991	206.9	879.5	-76%
1992	SA4	3000	0.32	0.000779	216.4	168.4	29%
	SA1	3000	0.64	0.000729	217.5	203.0	7%
	SA2	3000	0.42	0.000779	215.7	248.2	-13%
	SA3	3000	0.77	0.000885	208.6	479.3	-56%
2002	SA4	3000	0.37	0.000779	216.1	175.7	23%
	SA1	3000	1.66*	0.000734	214.3	215.1	0%
	SA2	3000	1.66	0.000736	214.1	295.8	-28%
	SA3	3000	0.29	0.000766	217.4	385.0	-44%
2012	SA4	3000	0.25	0.000993	206.6	204.2	1%

* 2012 grain size for SA1 not available, approximated with value from SA2

3.9 Geomorphic Conceptual Model

Massong et al. (2010) developed a channel planform evolution model for the Rio Grande based on historic observations. The sequence of planform evolution is outlined in Figure 31. Stage 1 describes a large channel with a high sediment load and frequent floods such that a wide, clear channel is maintained. As water levels fall, Stage 2 occurs and dunes from Stage 1 begin to stabilize into bars. In Stage 3, this stabilization is maintained by encroaching vegetation, regardless of flow levels. Only after the third stage does sediment transport become important in determining future stages. A lack of transport capacity leads to avulsion, as the channel aggrades and eventually the main flow shifts on to the now lower floodplain, processing to the A (aggrading) stages. Excessive transport capacity leads to the M (migrating) stages. Bends occur where bed and bank material erode both laterally and vertically. Transition between the M stages and the A stages can occur, but a reset to a Stage 1 requires a large, prolonged flood (Massong et al., 2010).

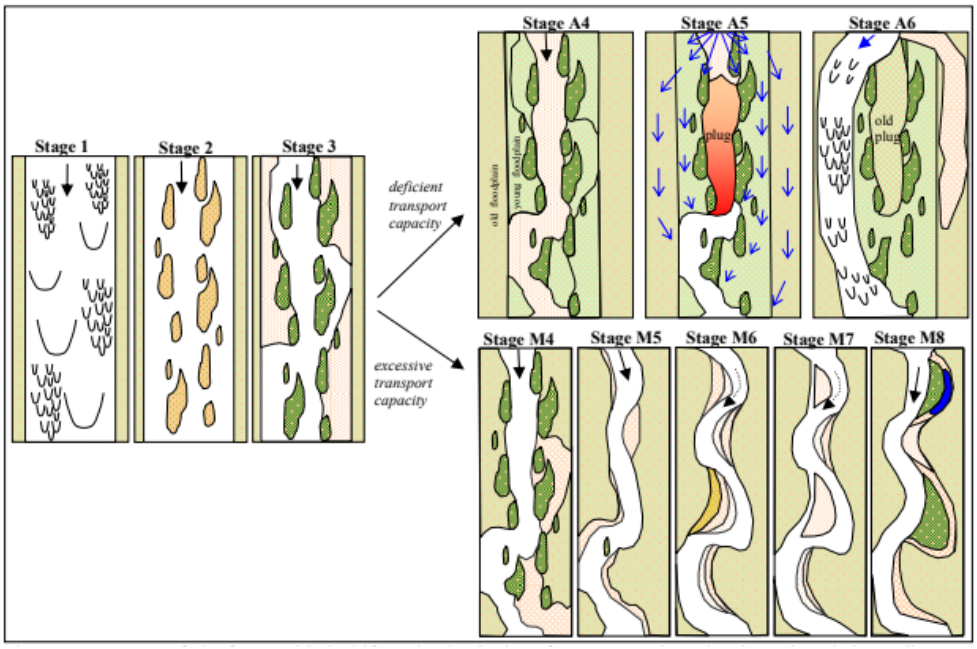

Figure 31 Planform evolution model from Massong et al. (2010). The river undergoes stages 1-3 first and then A4-A6 or M4-M8 depending on transport capacity.

Stages M4-M8 are the most relevant to the San Acacia reach, because it has excess transport capacity, as shown by the degradation seen in Section 3.5 Bed Elevation. Massong et al. classified the transition from Stage 1 to Stage 2 on most of the Middle Rio Grande as occurring during the drought of 1999-2004. As seen in Figure 8, during that time period, flows rarely topped 1,000 cfs (less than 6% of the time). Once flows returned to normal levels in 2005, many of the islands that formed in the previous five years became vegetated (Massong et al., 2010). Although this generalization holds true for much of the Rio Grande, in some areas, different patterns were seen. This evolution is demonstrated in Figure 32.

Each of the subreaches is evaluated individually in the following pages. SA1 and SA4 appear to be more entrenched compared to SA2 and SA3. SA2 shows full evolution through the M-stages. SA3 can still be classified in the early stages of the Massong model.

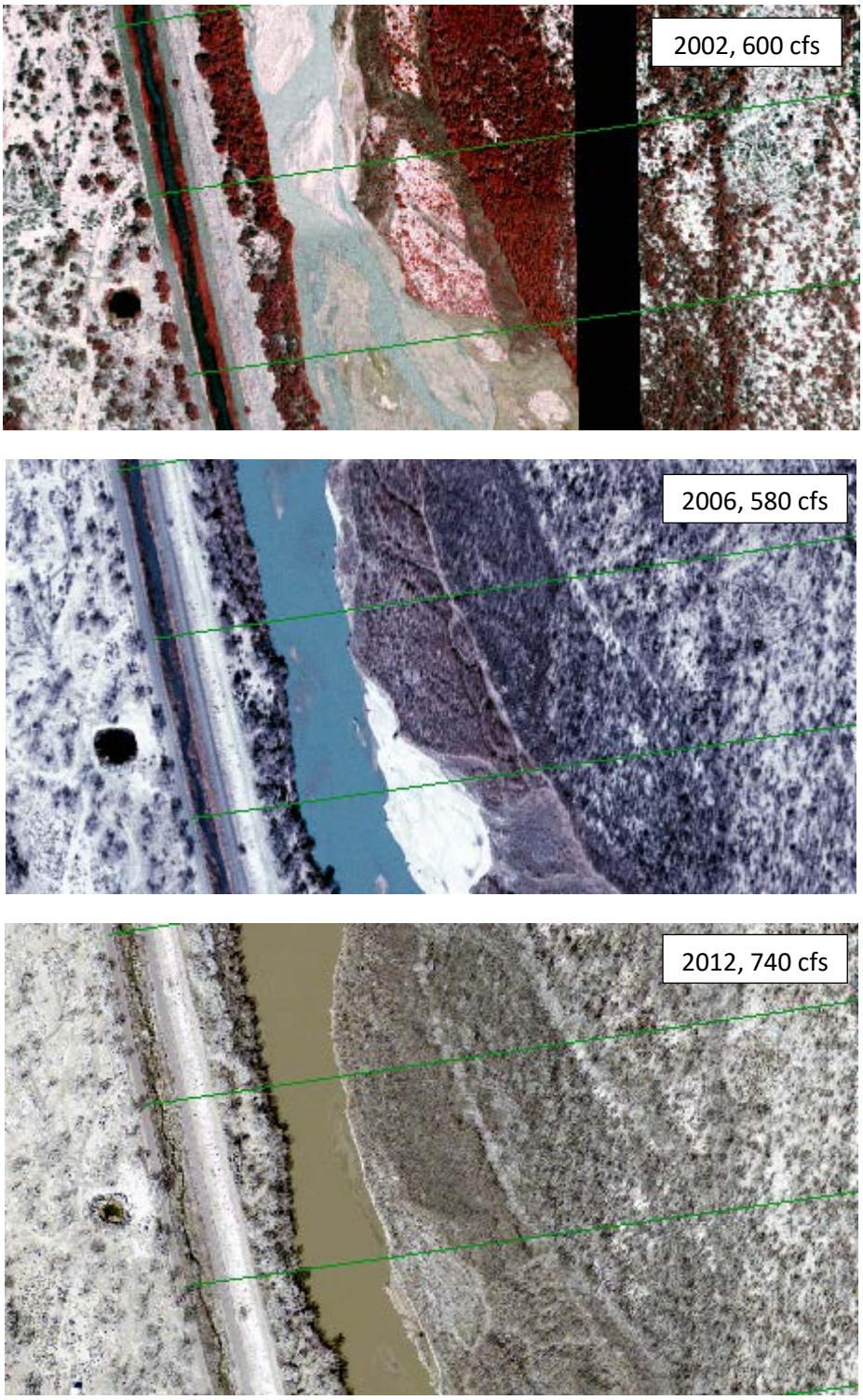

Figure 32 Geomorphic conceptual model evolution (Top: 2002; Middle: 2006; Bottom: 2012); flow direction from top to bottom

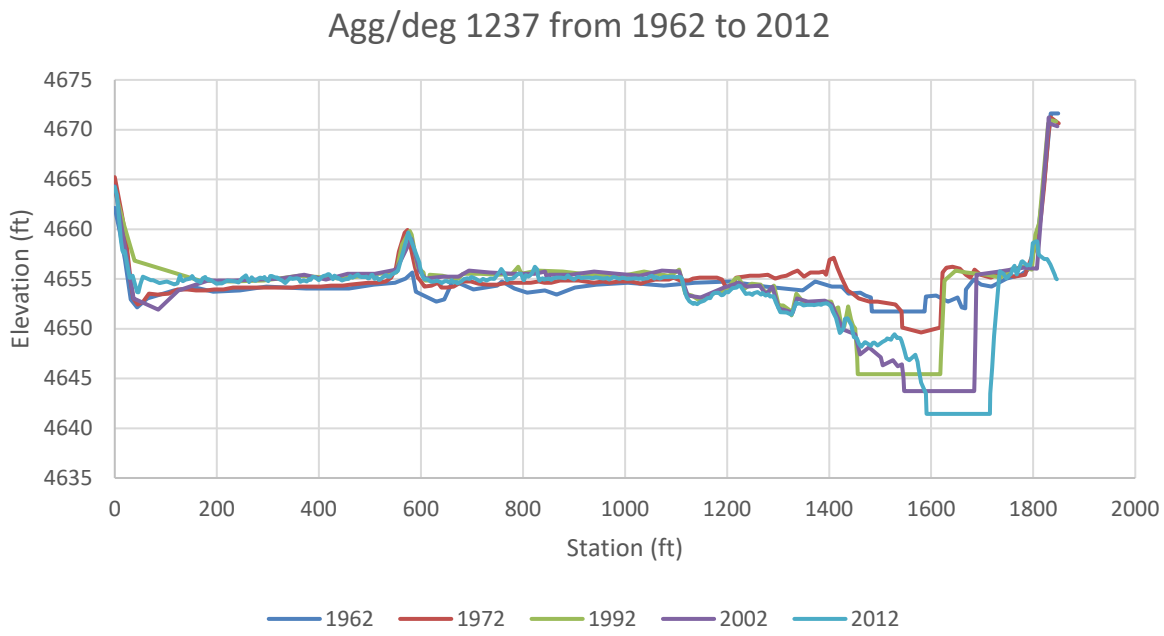

Figure 33 Evolution of cross-section 1237 from 1962 to 2012

Agg/deg line 1237 is in subreach SA1. It shows significant incision over the time period from 1962 to 2012. Slight migration towards the levee is shown as well, although this migration is likely to slow down in the future due to the placement of Kellner jetty jacks. Figure 34 on the next page shows each of these individually assigned a classification through Massong's model.

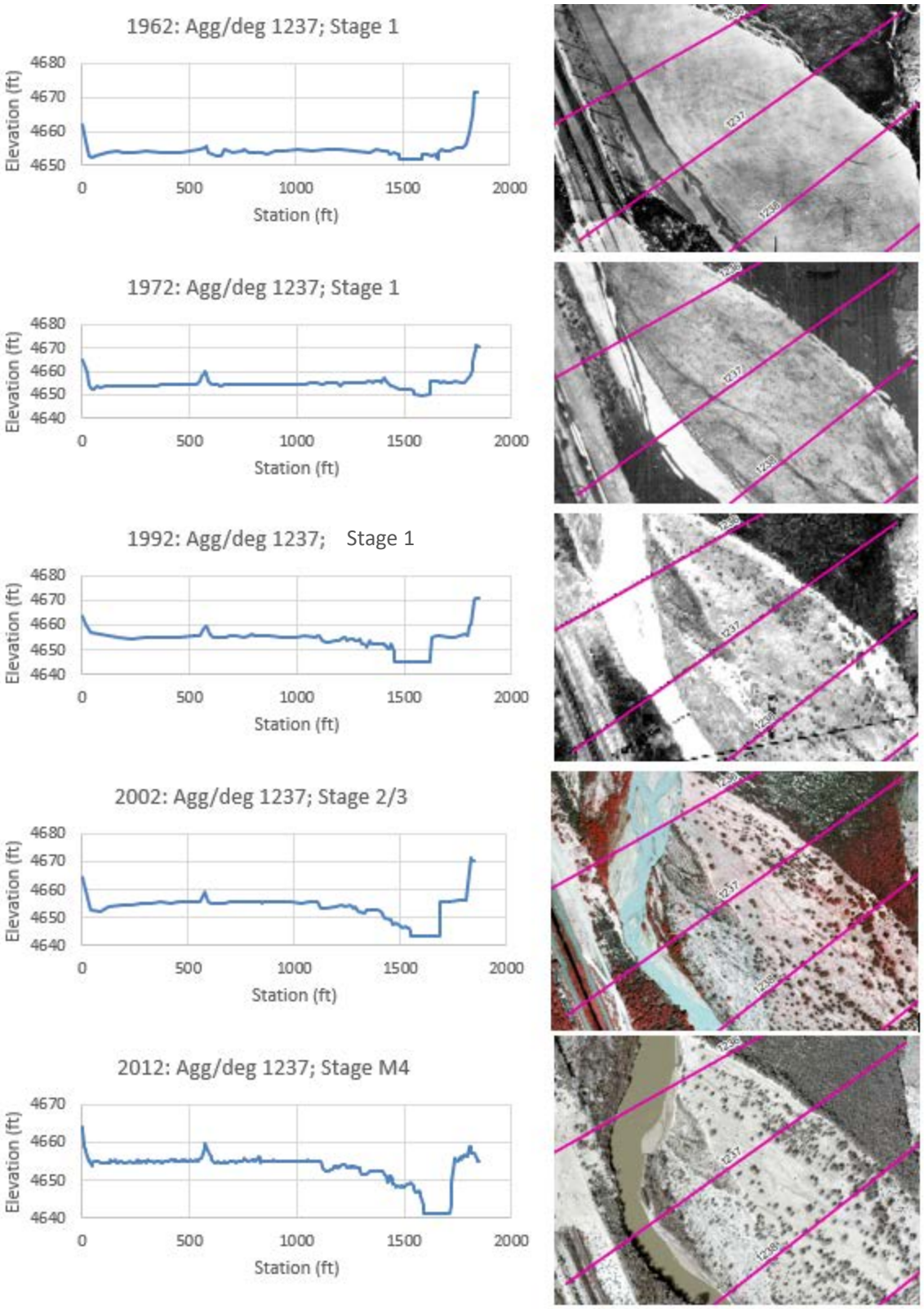

Figure 34 Evolution of cross-section 1237 from 1962 to 2012

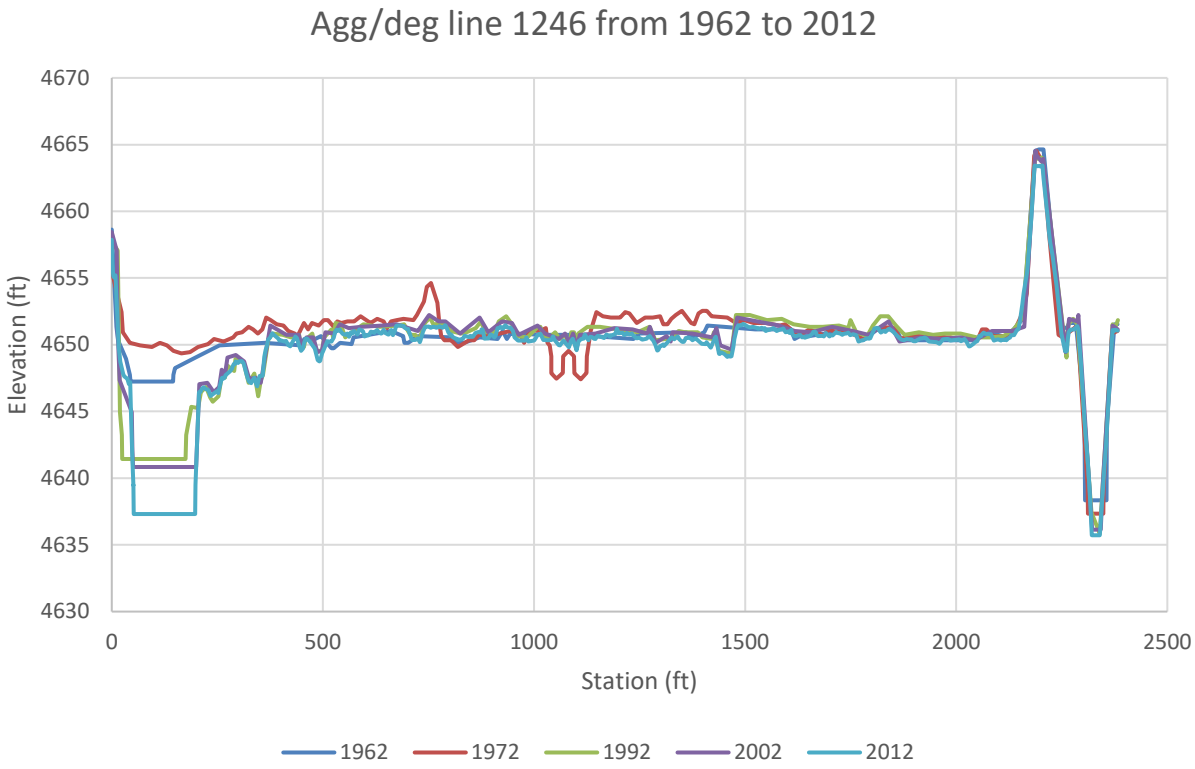

Figure 35 Evolution of cross-section 1246 from 1962 to 2012

Subreach SA2 shows the full evolution through the M-stages, as seen in Figure 37 below. In 1992, this section of the river appeared to be in Stage 2, with un-vegetated bars and islands. Substantial change was then seen with a dramatic increase in the degree of sinuosity, as the bends laterally eroded. In 2005, M6 is most closely represented. Stages 3, M4 and M5 occurred in the period of time between these two images. Shortly after, in 2006, a cutoff formed, with flow split between the more direct path and the larger bend. By 2009, this bend was inactive, resembling stage M8. Sand deposits likely filled the previous channel, and vegetation continued to colonize the old bars and islands formed by this cutoff. It is likely that the channel reverted to M4, but can now be classified as M5, with smoother banks. The median width cross-section in this channel is shown in Figure 37.

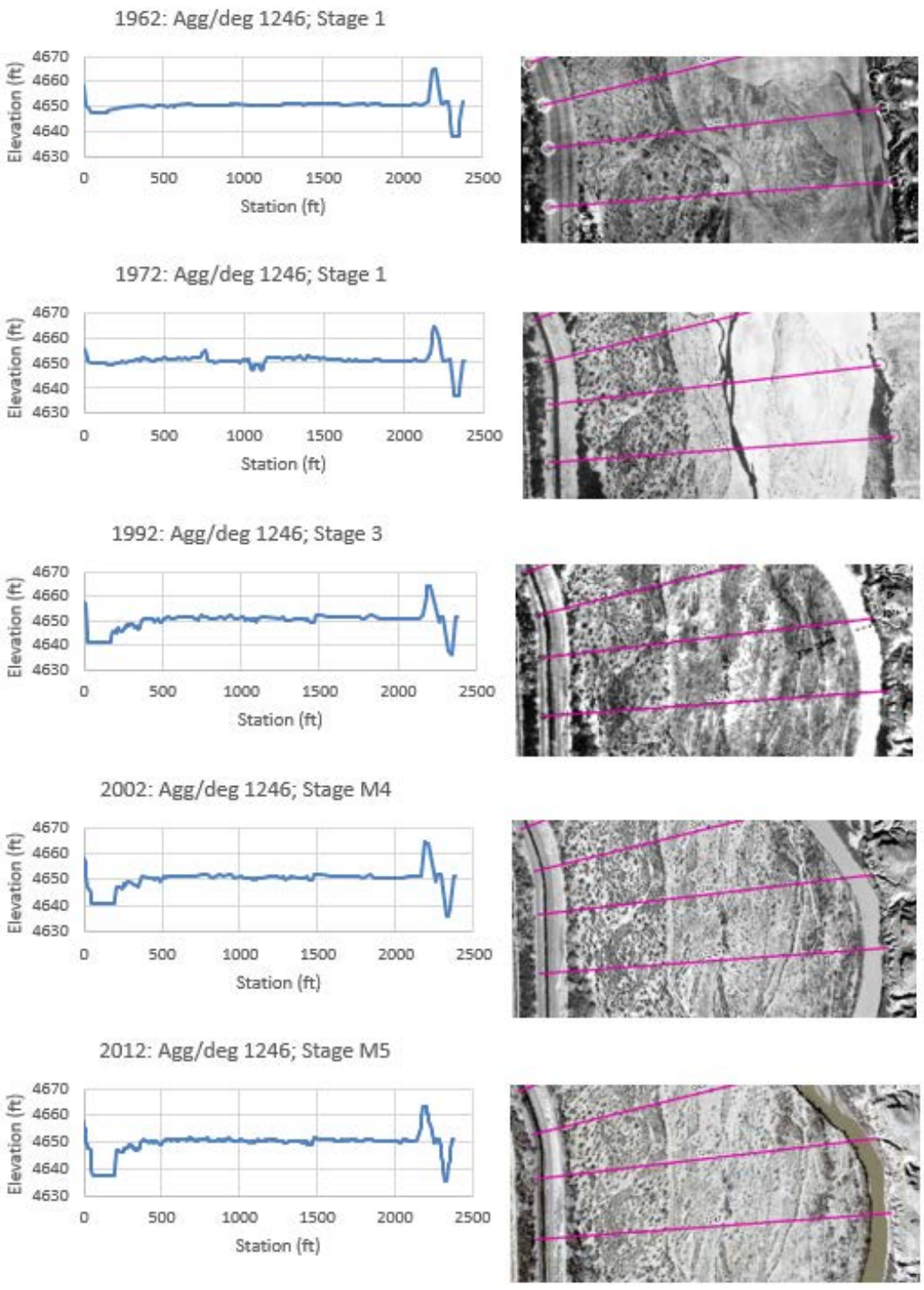

Figure 36 Evolution of cross-section 1246 from 1962 to 2012

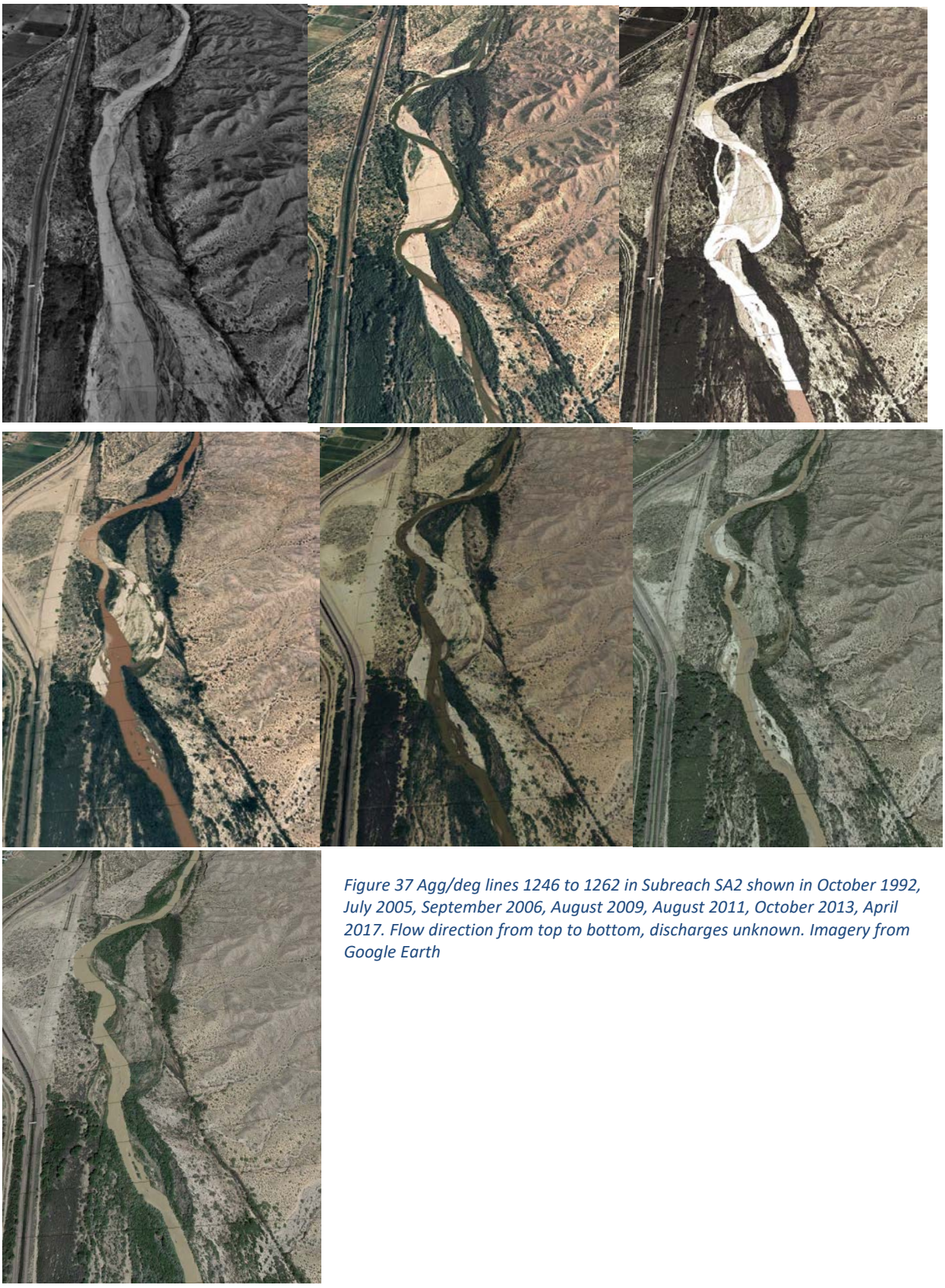

Figure 37 Agg/deg lines 1246 to 1262 in Subreach SA2 shown in October 1992, July 2005, September 2006, August 2009, August 2011, October 2013, April 2017. Flow direction from top to bottom, discharges unknown. Imagery from Google Earth

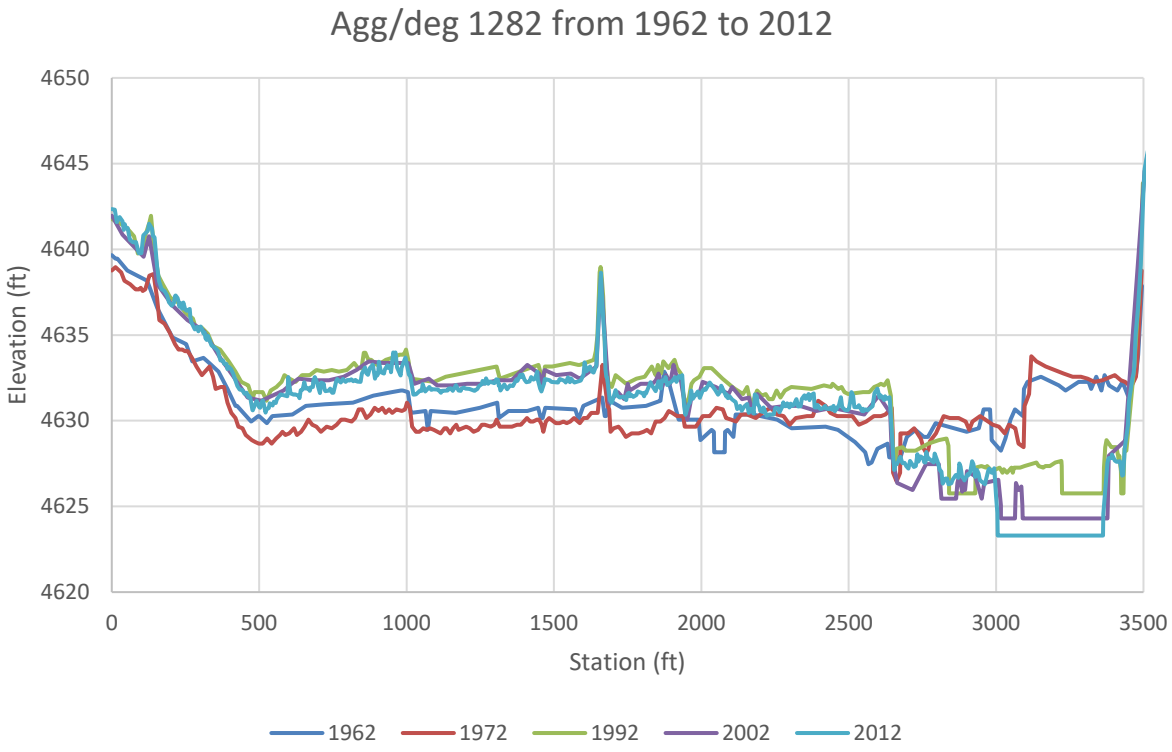

Figure 38 Evolution of cross-section 1282 from 1962 to 2012

Although Subreach SA3 has changed dramatically since 1962, in comparison to the other subreaches, it is still significantly wider, as seen in Figure 25. Therefore, through 2012, it can still be classified in the early stages of the Massong channel evolution model. However, vegetation encroachment happens rapidly from 2013 to 2017, indicating that it may be proceeding to the other M-stages relatively soon, as seen in Figure XXX. Although in Figure 40, it is classified as Stage 3 in 2012, its classification today is somewhere between Stage 3 and Stage M4.

Figure 39 Subreach SA3 from October 2013 to April 2017 showing vegetation encroachment and narrowing in the main channel. Flow direction is from top to bottom, discharges unknown. Imagery from Google Earth

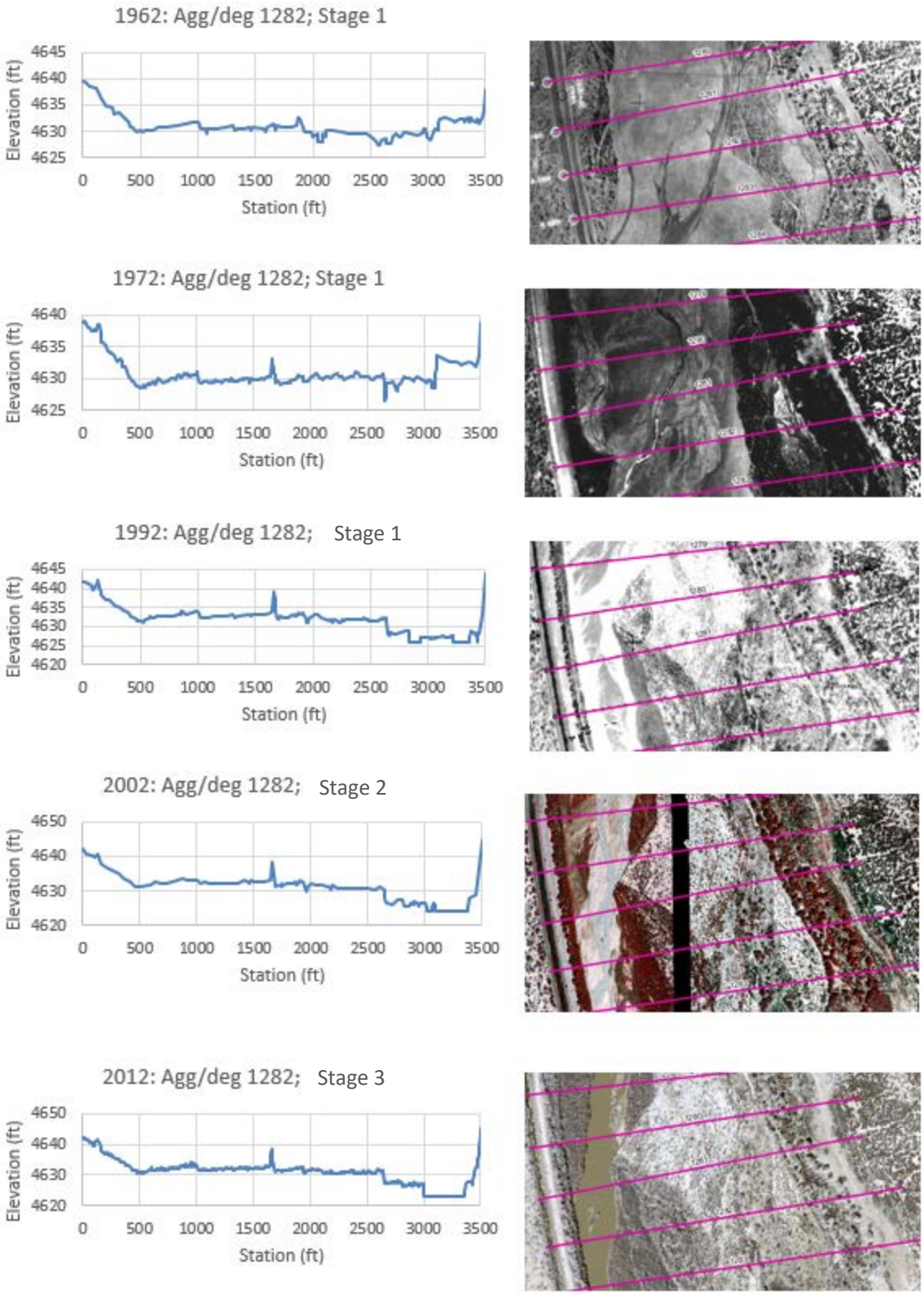

Figure 40 Evolution of cross-section 1282 from 1962 to 2012

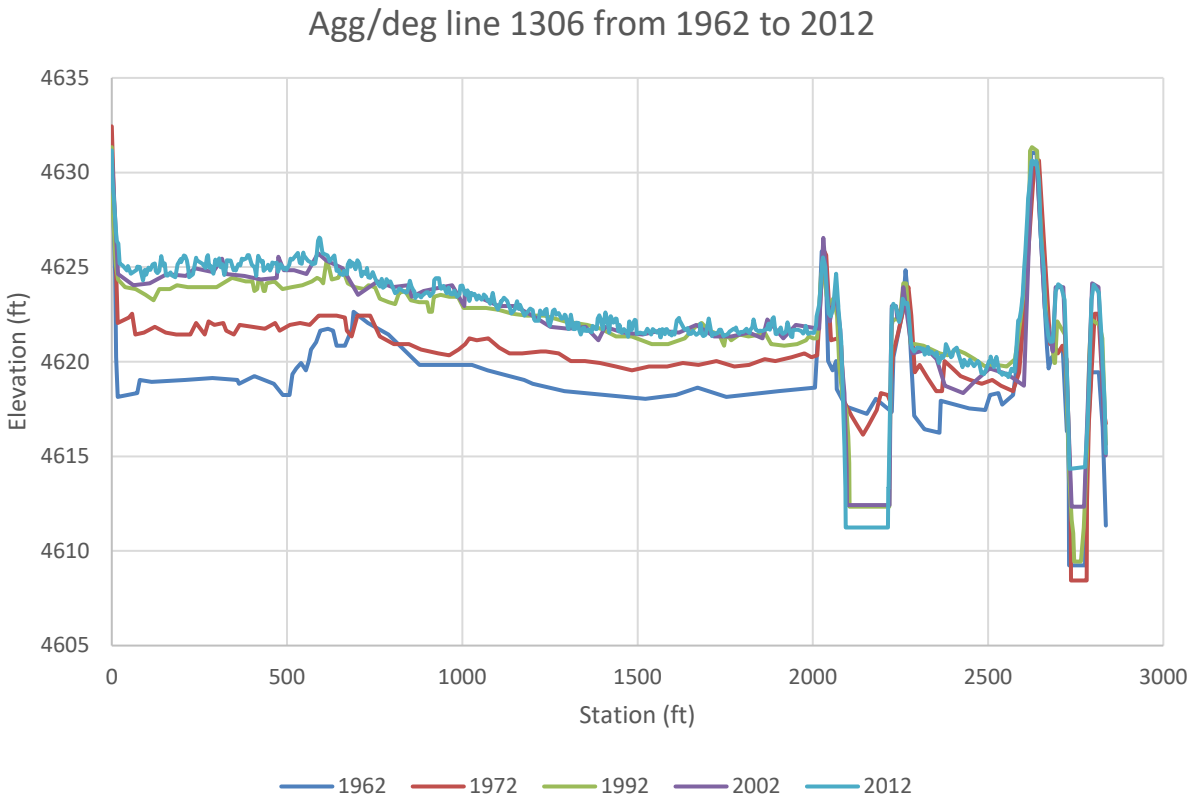

Figure 41 Evolution of cross-section 1306 from 1962 to 2012

SA4 shows very little movement besides incision over time, and has a nearly constant average width from 1962 to the present. Although the characteristics of vegetation and the depth of the channel in that subreach have changed since 1962, the lack of meandering shows that stage M4 can have different lag times in different areas of the river. This may be so severe in this reach because the main channel of SA4 was straightened and altered away from the historic river channel. In Figure 42, the channel on the right side of each of the figures was the historic channel. After the 1950s, flow rarely passed through this channel, and instead was concentrated in the channel on the left side.

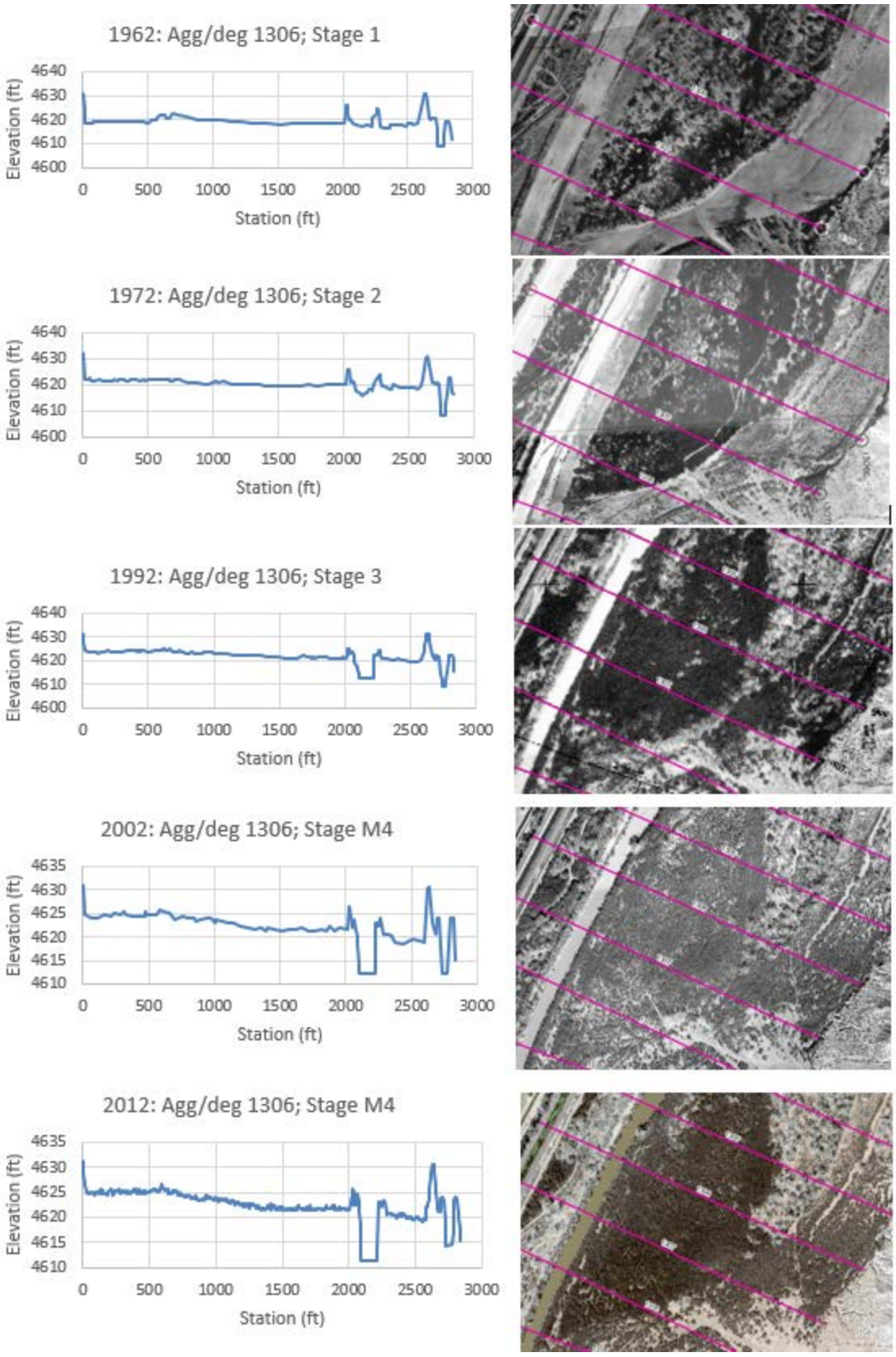

Figure 42 Evolution of cross-section 1306 from 1962 and 2012

4. HEC-RAS Modeling for Silvery Minnow Habitat

The Rio Grande Silvery Minnow is an endangered fish species that is native to the Middle Rio Grande. It currently occupies only about seven percent of its historic range (U.S. Fish and Wildlife Service, 2010). It was listed by the US Fish and Wildlife Service in 1994.

One of the most important aspects of silvery minnow habitat is the connection of the main channel to the floodplain. Spawning is stimulated by peak flows in late April to early May. These flows should create shallow water conditions on the floodplains, which are ideal nursery habitat for the silvery minnow (Mortensen et al., 2019). Silvery minnows prefer specific velocities and depths for different stages of their life histories. Table 11 outlines these velocity and depth guidelines.

Table 11 RGSM habitat velocity and depth requirements (from Mortensen et al., 2019)

	Velocity (cm/s)	Depth (cm)
Adult Habitat	<40	>5 and <60
Juvenile Habitat	<30	>1 and <50
Larvae Habitat	<5	<15

4.1 Modeling Background and Methodology

Peak spring flows have varied drastically from 1992 to the present, with some years maintaining flows over 5,000 cfs for many days in a row, and some years where flows did not even reach 2,000 cfs. Therefore, a wide variety of flows were modeled to represent this spread of peak runoff values, using an increment of 500 cfs up to 10,000 cfs.

Existing cross-sections developed by the USBR were used in a steady-state HEC-RAS model. Levee points were set at each cross-section to prevent flow in inaccessible side channels and in the low flow channel on the other side of the levee for the highest flow profile used (10,000 cfs). The 1-D results produced by the HEC-RAS model were processed through RAS-Mapper to provide quasi 2-D results. This was possible in 2012 because LiDAR was collected on the floodplain, which was used to develop a terrain for RAS-Mapper. RAS-Mapper generated rasters of velocity and depth, which were merged in ArcGIS and exported by subreach.

Although modeling was done at low flows (<1,000 cfs), these results are considered inaccurate. In developing the HEC-RAS geometry cross-sections and the RAS-Mapper terrain, LiDAR was not available under the water surface. Therefore, an underwater prism was developed by the USBR based on water surface elevation measurements. This underwater prism was approximated as a trapezoidal cross-section and lacks the complexity of the actual channel. Those interested in understanding RGSM habitat at low flows should look at the 2008 report “Streamflow and Endangered Species Habitat in the Lower Isleta Reach of the Middle Rio Grande” by Bovee et al, which analyzed fish habitat at flows below 1,000 cfs.

4.2 Habitat Results in 2012

The results of this analysis are shown in Figure 47 through Figure 50. Larval habitat peaks at 2,500 cfs to 3,000 cfs, juvenile habitat peaks at 4,500 cfs and adult habitat peaks at 5,500 cfs. The graphs of habitat by subreach show considerable differences across subreaches. Larval habitat is hardly present in subreaches SA1 and SA4. The 2,500 cfs peak is controlled primarily by subreach SA3, while a secondary peak occurs at 5,500 cfs from subreach SA2. Similarly, for juveniles, habitat in SA3 peaks first at 4,000 cfs with a lower peak at 6,000 cfs for SA2. SA1 remains low throughout while SA4 begins to increase once flows are higher than 6,000 cfs. For adult habitat, SA3 peaks at 4,500 cfs and SA3 peaks at 6,000 cfs. SA1 remains constant while SA4 begins to increase above 6,000 cfs.

Mapping for adult habitat can be seen in Figure 43 through Figure 46. Discharges 1,500, 3,000, 4,000, and 6,000 cfs were selected for mapping. An aerial view provides further insight into the habitat conditions and where habitat conditions are being met. Additional mapping for larvae and juvenile habitat is in Appendix 7.2 Additional Figures.

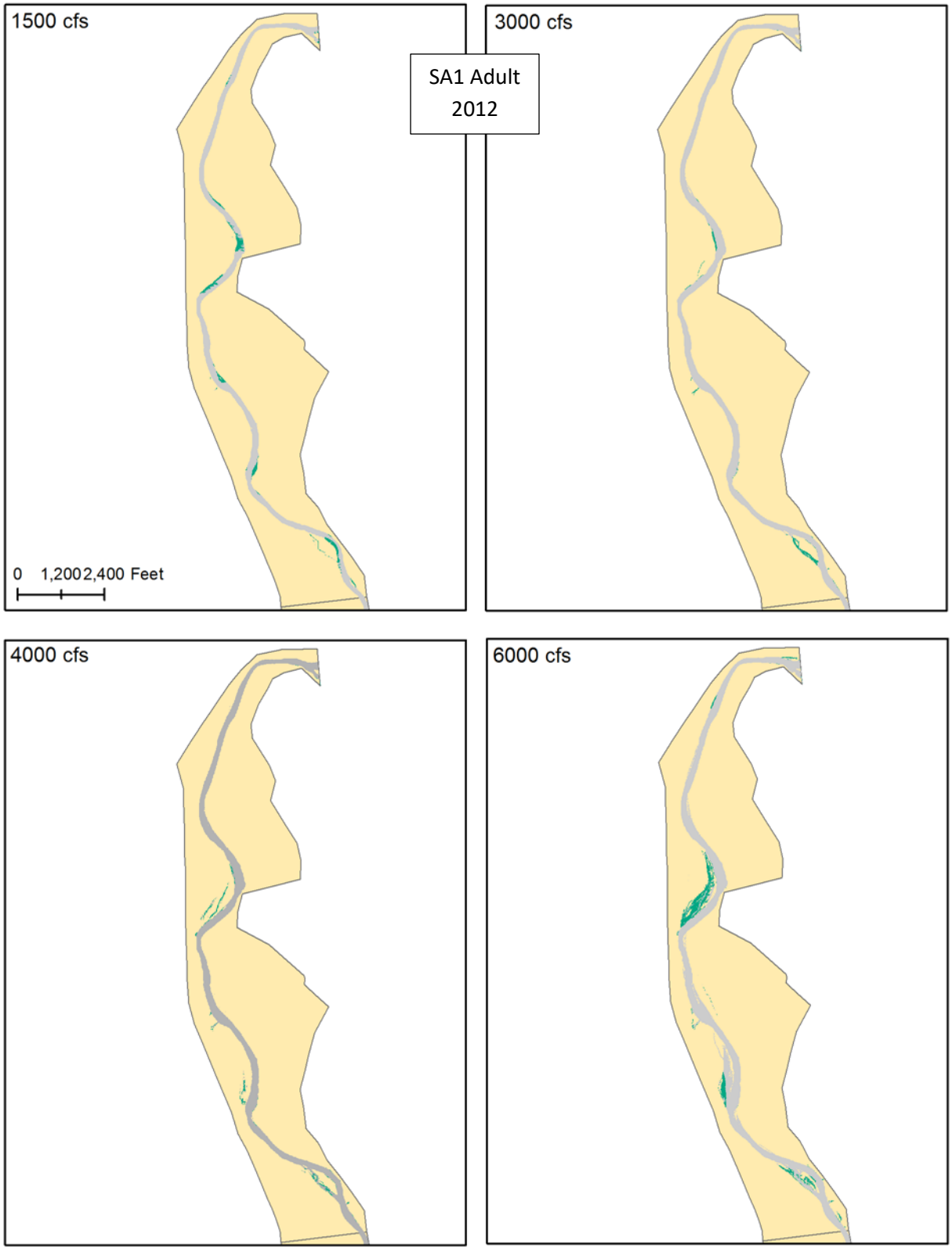

Figure 43 Adult habitat at subreach SA1 in 2012; flow direction is from top to bottom

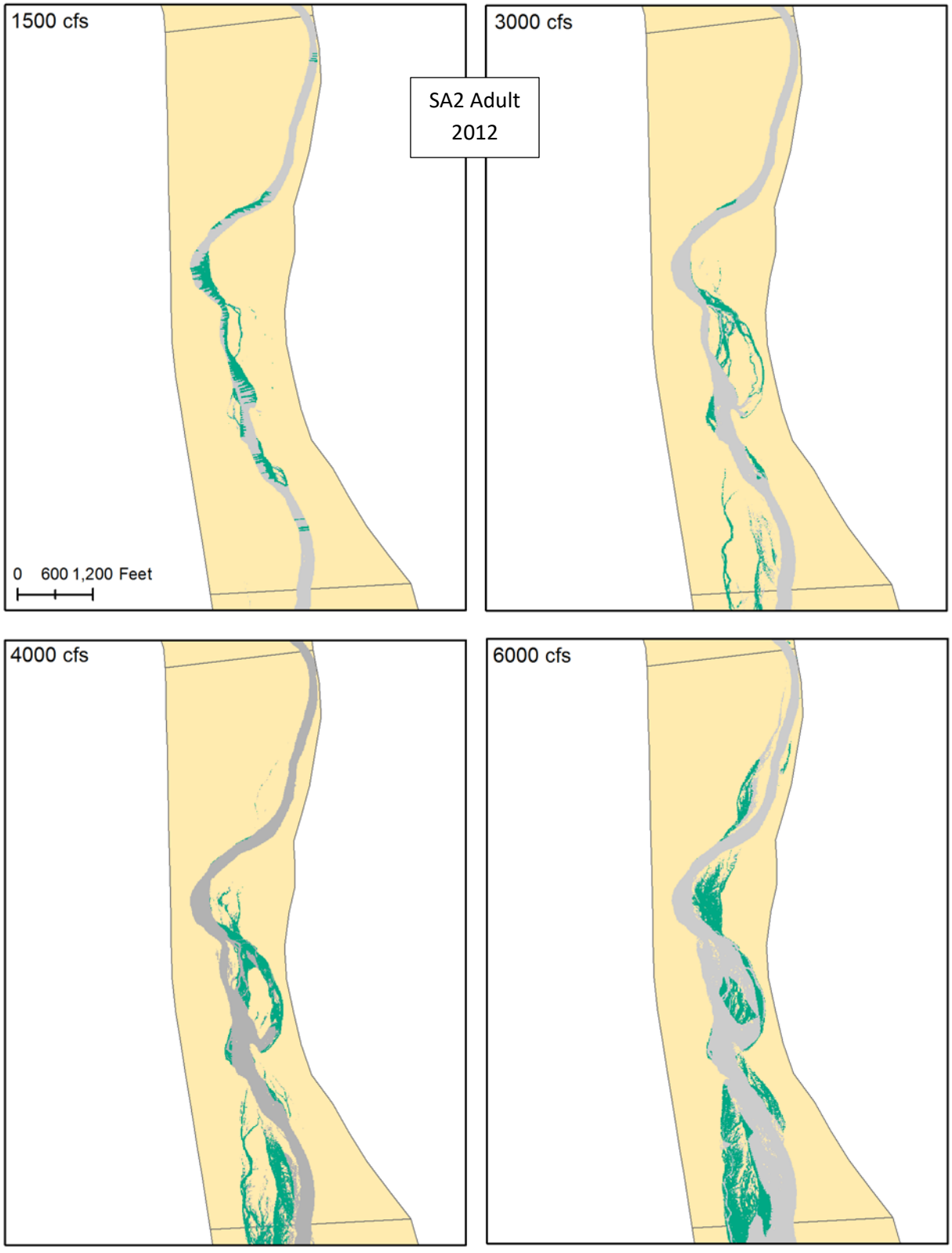

Figure 44 Adult habitat at subreach SA2 in 2012; flow direction is from top to bottom

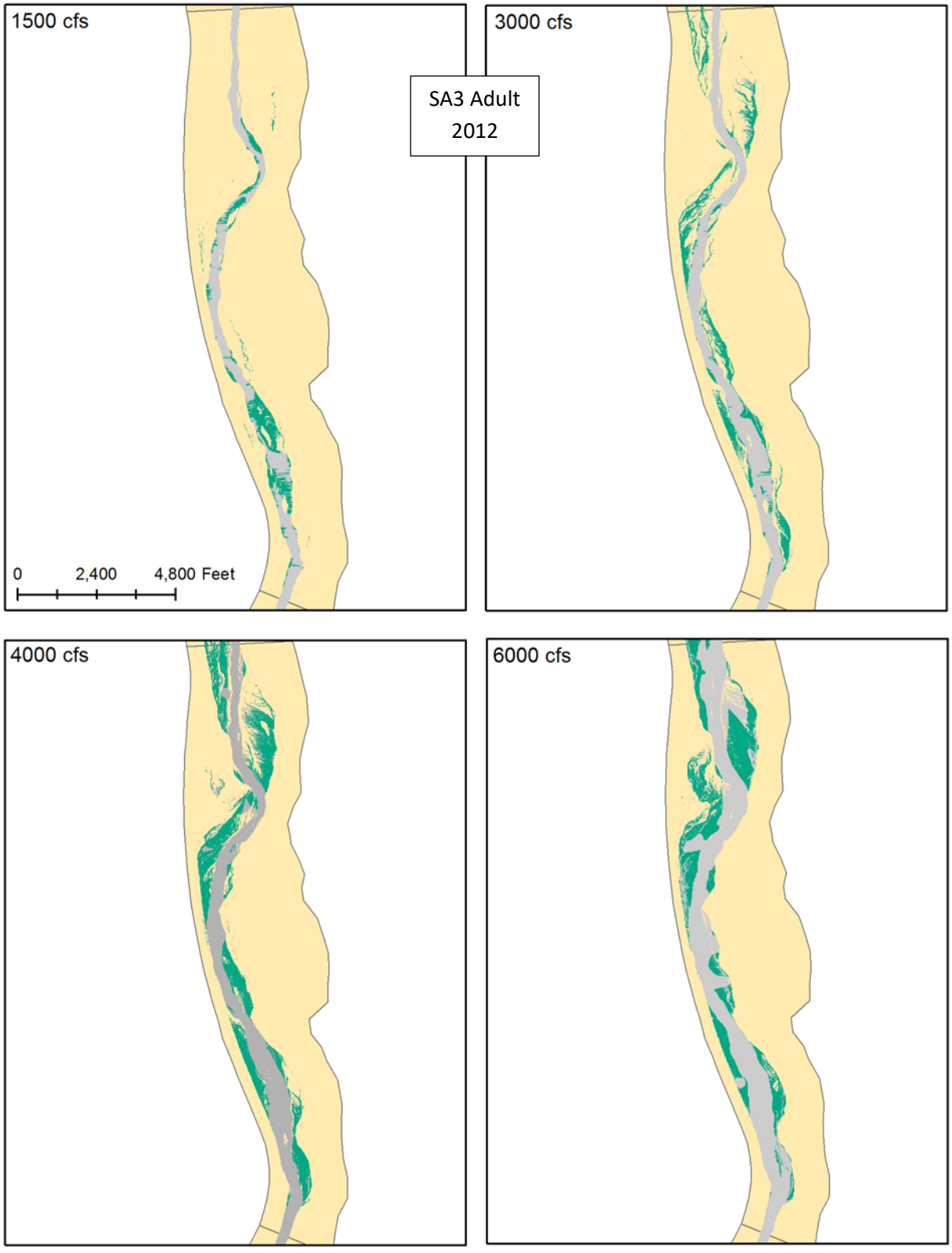

Figure 45 Adult habitat at subreach SA3 in 2012; flow direction is from top to bottom

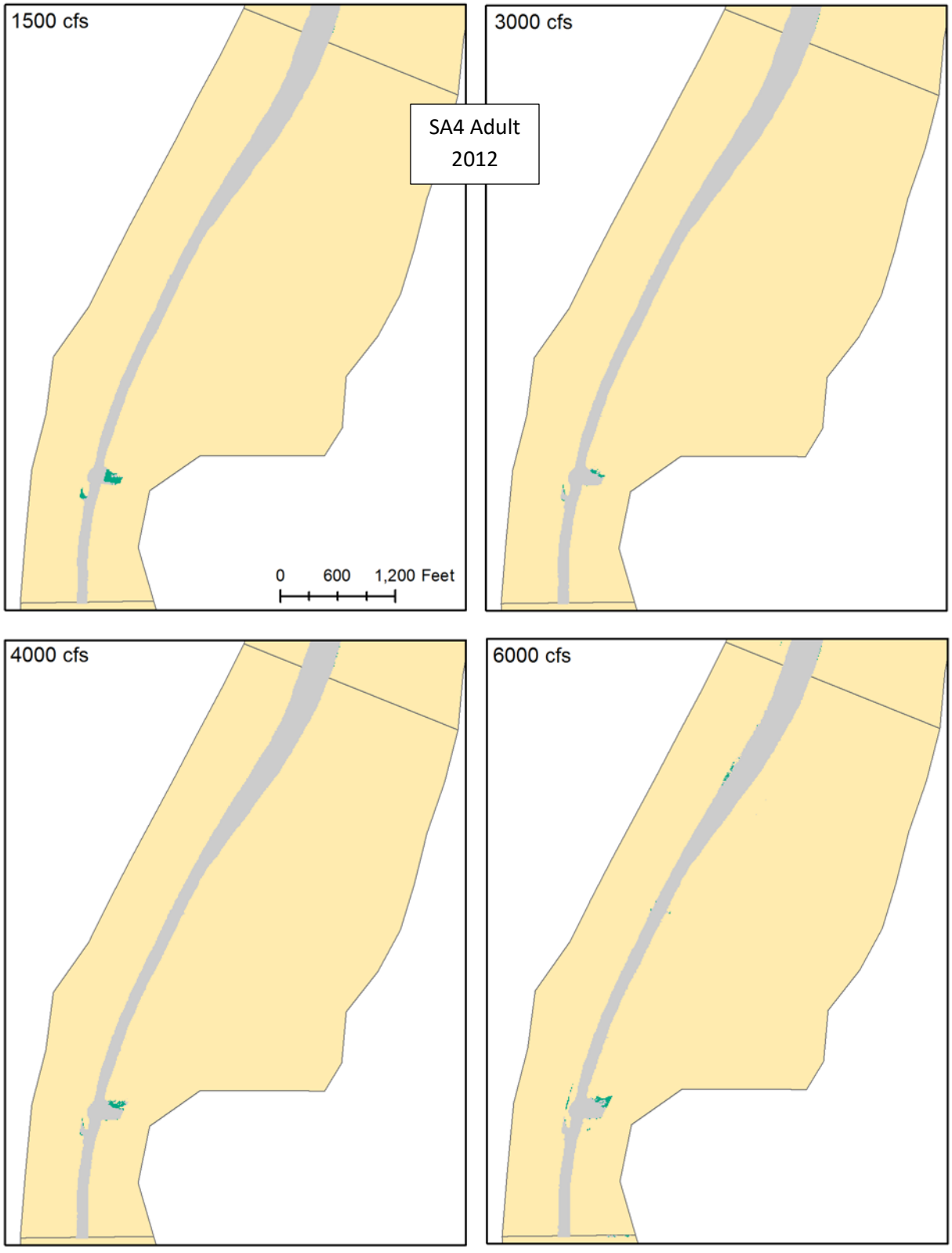

Figure 46 Adult habitat at subreach SA4 in 2012; flow direction is from top to bottom

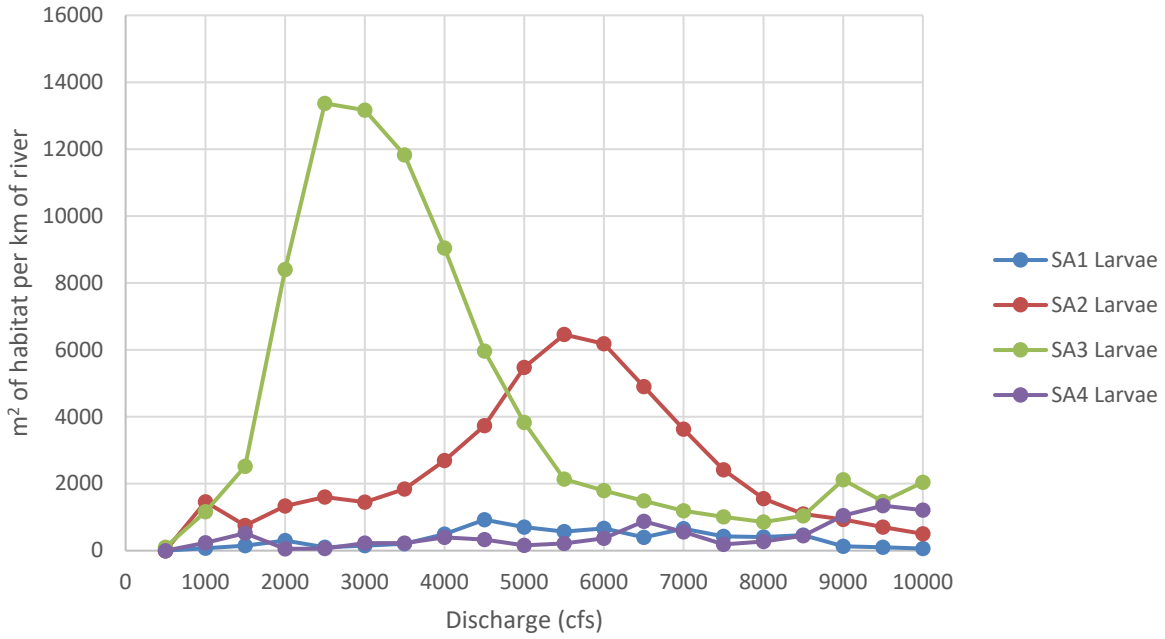

Figure 47 Larvae habitat by subreach in 2012

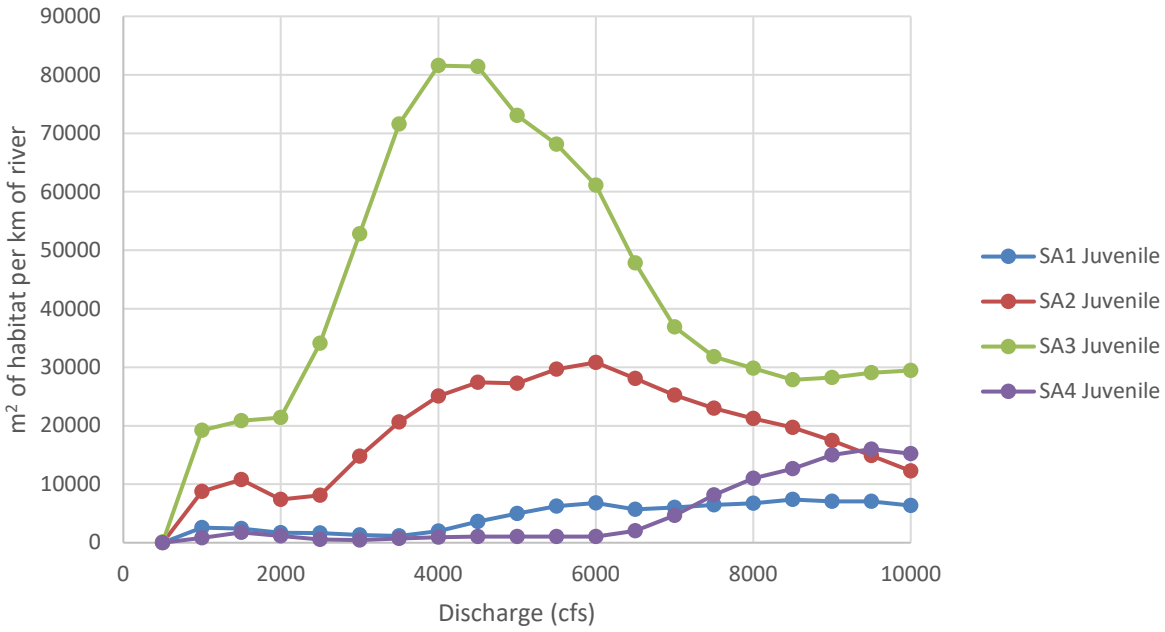

Figure 48 Juvenile habitat by subreach in 2012

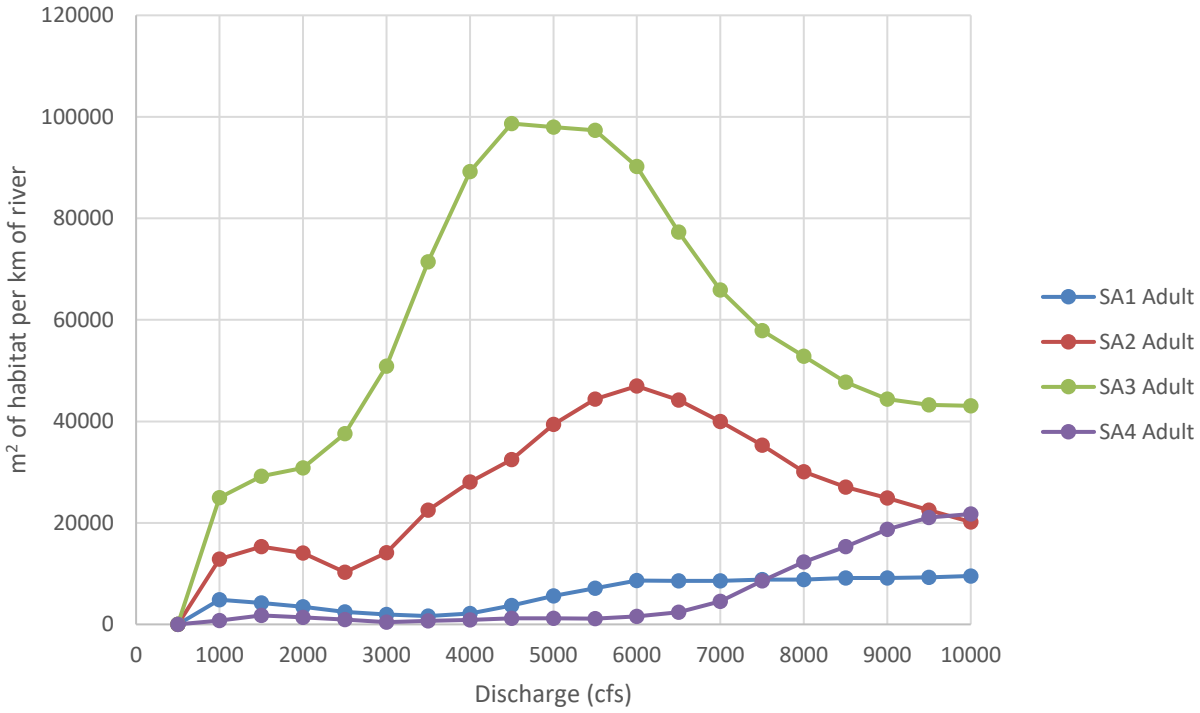

Figure 49 Adult habitat by subreach in 2012

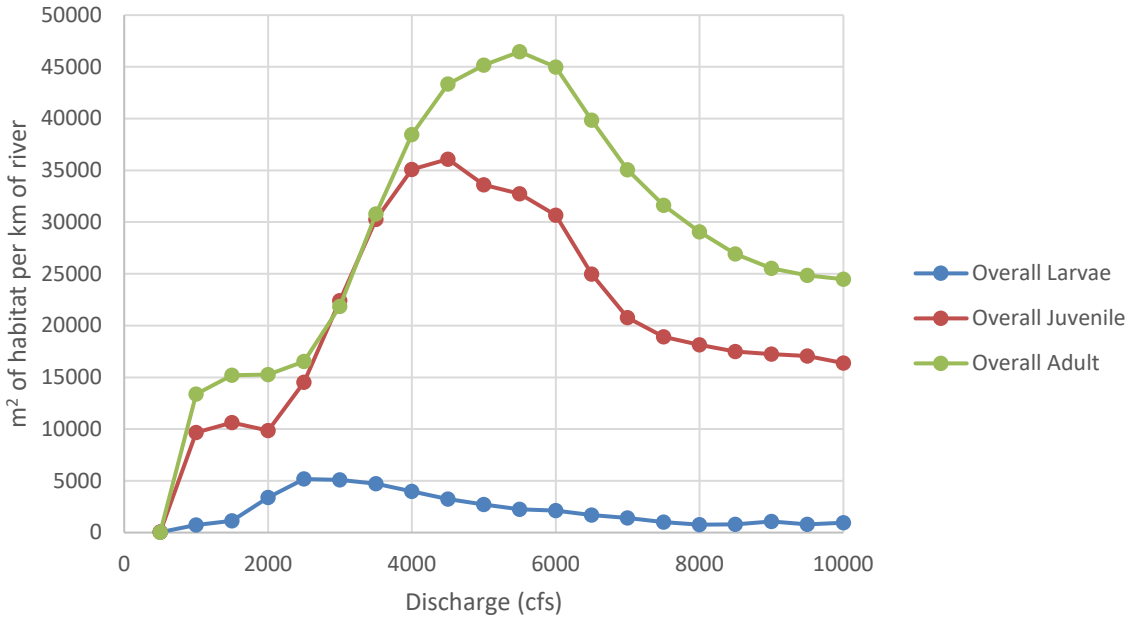

Figure 50 Larvae, juvenile and adult habitat for the overall San Acacia reach in 2012

4.3 Velocity versus Depth in 2012

Areas produced by the RAS-Mapper method were also broken apart into their component parts, looking at velocity and depth across areas individually. Figure 51 shows a comparison of the areas meeting depth and velocity criteria individually versus combined. The overall shape of the velocity curve more closely resembled the actual habitat availability curve that considers both depth and velocity. However, the depth only curve shows two peaks, with the first occurring around 1,500 cfs. Additional figures for juveniles and larvae are in Appendix 7.2 Additional Figures. Figure 52 shows that for some discharges, almost 100% of the areas meeting velocity criteria become overall acceptable habitat (meeting both velocity and depth criteria).

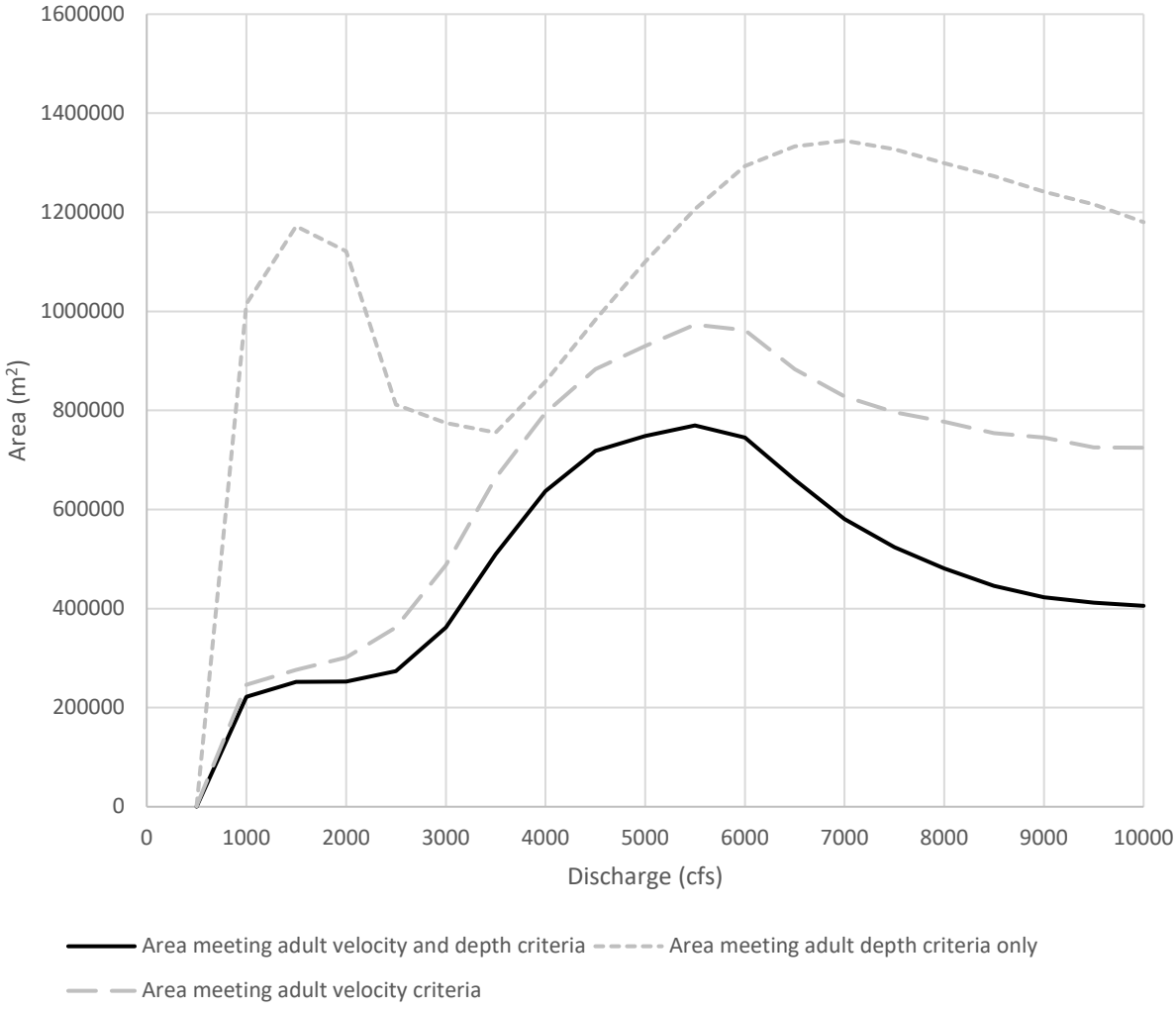

Figure 51 Comparison of areas meeting depth and velocity criteria individually and combined for adults

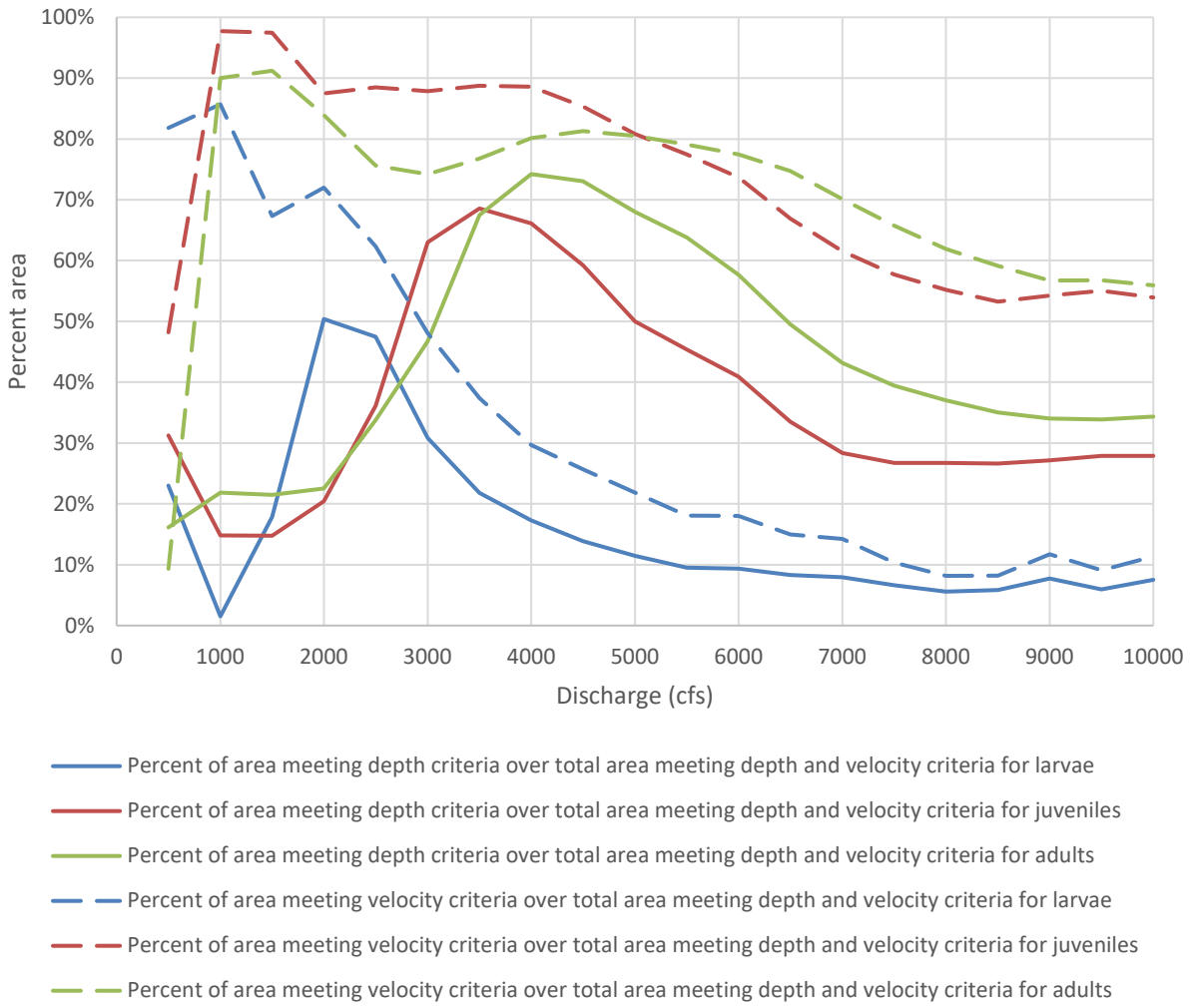

Figure 52 Percent of areas meeting depth and velocity criteria over the total acceptable habitat area

4.4 Habitat Analysis

The first trend observed was that subreach SA3 had the most available habitat across larvae, juvenile and adult life stages. This indicates that there are distinct subreach level differences in suitability for RGSM. There are potential links to the geomorphology of the subreach. Note that subreach SA3, the widest subreach historically and currently, experienced the least amount of degradation in the time period analyzed (see Sections 3.3 and 3.5). SA3 can be considered the major driver of overall habitat trends in the San Acacia reach.

A second observation is that the limiting factor for habitat availability was velocities, not depths. This is particularly true at discharges at or below 3,000 cfs. For example, of the areas meeting velocity criteria for adults alone, 91% ultimately became areas that fit velocity and depth criteria. In contrast, only 21% of the areas meeting depth criteria for adults alone were utilized. This suggests that there are many areas where depths are acceptable for RGSM habitat in the channel, but velocities are too

high. These initial results suggest that restoration efforts could potentially focus on creating areas of low velocity in places where the existing depths meet criteria for RGSM.

5. Conclusions

The San Acacia reach was analyzed for hydrologic, hydraulic and geomorphic trends between 1918 and 2018. This reach covers around 11.6 miles from the San Acacia Diversion Dam to the Escondida Bridge.

HEC-RAS and GIS were used to find geomorphic and river characteristics such as sinuosity, width, bed elevation and other hydraulic parameters. These analyses were broken down by each of the four subreaches, allowing trends to be seen on a smaller scale.

Major findings include:

- The annual water volume has been reduced since 1995. Peak discharges are lower and of shorter duration.
- The annual suspended sediment discharge in the Rio Grande has decreased since 1995.
- Degradation has occurred in all subreaches.
- Most subreaches are currently in stage M4 of the geomorphic conceptual model, representing more incision and less connection to the floodplain.
- Significant narrowing has occurred in all subreaches, and some are approaching the theoretical equilibrium width predicted by the JW equations.
- Sinuosity has decreased overall since 1918 but has been increasing since 1985 on Subreaches SA1-SA3.
- Evidence of coarsening downstream of the San Acacia Diversion Dam is present.
- Subreach SA3 has the most habitat and is a major driver of habitat trends on the entire San Acacia reach.
- Velocity is the limiting factor for habitat availability, not depth.

6. Works Cited

Bovee, K.D., Waddle, T.J., and Spears, J.M. (2008). “Streamflow and endangered species habitat in the lower Isleta reach of the middle Rio Grande.” *U.S. Geological Survey Open-File Report 2008-1323*.

LaForge, K., Yang, C.Y., Julien, P.Y., and Doidge, S. (2019). Draft Report. *Rio Puerco Reach: Hydraulic Modeling and Silvery Minnow Habitat Analysis*, Colorado State University, Fort Collins, CO.

Klein, M., Herrington, C., AuBuchon, J., and Lampert, T. (2018a). *Isleta to San Acacia Geomorphic Analysis*, U.S. Bureau of Reclamation, Reclamation River Analysis Group, Albuquerque, New Mexico.

Klein, M., Herrington, C., AuBuchon, J., and Lampert, T. (2018b). *Isleta to San Acacia Hydraulic Modeling Report*, U.S. Bureau of Reclamation, Reclamation River Analysis Group, Albuquerque, New Mexico.

Julien, P.Y. (2002). *River Mechanics,* Cambridge University Press, New York

Julien, P. Y., and Wargadalam, J. (1995). “Alluvial channel geometry: theory and applications.” *Journal of Hydraulic Engineering*, American Society of Civil Engineers, 121(4), 312–325.

Massong, T., Paula, M., and Bauer, T. (2010). “Planform Evolution Model for the Middle Rio Grande, NM.” *2nd Joint Federal Interagency Conference, Las Vegas, NV, June 27 - July 1, 2010*.

MEI. (2002). *Geomorphic and Sedimentologic Investigations of the Middle Rio Grande between Cochiti Dam and Elephant Butte Reservoir*, Mussetter Engineering, Inc., Fort Collins, CO, 220 p.

Mortensen, J.G., Dudley, R.K., Platania, S.P., and Turner, T.F. (2019). Draft report. *Rio Grande Silvery Minnow Habitat Synthesis,* University of New Mexico with American Southwest Ichthyological Researchers, Albuquerque, NM.

Posner, A. J. (2017). Draft report. *Channel conditions and dynamics of the Middle Rio Grande River,* U.S. Bureau of Reclamation, Albuquerque, New Mexico.

Scurlock, D. (1998). “From the Rio to the Sierra: an environmental history of the Middle Rio Grande Basin.” *General Technical Report RMRS-GTR-5. Fort Collins, CO: US Department of Agriculture, Forest Service, Rocky Mountain Research Station, 440 p.*

Shah-Fairbank, S. C., Julien, P. Y., and Baird, D. C. (2011). “Total sediment load from SEMEP using depth-integrated concentration measurements.” Journal of Hydraulic Engineering, 137(12), 1606–1614.

U.S. Bureau of Reclamation. (2012). “Middle Rio Grande River Maintenance Program - Comprehensive Plan and Guide.” Albuquerque Area Office, Albuquerque, New Mexico, 202p.

U.S. Fish and Wildlife Service. (2007). “Rio Grande Silvery Minnow (Hybognathus amarus).” Draft Revised Recovery Plan, Albuquerque, New Mexico, 174 p.

Varyu, D. (2013). *Aggradation / Degradation Volume Calculations: 2002-2012*. U.S. Department of the Interior, Bureau of Reclamation, Technical Services Center, Sedimentation and River Hydraulics Group. Denver, CO.

Varyu, D. (2016). *SRH-1D Numerical Model for the Middle Rio Grande: Isleta Diversion Dam to San Acacia Diversion Dam*. U.S. Department of the Interior, Bureau of Reclamation, Technical Services Center, Sedimentation and River Hydraulics Group. Denver, CO.

Yang, C.Y. (2019). *The Sediment Yield of South Korean Rivers*, Colorado State University, Fort Collins, CO.

Yang, C.Y. and Julien, P.Y. (2019). “The ratio of measured to total sediment discharge.” *International Journal of Sediment Research*, 34(3), pp.262-269.

Yang, C.Y., LaForge, K., Julien, P.Y., and Doidge, S. (2019). Draft Report. *Isleta Reach: Hydraulic Modeling and Silvery Minnow Habitat Analysis*, Colorado State University, Fort Collins, CO.

7. Appendix

7.1 Subreach Delineation

The following figures were used to aid subreach delineation.

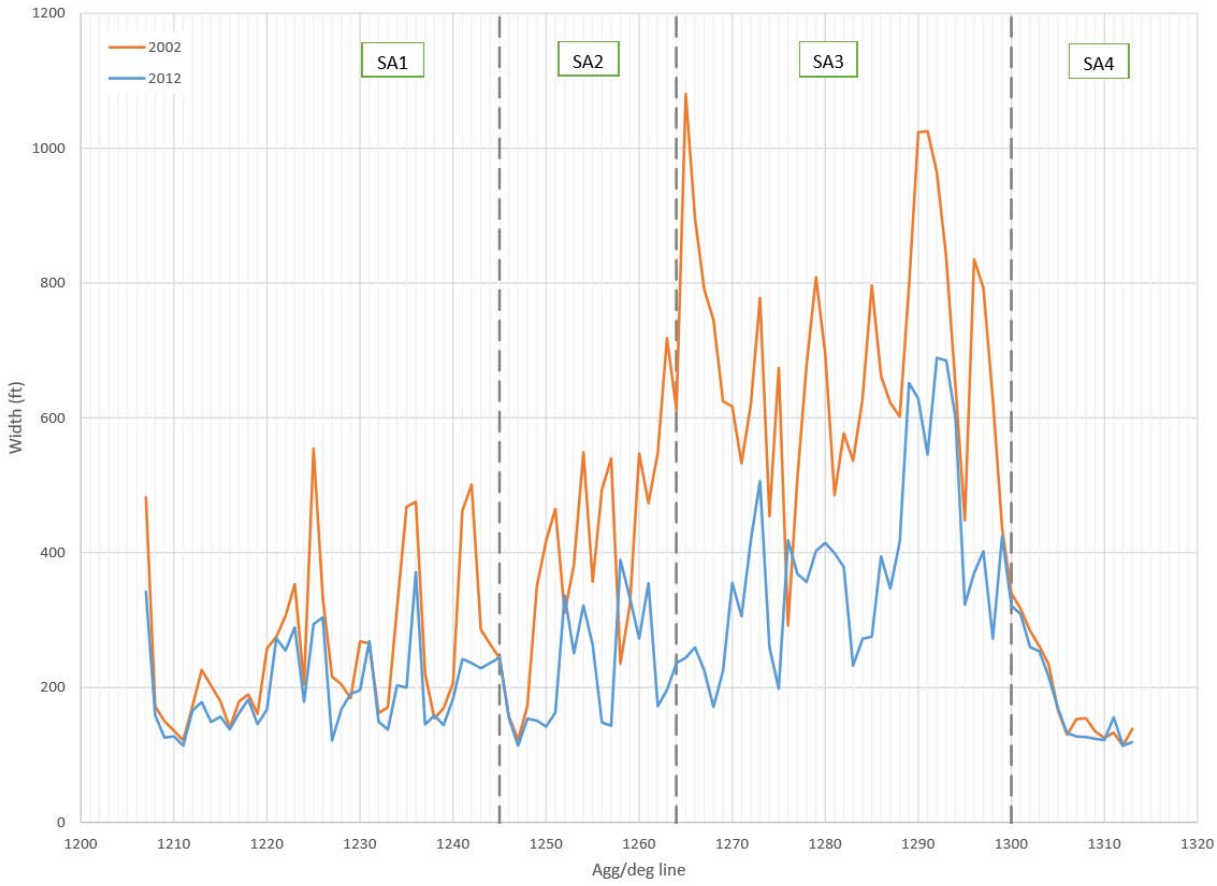

Figure 53 Subreach delineation width

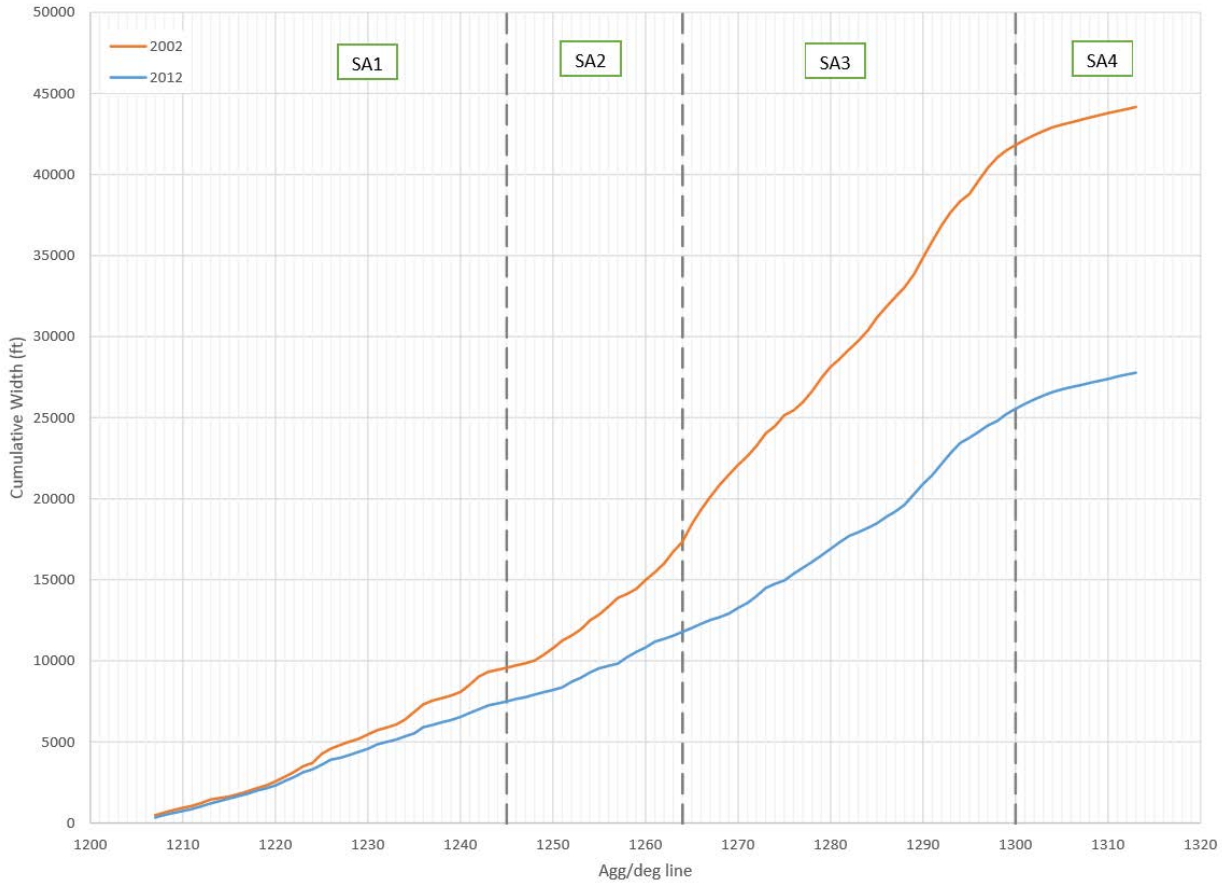

Figure 54 Subreach delineation cumulative width

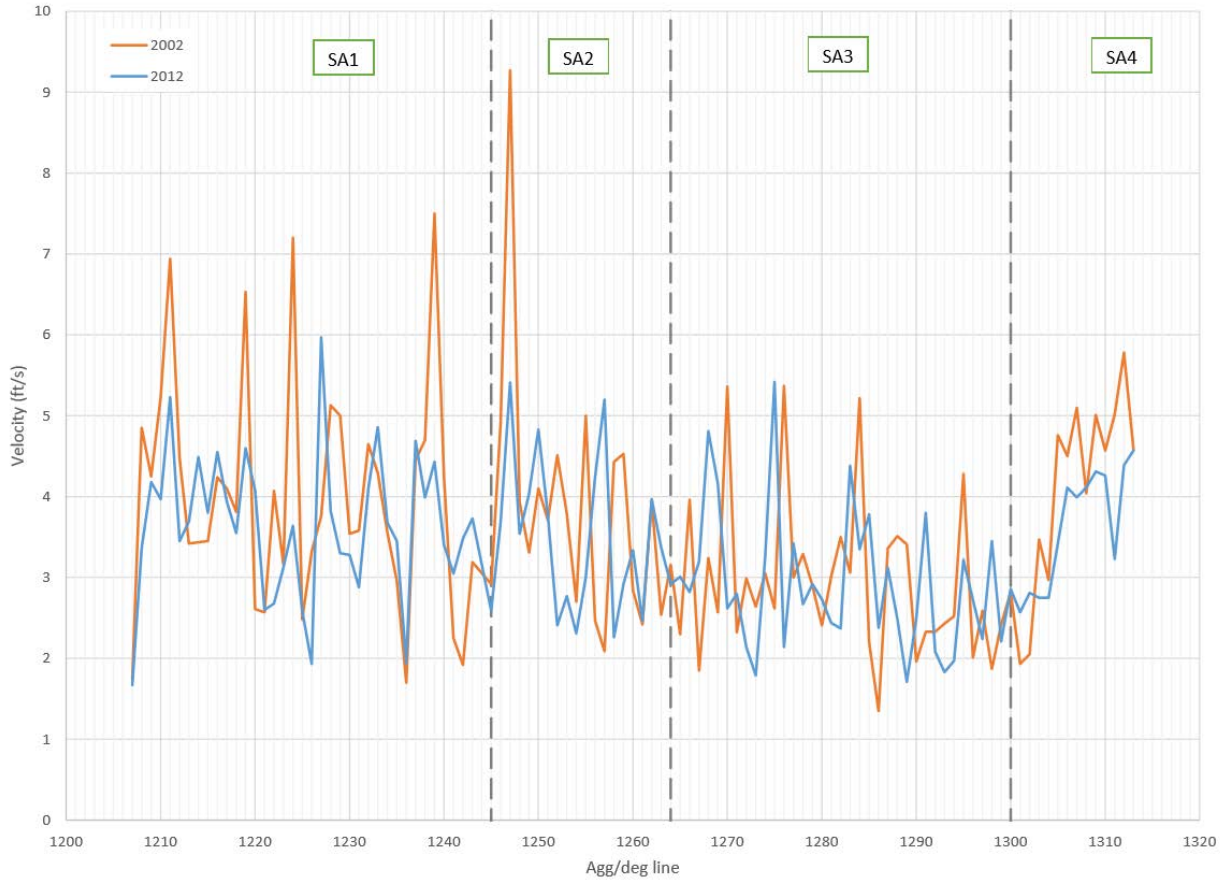

Figure 55 Subreach delineation velocity

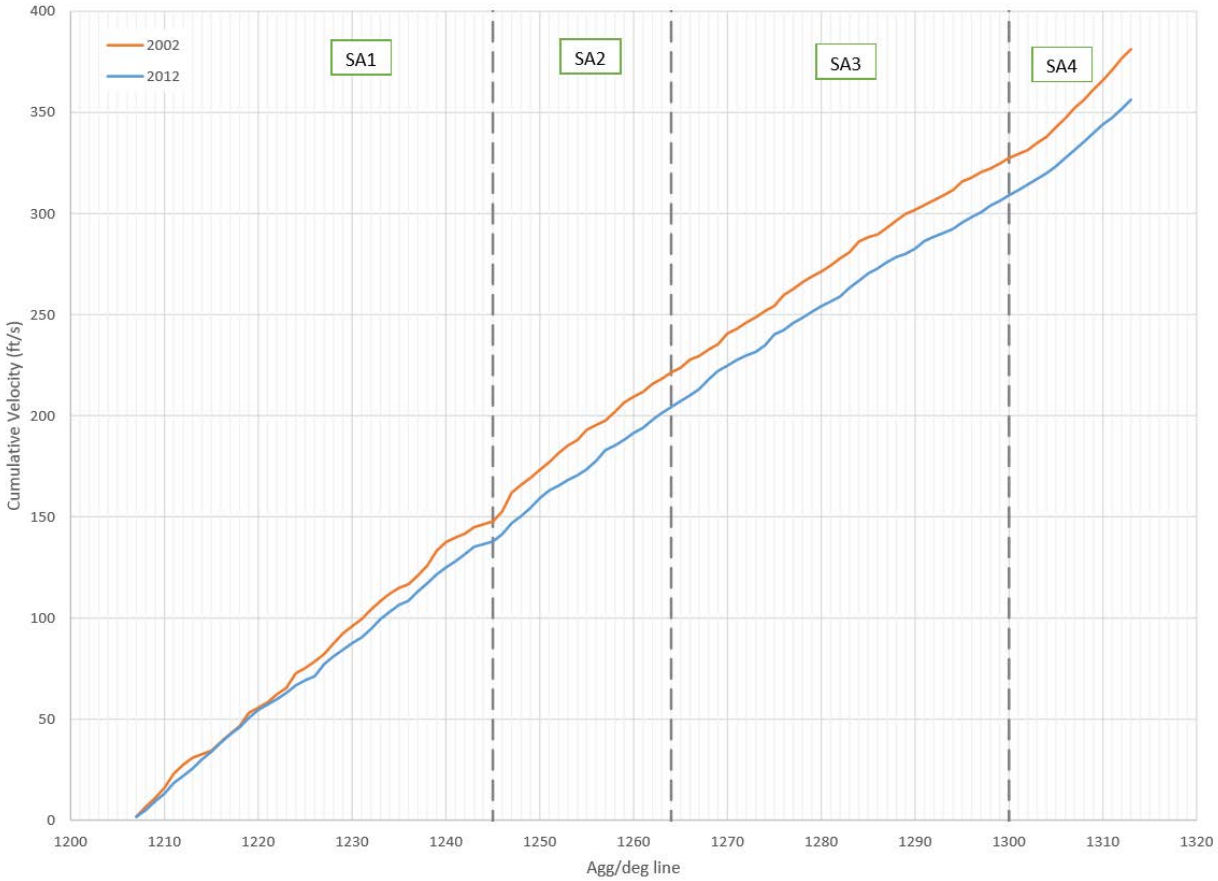

Figure 56 Subreach delineation cumulative velocity

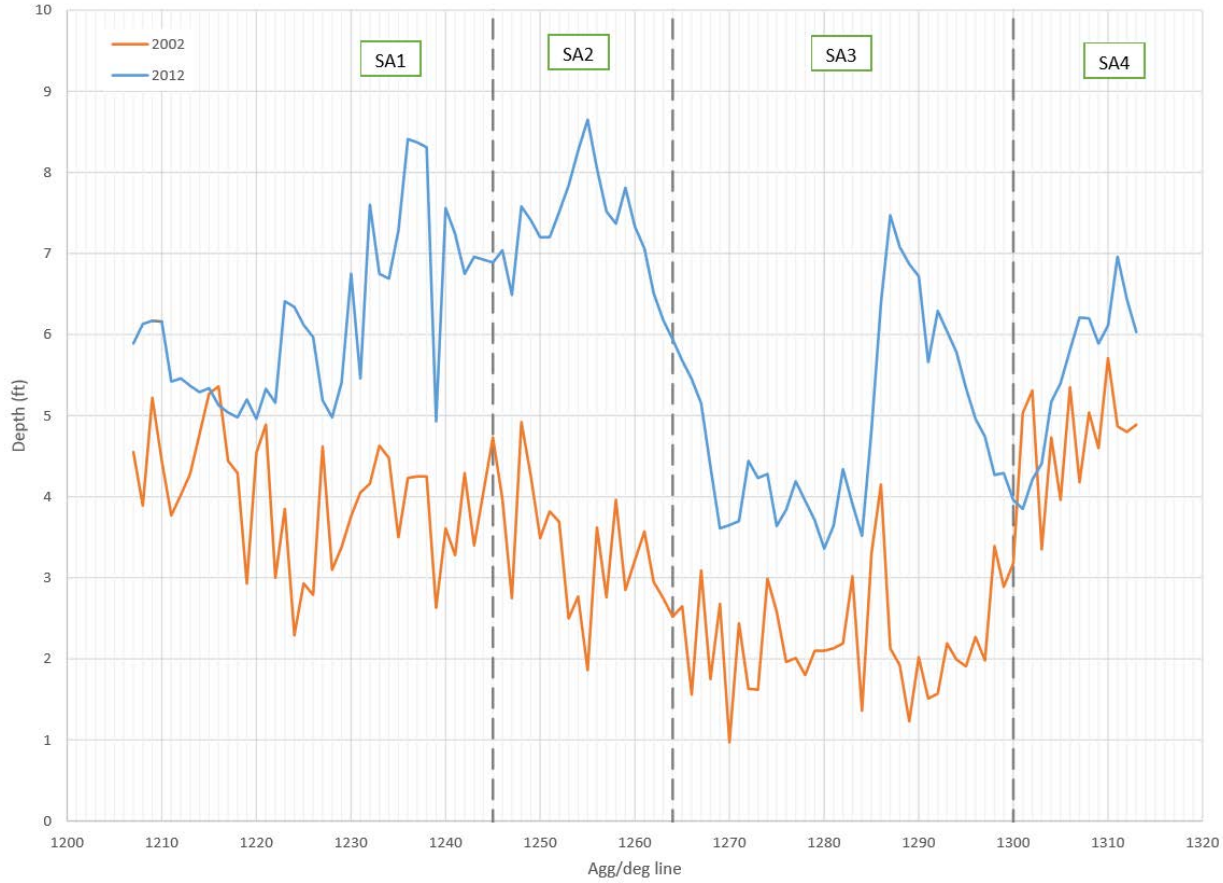

Figure 57 Subreach delination depth

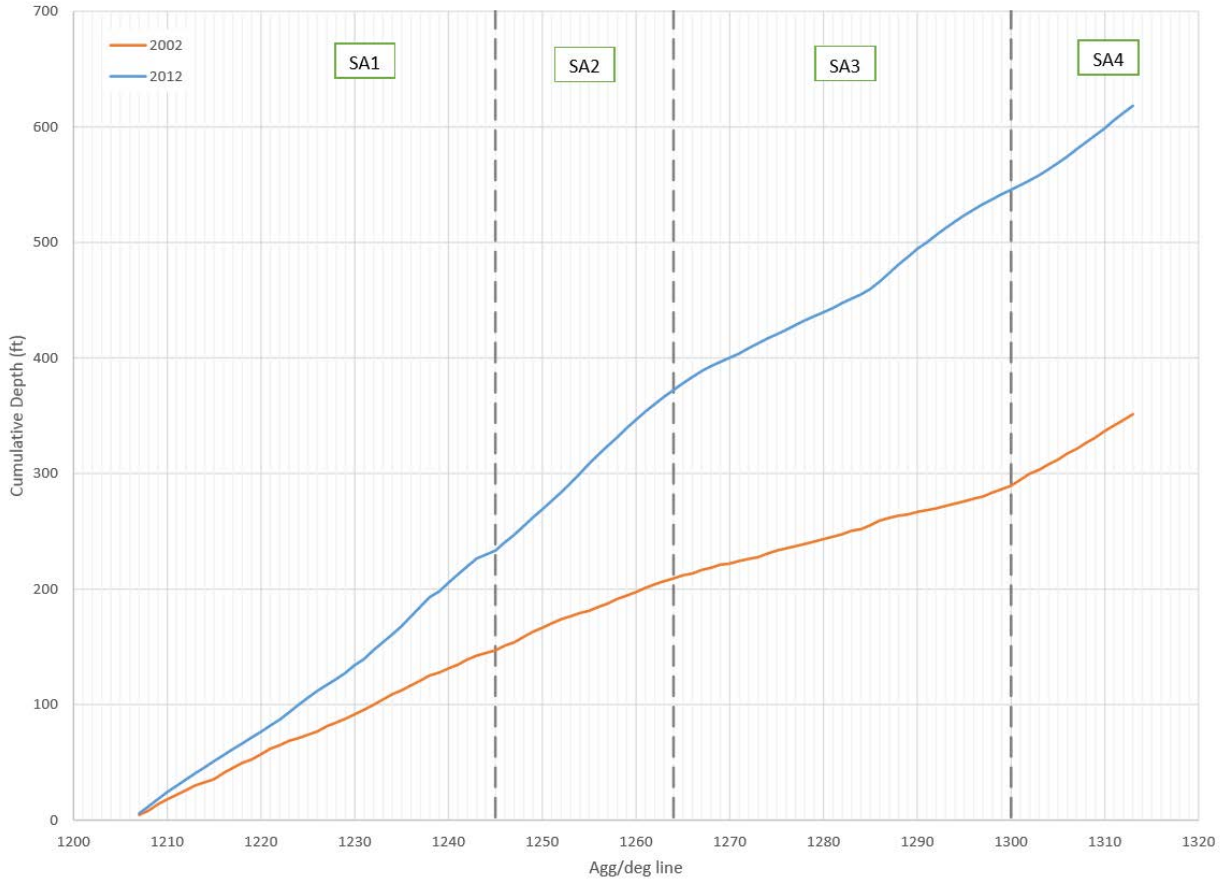

Figure 58 Subreach delineation cumulative depth

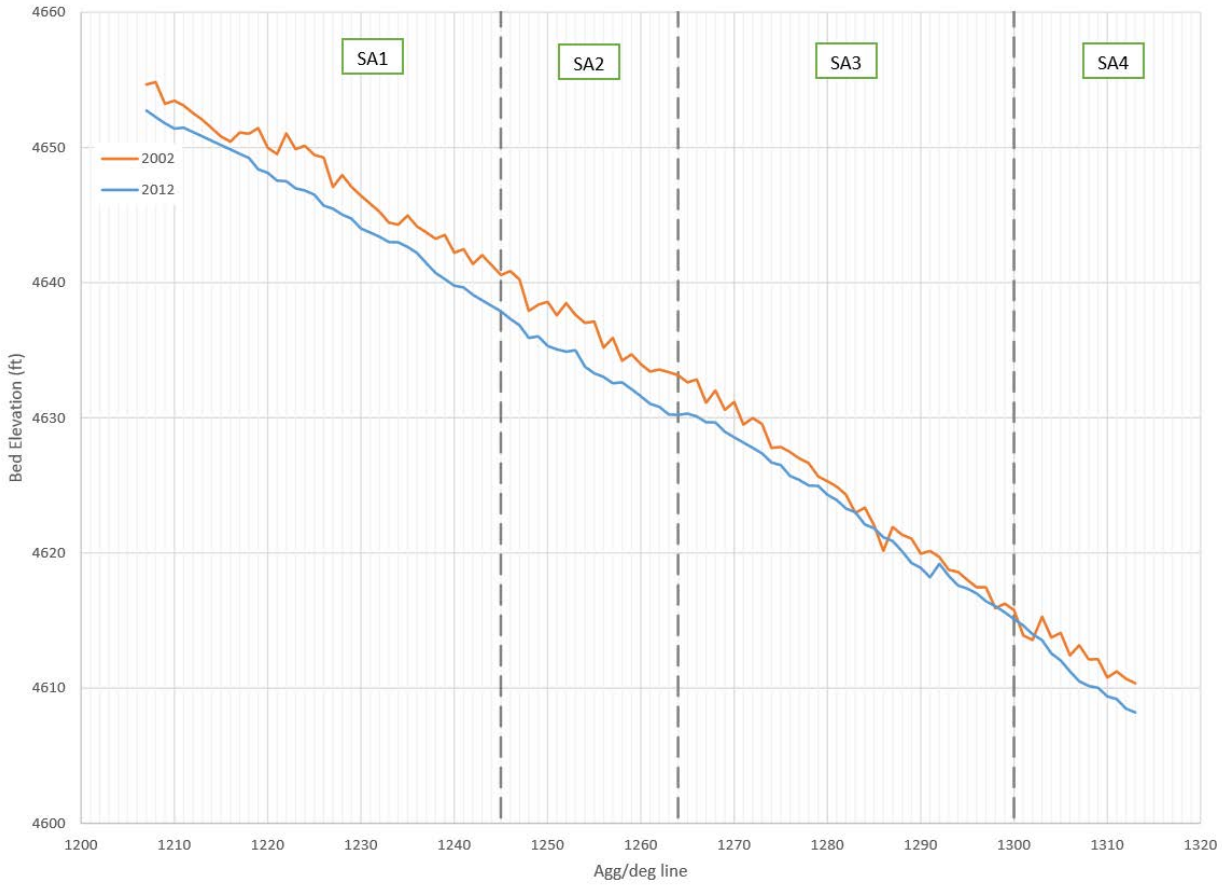

Figure 59 Subreach delination bed elevation

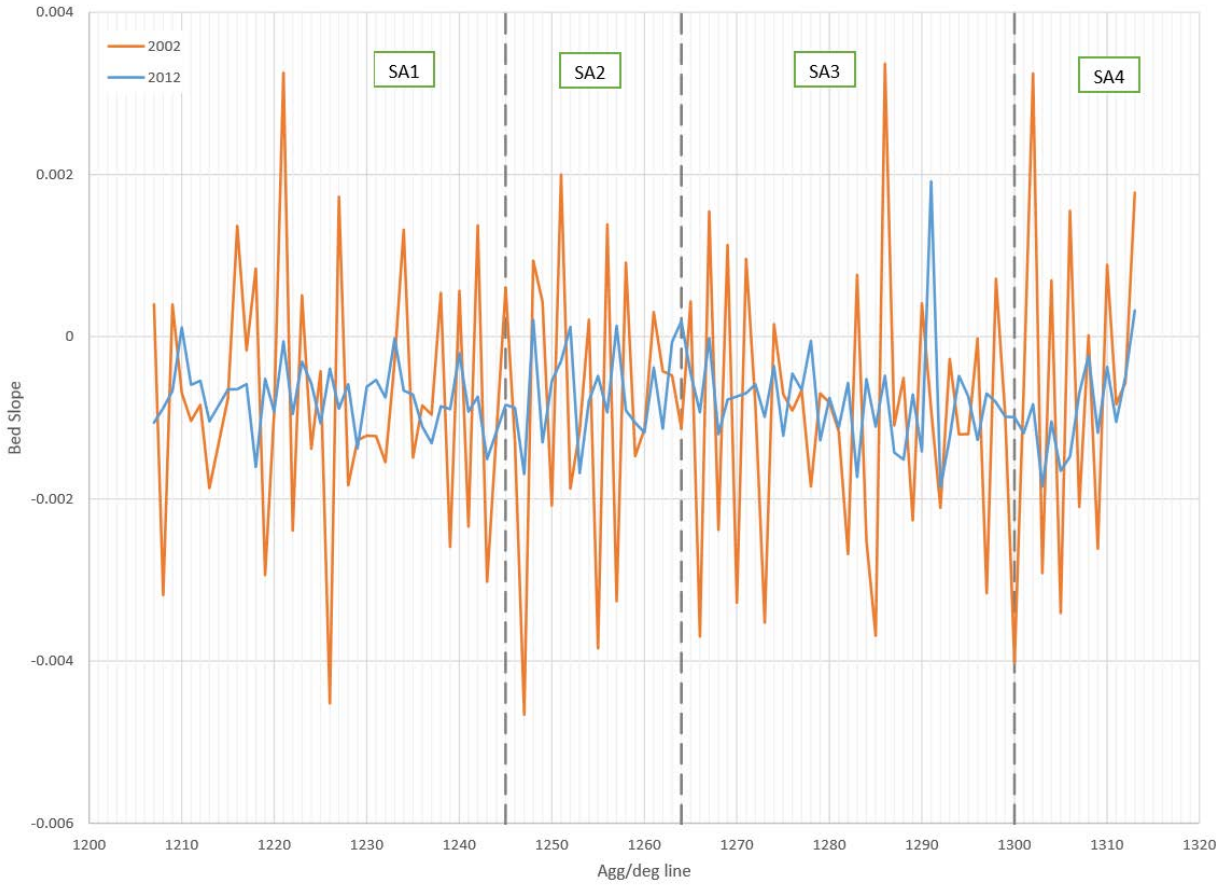

Figure 60 Subreach delineation slope

7.2 Additional Figures

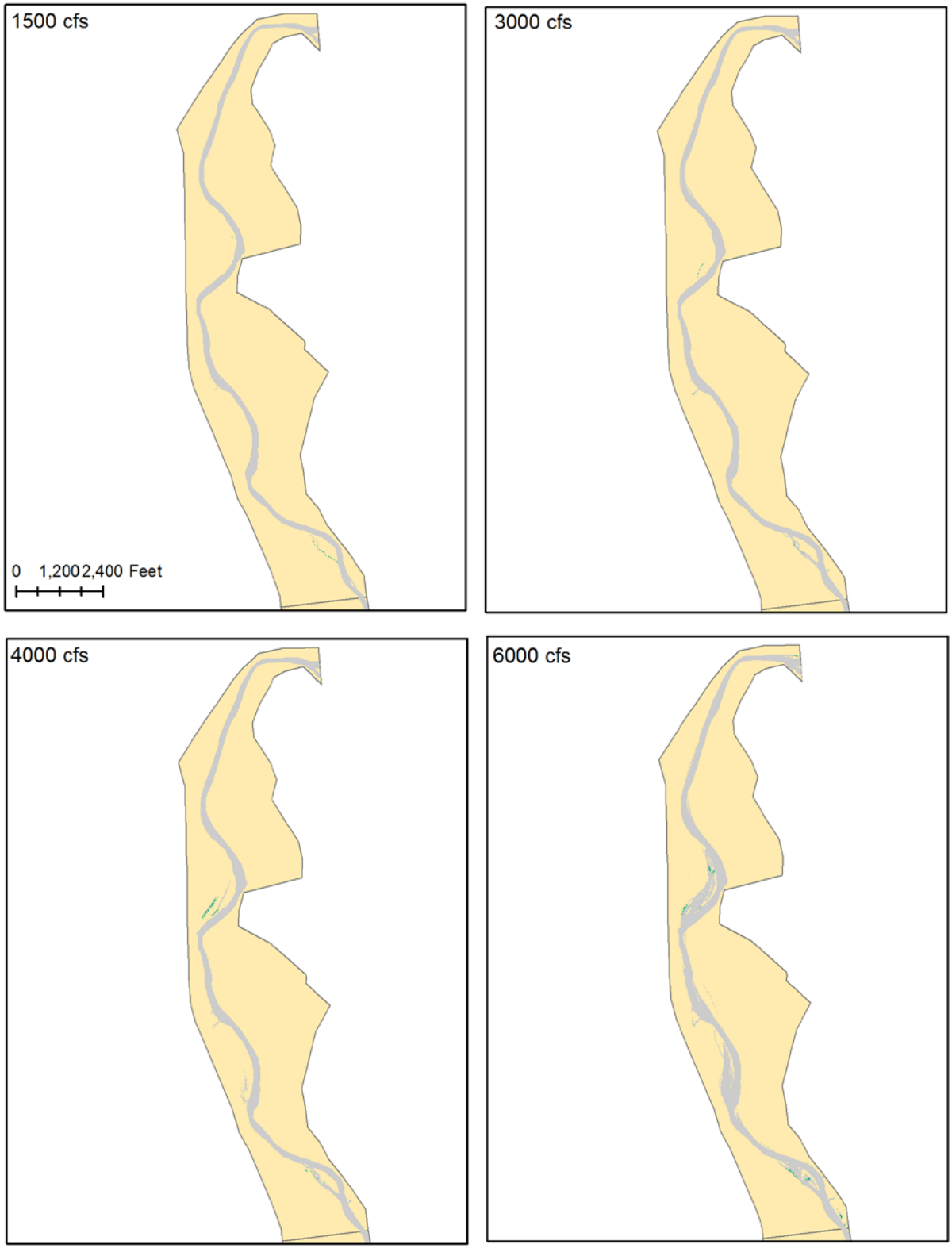

Figure 61 Larvae habitat at subreach SA1; flow direction is from top to bottom

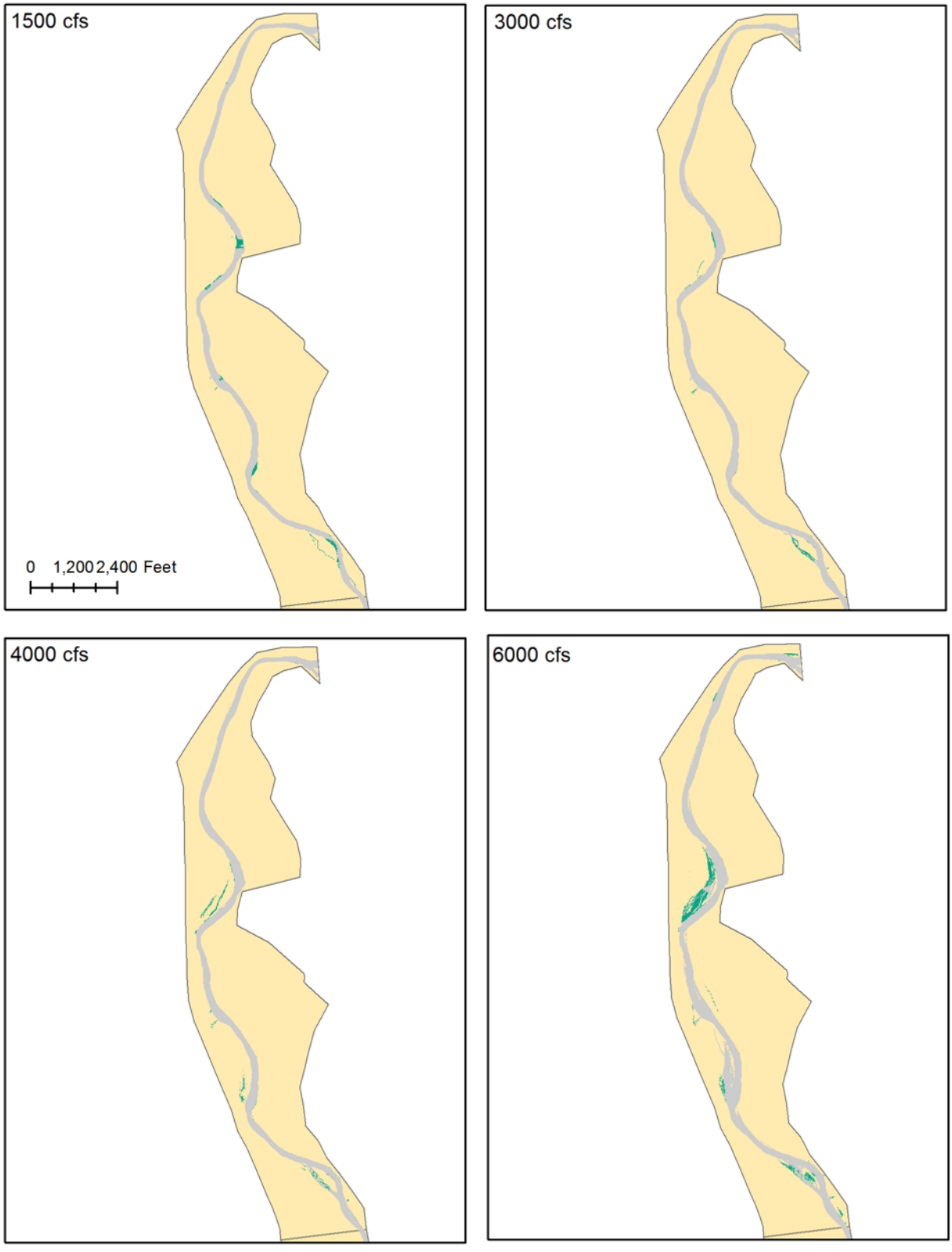

Figure 62 Juvenile habitat at subreach SA1; flow direction is from top to bottom

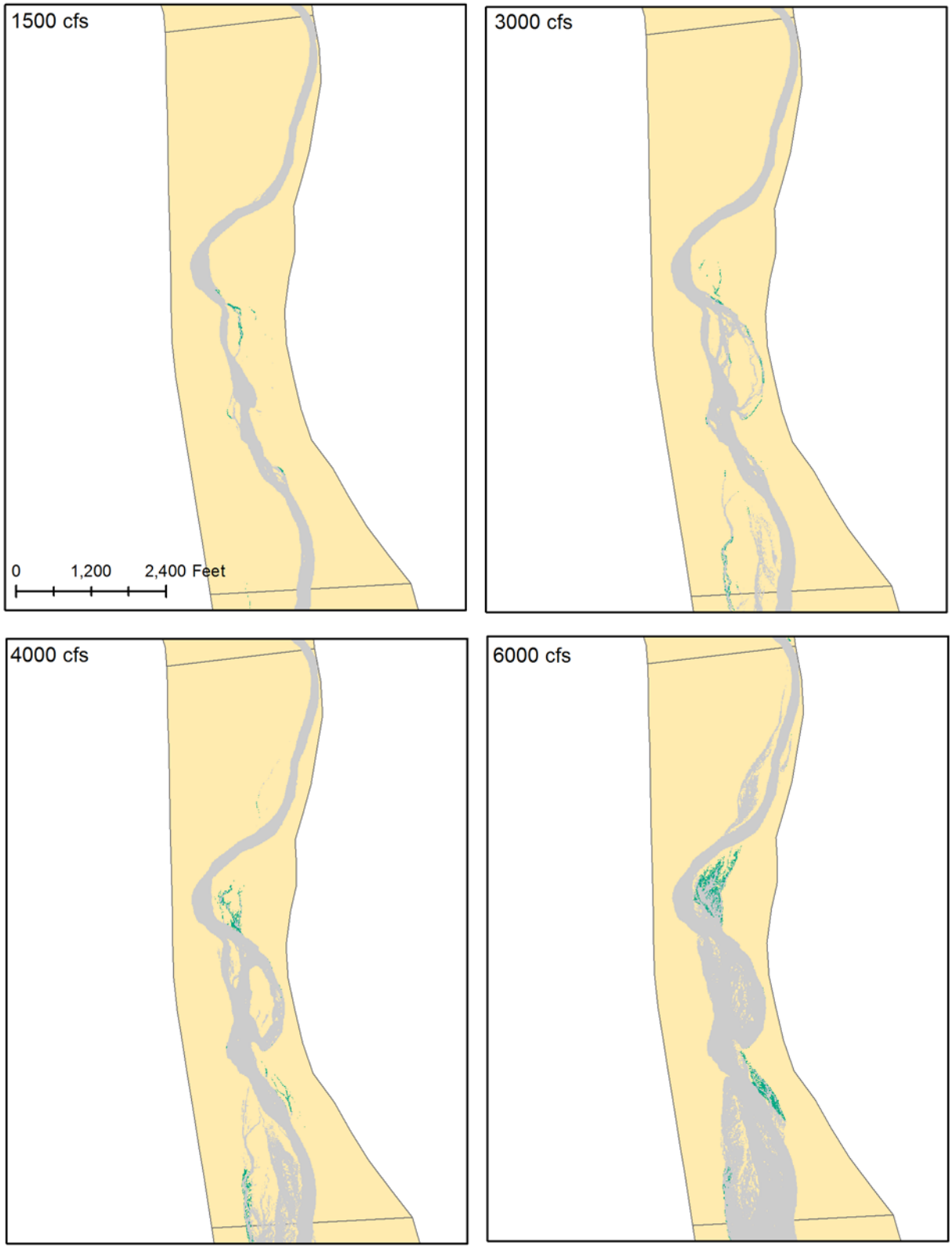

Figure 63 Larvae habitat at subreach SA2; flow direction is from top to bottom

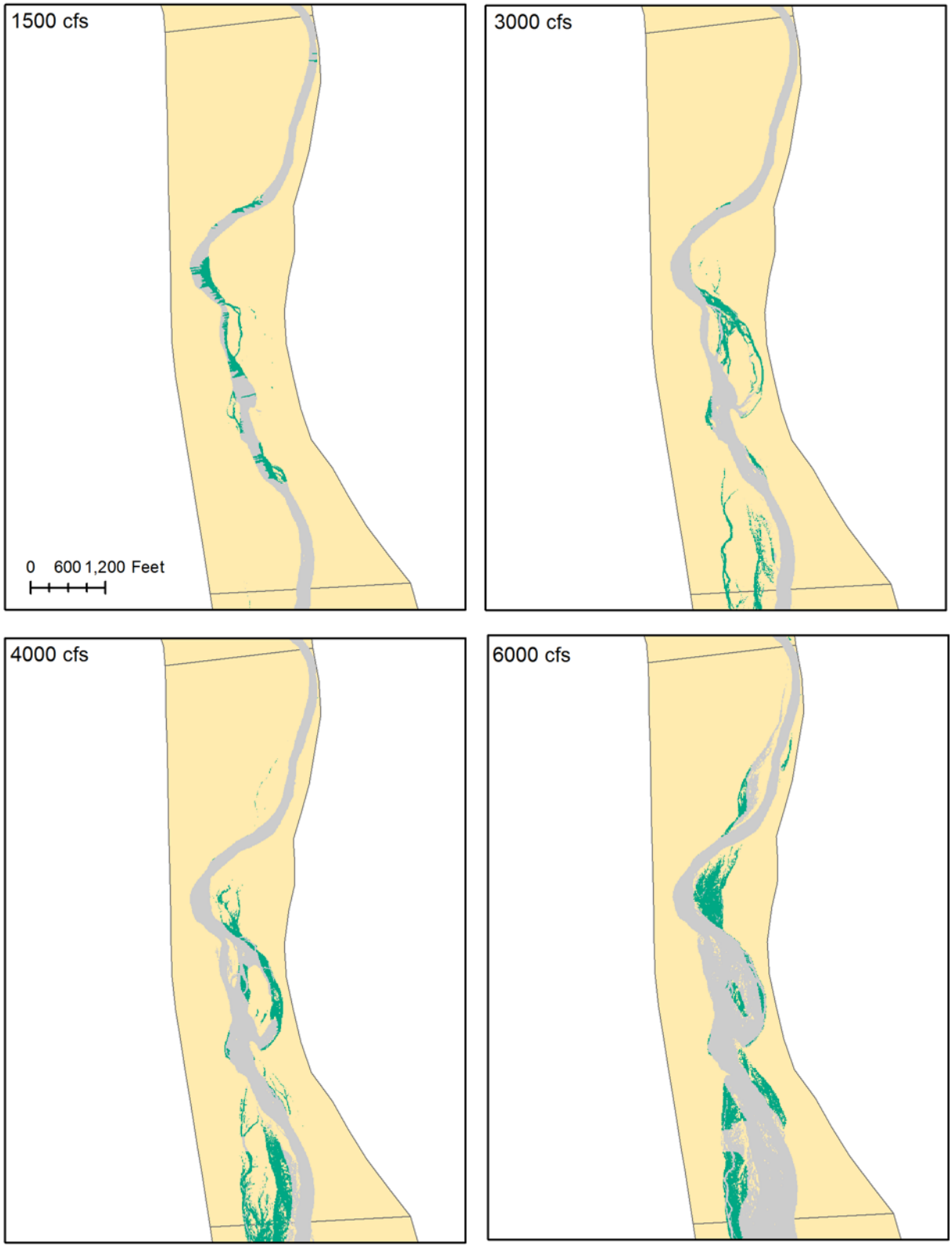

Figure 64 Juvenile habitat at subreach SA2; flow direction is from top to bottom

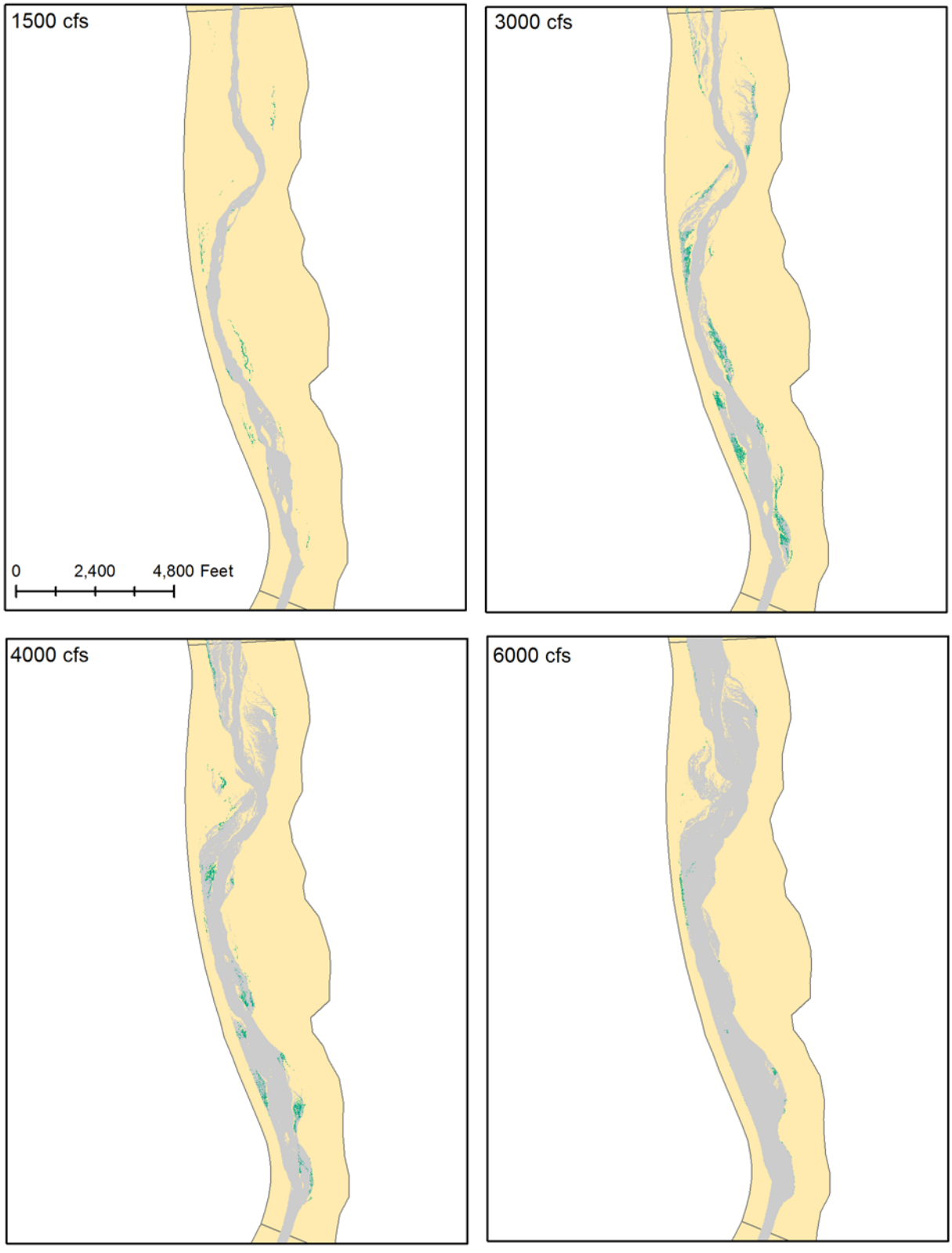

Figure 65 Larvae habitat at subreach SA3; flow direction is from top to bottom

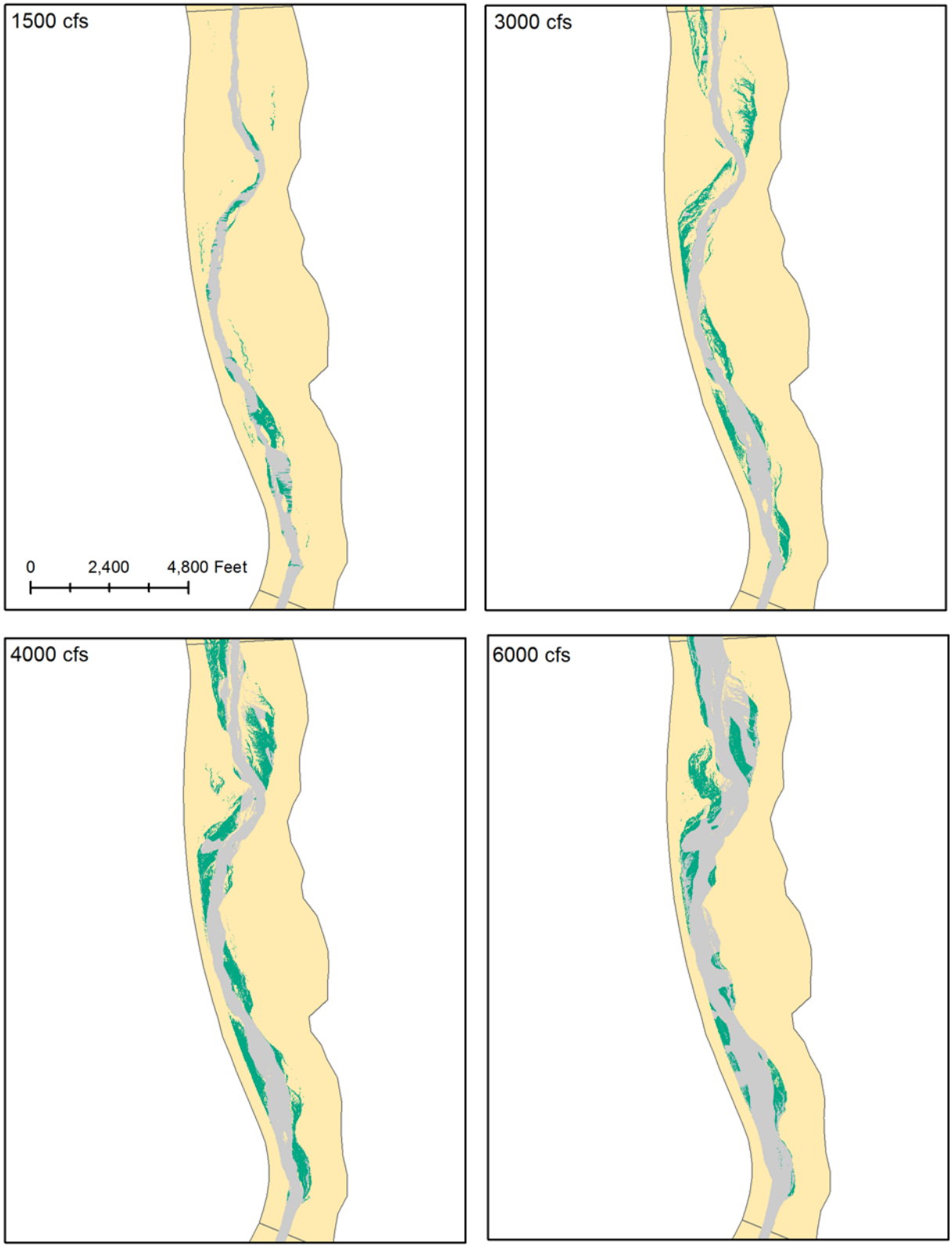

Figure 66 Juvenile habitat at subreach SA3; flow direction is from top to bottom

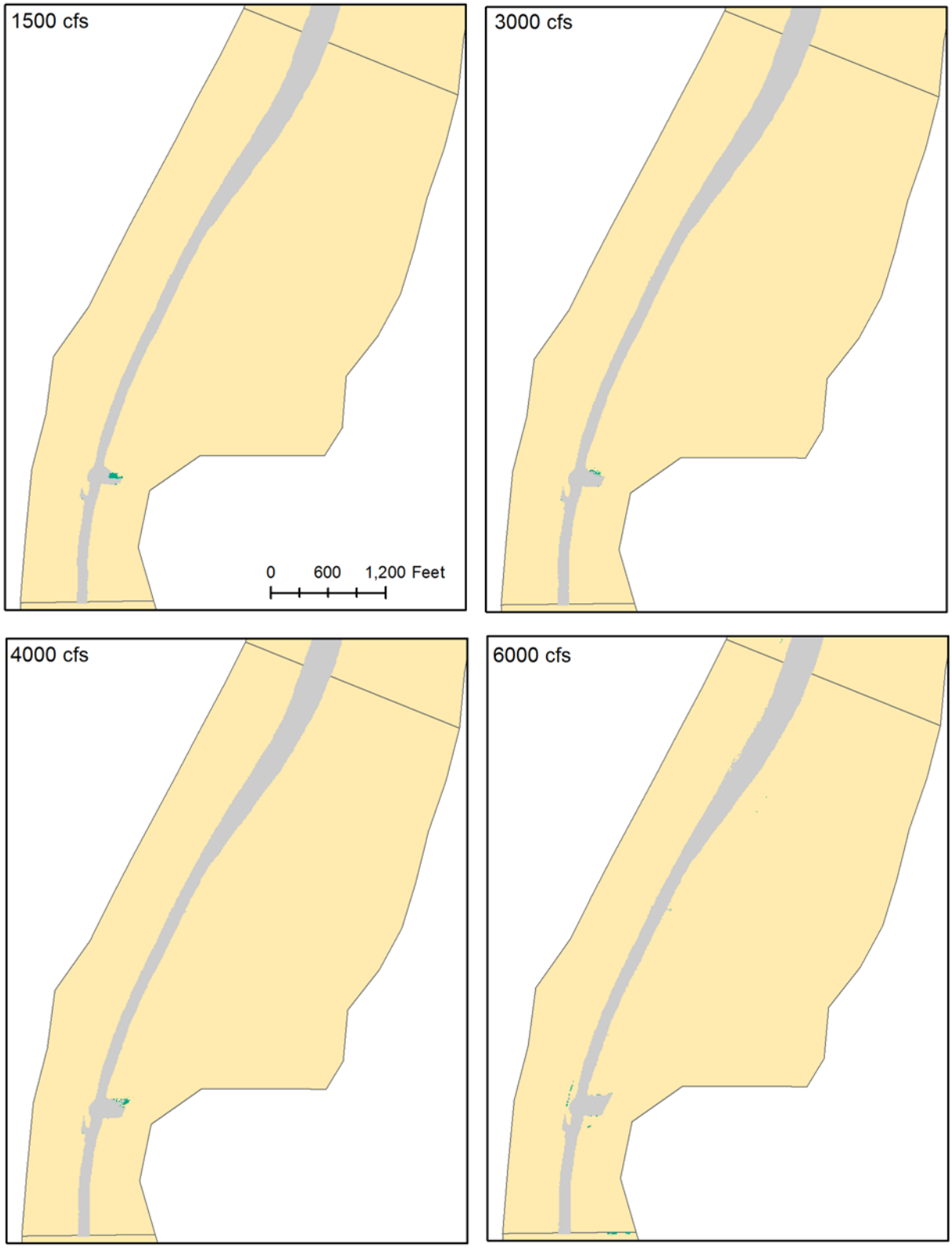

Figure 67 Larvae habitat at subreach SA4; flow direction is from top to bottom

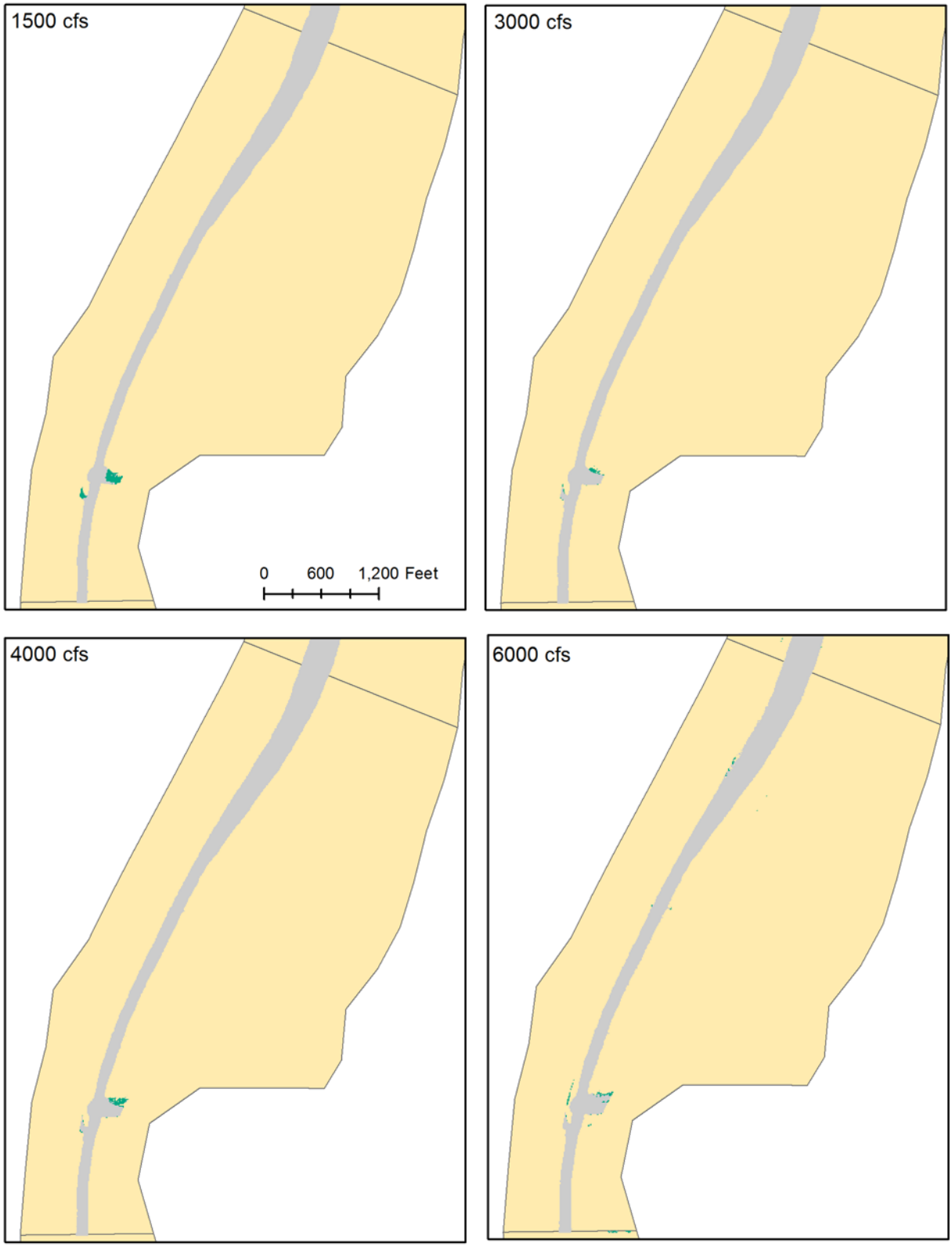

Figure 68 Juvenile habitat at subreach SA4; flow direction is from top to bottom

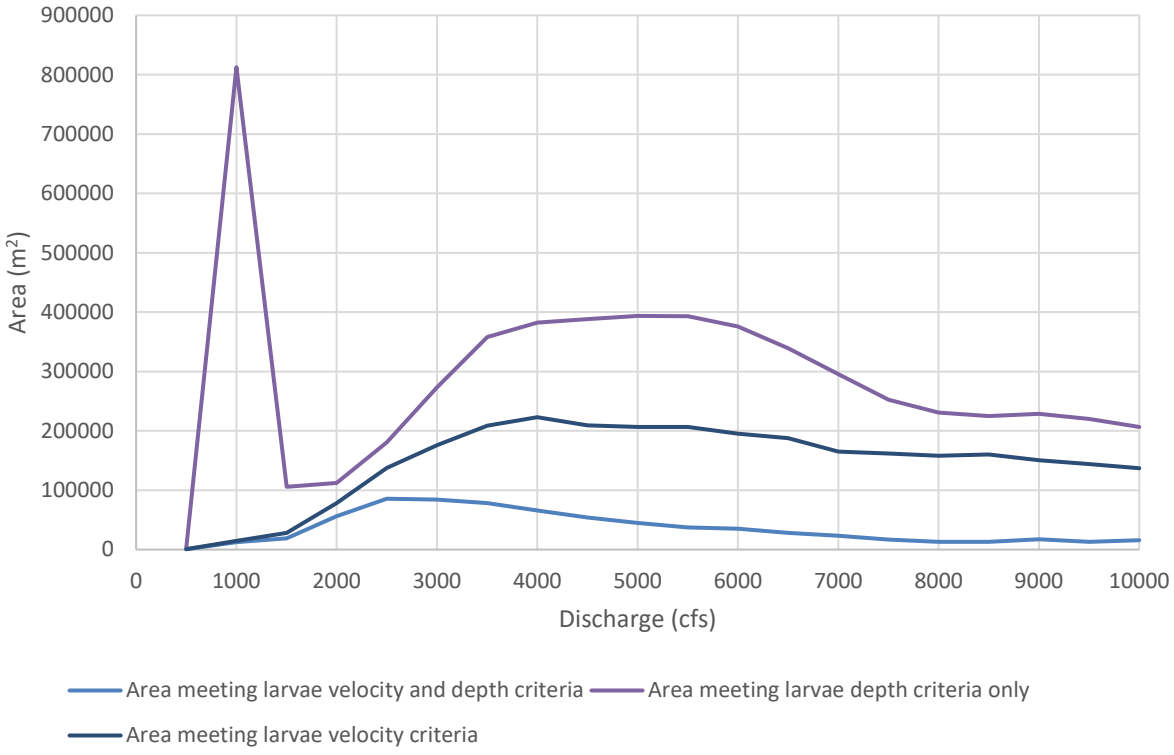

Figure 69 Comparison of areas meeting depth and velocity criteria individually and combined for larvae

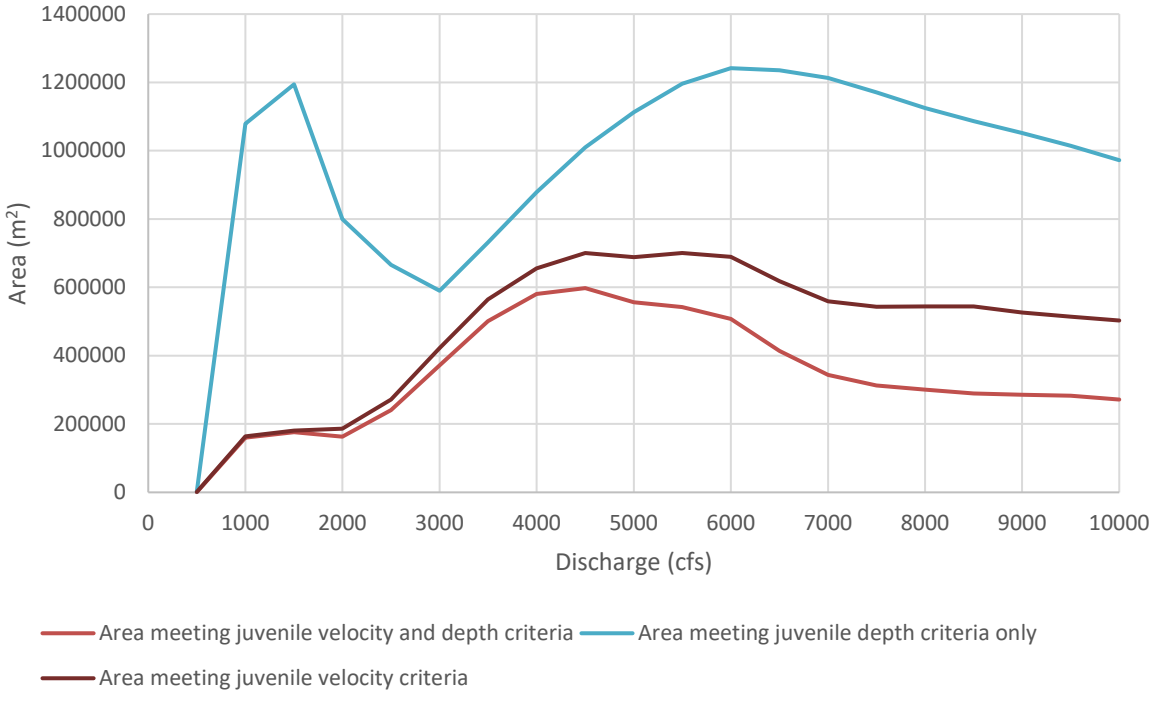

Figure 70 Comparison of areas meeting depth and velocity criteria individually and combined for juveniles